

Assen Zlatarov University
Burgas, Bulgaria



ANNUAL

VOLUME XLIX, BOOK 1, 2020

TECHNICAL AND NATURAL SCIENCES

1

ASSEN ZLATAROV UNIVERSITY
BURGAS, BULGARIA

ANNUAL

Vol. XLIX, BOOK 1, 2020

TECHNICAL AND NATURAL SCIENCES



Assen Zlatarov University

Assen Zlatarov University
Annual, Vol. XLIX, Book 1, 2020
Burgas 8010, Bulgaria
ISSN 2603-3968

**ASSEN ZLATAROV UNIVERSITY
BURGAS, BULGARIA**

ANNUAL

Vol. XLIX, BOOK 1, 2020

TECHNICAL AND NATURAL SCIENCES



BURGAS • 2020

Editor-in-Chief

Prof. Margarita Terzieva, DSc

Co-editors

Assoc. Prof. Penka Peeva, PhD
Assoc. Prof. Liliya Staneva, PhD
Asst. Prof. Ivan Sokolov

Editorial Boards

Section I: Technical Sciences

Prof. Magdalena Mitkova, PhD
Prof. Valentin Nenov, PhD
Prof. Sotir Sotirov, PhD
Prof. Irena Markovska, PhD
Assoc. Prof. Yovka Nikolova, PhD
Assoc. Prof. Dimitrina Kiryakova, PhD
Assoc. Prof. Husein Yemendzhiev, PhD
Prof. A. Baran Dural (Turkey)
Prof. Yordan Nikov (France)

Section II: Natural Sciences

Assoc. Prof. Svetlana Zheleva, PhD
Prof. Nina Sultanova, PhD
Assoc. Prof. Zhechka Mihailova, PhD

Technical Assistant: Iliana Ishmerieva

Reviewers

Prof. Ts. Godzhevargova, DSc
Prof. N. Sultanova, PhD
Assoc. Prof. N. Koleva, DSc
Assoc. Prof. Z. Burieva-Nikolaeva, PhD
Assoc. Prof. I. Vardeva, PhD
Assoc. Prof. D. Yordanov, PhD
Assoc. Prof. D. Dobrudzhaliev, PhD
Assoc. Prof. Y. Tasheva, PhD
Assoc. Prof. L. Staneva, PhD
Assoc. Prof. T. Kostadinov, PhD
Assoc. Prof. I. Belovski, PhD
Chief Asst. Prof. I. Ivanov, PhD
Chief Asst. Prof. G. Yordanova, PhD
Chief Asst. Prof. B. Midyurova, PhD

Section III: Social Sciences and Humanities

Prof. Bratoy Koprinarov, PhD
Assoc. Prof. Todor Palichev, PhD
Prof. Valentina Terentieva (Russia)
Prof. Kiril Chekalov (Russia)
Prof. Marina Yanich (Serbia)
Prof. Zaur Zavrumov (Russia)
Assoc. Prof. Galina Petrova, PhD

Section IV: Public Health and Health Care

Prof. Hristo Bozov, PhD
Assoc. Prof. Antoaneta Grozeva, PhD

VOLUME XLIX (1). CONTENTS

<i>Yana Koleva</i>	Study of Metabolic Activation in Liver and Skin for Similar Compounds of Tazarotene	7
<i>Dimo Hristozov, Zdravka Nikolaeva, Todorka Dimitrova</i>	Osmometer with Natural and Artificial Cylindrical Membranes	13
<i>Irena Markovska, Fila Yovkova, Tsvetan Dimitrov</i>	Color Characteristics of Zircon Pigments Synthesized from Agricultural Waste	18
<i>Nikola Todorov, Emiliya Ivanova, Vladilena Deyanova, Violeta Zheleva</i>	Estimation of Noise Levels on the Territory around the Inorganic Chemistry Building of Prof. Dr Assen Zlatarov University	23
<i>Yordanka Tasheva, Aleksandar Dimitrov, Milena Dimitrova</i>	Removal of Sulfur Compounds by Adsorption	28
<i>Dimitrina Krasteva, Yavor Ivanov, Katya Gabrovska</i>	Counting of CD45+ Cells with Easycounter BC Automatic Fluorescence Microscope Using Anti-CD45 Antibody Conjugate	34
<i>Milka Atanasova, Yavor Ivanov, Katya Gabrovska</i>	Determination of Total Cell Count and Viability of Leukocytes in Blood by Double Fluorescent Staining	40
<i>Desislava Nikolova</i>	A Sustainable Approach to Creating a Biodiesel Supply Chain from Dairy Waste Scum	45
<i>Galina Grigorova</i>	Study of the Macronutrient Composition of Confectionery Offered on the Market and its Physiological Influence	48
<i>Ivaylo Belovski</i>	Ultrasonic Distance Measurement System	52
<i>Radostin Kasarov</i>	Selection of Immersion Transducers for Investigation of Peltier Module	57
<i>Radostin Kasarov, Plamena Atanasova, Sabina Nedkova</i>	Radiological Monitoring of the Working Environment	61
<i>Mladen Proykov</i>	Rehabilitation of Bicycle Lane Lighting	64
<i>Mladen Proykov</i>	Energy Efficiency in the Modern Home	70

<i>Vasil Ivanov</i>	Modeling of Single Phase Inverter System in Simulink Software	75
<i>Yuliyana Petrova</i>	Determining the Area of the Automobile Tire Contact Footprint Using Generalized Nets	79
<i>Yuliyana Petrova, Stanko Pavlov</i>	Finding the Velocity of an Object Situated on a Moving Object when Colliding with a Stationary Object and the Mobile Part Is Ejected	82
<i>Magdalena Dyulgerova, Toncho Boyukov</i>	Developing Competences by Training Students in Automotive Diagnostics	85

STUDY OF METABOLIC ACTIVATION IN LIVER AND SKIN FOR SIMILAR COMPOUNDS OF TAZAROTENE

Yana Koleva
E-mail: yanuriana@abv.bg

ABSTRACT

This study aimed to predict possible hepatic and skin metabolites (in vivo and in vitro rat) and their DNA and protein binding (mechanism of action) of the similar compounds of tazarotene by in silico methods (QSAR Toolbox software). The probable hepatic and skin metabolites of the three similar compounds of tazarotene were predicted by QSAR Toolbox (in vivo, in vitro rat metabolism simulator and skin metabolism simulator). The three similar compounds of tazarotene have from eleven to twenty metabolites for in vivo rat metabolism simulator and five to nine metabolites for in vitro rat metabolism simulator. Metabolites that are active against DNA binding have the following mechanisms of action - Radical mechanism via ROS formation (thiols) and Michael addition on polarised alkynes (polarised alkynes – alkinyl pyridines, pyrazines, pyrimidines, triazines), Michael addition on polarised alkenes (polarised alkenes – sulfinyl), Nucleophilic addition (Addition to carbon-hetero double bonds (ketones)) and Schiff base formation with carbonyl compounds (aldehydes) for protein binding by OASIS. The possible skin metabolites after metabolic activation of the three similar compounds of tazarotene are two. The metabolites are not active against protein binding and their mechanisms of action against DNA binding are Michael addition on polarised alkynes (polarised alkynes – alkinyl pyridines, pyrazines, pyrimidines, triazines) and Michael addition on polarised alkenes (polarised alkenes – sulfinyl).

Keywords: tazarotene, similar compounds, predict, metabolic activation, liver, skin

INTRODUCTION

The importance of retinol (vitamin A) was discovered during World War I and subsequent research showed that its deficiency gives rise to xerosis and follicular hyperkeratosis. The retinoid drug project was launched in 1968 to synthesize compounds similar to vitamin A by chemical manipulation of its molecule to improve clinical efficacy and safety. The use of these substances in therapy dates back some 3,000 years to ancient Egypt, where liver was used to treat endemic night blindness. The modern history of retinoids, however, began in 1909 when an essential factor in the viability of an embryo in the fatty extract of the egg yolk, called vitamin A, was discovered. Retinoids were finally introduced into the treatment of dermatoses including photo aging more than two decades ago [1].

Tazarotene is a novel acetylenic retinoid known to be effective in the topical treatment of psoriasis and acne. Tazarotene is a prodrug, rapidly metabolized to its active metabolite tazarotenic acid. Due to its rigid polyaromatic structure, it does not undergo any isomerization or

conformational change in the skin. Although tazarotene belongs to the retinoid family, it displays a receptor selectivity pattern different from the one found with tretinoin. Tretinoin directly activates all RAR subtypes and indirectly RXRs, whereas tazarotenic acid selectively binds to RAR- β and RAR- γ but not to RXRs. Tazarotenic acid modulates the expression of retinoid-responsive genes, including those that regulate cell proliferation, cell differentiation, and inflammation, corresponding to its binding capacities to various RAR receptors. Tazarotene also down-regulates the abnormal expression of keratinocytes, epidermal growth factor receptor, and hyper proliferative keratins [2-5].

This study aimed to predict possible hepatic and skin metabolites (*in vivo* and *in vitro* rat) and their DNA and protein binding (mechanism of action) of the similar compounds of tazarotene by *in silico* methods (QSAR Toolbox software). The probable hepatic and skin metabolites of the three similar compounds of tazarotene were predicted by QSAR Toolbox (*in vivo*, *in vitro* rat metabolism simulator and skin metabolism simulator). The three similar compounds of tazarotene

have from eleven to twenty metabolites for *in vivo* rat metabolism simulator and five to nine metabolites for *in vitro* rat metabolism simulator. Metabolites that are active against DNA binding have the following mechanisms of action – Radical mechanism via ROS formation (thiols) and Michael addition on polarised alkynes (polarised alkynes – alkinyl pyridines, pyrazines, pyrimidines, triazines), Michael addition on polarised alkenes (polarised alkenes – sulfinyl), Nucleophilic addition (Addition to carbon-hetero double bonds (ketones)) and Schiff base formation with carbonyl compounds (aldehydes) for protein binding by OASIS. The possible skin metabolites after metabolic activation of the three similar compounds of tazarotene are two. The metabolites are not active against protein binding and their mechanisms of action against DNA binding are Michael addition on polarised alkynes (polarised alkynes – alkinyl pyridines, pyrazines, pyrimidines, triazines) and Michael addition on polarised alkenes (polarised alkenes – sulfinyl).

MATERIAL AND METHODS

Compound Data. Tazarotene [6] is a third-generation retinoid with CAS number 118292-40-3 and its similar compounds (6-[(4,4-dimethyl-3,4-dihydro-2H-1-benzothiopyran-6-yl)ethynyl]pyridine-3-carboxylic acid, 6-[(2,2,4,4-tetramethyl-3,4-dihydro-2H-1-benzothiopyran-7-yl)ethynyl]pyridine-3-carboxylic acid, 6-[(4,4-dimethyl-1-oxo-1,2,3,4-tetrahydro-1-benzothiopyran-6-yl)ethynyl]pyridine-3-carboxylic acid), which were defined with CompTox Chemistry Dashboard.

CompTox Chemistry Dashboard. The Dashboard is a freely accessible web-based application and data hub providing access to data associated with chemical substances. It accesses data from nine component databases housing generic data types. The Dashboard also integrates data from other platforms (specifically PubChem and PubMed) via web services and visualization widgets. The Dashboard represents a first step in building a comprehensive chemical substance-centric informatics architecture to provide flexible access to data, models and analysis tools in support of EPA's research programs [7, 8].

Similar molecules. The similar molecules tab shows the results of a structural similarity search, underpinned by a Tanimoto similarity calculated using the Bingo Molecular Search Cartridge (with the associated Indigo fingerprints) [9]. The search displays up to 50 of the topmost similar

molecules above a Tanimoto similarity metric of 0.8. The view also displays a selection of experimental and predicted chemical properties to help illustrate the consistency and concordance of these attributes within the identified set of structurally related molecules [7, 8].

Organisation for economic co-operation and development (OECD) (Q)SAR toolbox (version 4.3). (Quantitative) Structure-Activity Relationships [(Q)SARs] are methods for estimating properties of a chemical from its molecular structure and have the potential to provide information on the hazards of chemicals, while reducing time, monetary costs and animal testing currently needed. To facilitate practical application of (Q)SAR approaches in regulatory contexts by governments and industry and to improve their regulatory acceptance, the OECD (Q)SAR project has developed various outcomes such as the principles for the validation of (Q)SAR models, guidance documents as well as the QSAR Toolbox [10].

Liver metabolism (observed and simulator) – *in vivo* and *in vitro* for rat:

Observed rat *in vivo* metabolism. The observed (documented) metabolic pathways for 647 chemicals, extracted from the scientific literature, and associated with the *in vivo* biotransformations of xenobiotic chemicals in rodents (mostly rats) are stored in a database format that allows easy computer access to the metabolism information. This database includes structurally different chemicals of various functionalities such as aliphatic and aromatic hydrocarbons, halogenated hydrocarbons, alcohols and phenols, carbonyl compounds, carboxylic acids and esters, nitro compounds, amines, organic sulfides, heterocyclic and, mostly, multi-functional chemicals etc [10].

***In vivo* rat metabolism simulator.** The current *in vivo* rat liver metabolic simulator (transformation table) represents electronically designed set of 671 structurally generalized, hierarchically arranged abiotic and enzymatic transformation reactions, which are characteristic for the metabolism for *in vivo* experimental systems such as rodent (mostly rat). The principal applicability of this simulator is associated with the reproduction as well as the prediction of the metabolic activation reactions and pathways of xenobiotic chemicals, which may elicit *in vivo* genotoxicity effects [10].

Observed rat liver S9 metabolism. The documented metabolic pathways for 261 chemicals observed with the use of *in vitro* experimental

systems such as rodent (mostly rat) liver microsomes and S9 fraction are stored in a database format that allows easy computer access to the metabolism information. This database includes structurally different chemicals of various functionalities and fields of application such as aliphatic and aromatic hydrocarbons, halogenated hydrocarbons, carboxylic acids and esters nitro compounds, amines, heterocyclic and multi-functional chemicals, etc [10].

Rat liver S9 metabolism simulator. The current *in vitro* rat liver metabolic simulator (transformation table) represents electronically designed set of 551 structurally generalised, hierarchically arranged biotransformation reactions, which are characteristic for the metabolism for *in vitro* experimental systems such as rodent (mostly rat) liver microsomes and S9 fraction. The principal applicability of this simulator is associated with the reproduction as well as the prediction of the metabolic activation reactions and pathways of xenobiotic chemicals, which may elicit *in vitro* genotoxicity effects such as bacterial mutagenicity and chromosomal aberrations [10].

DNA binding by OASIS. The profiler is based on Ames Mutagenicity model part of OASIS TIMES system. The profiler consists of 85 structural alerts responsible for interaction with DNA analyzed in Ames Mutagenicity model. The scope of the profiler is to investigate presence of alerts within target molecules which may interact with DNA [10].

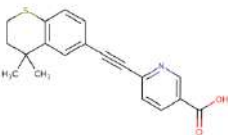
Protein binding by OASIS. The scope of the profiler is to investigate presence of alerts within

target molecules responsible for interaction with proteins. The list of 112 structural alerts has been separated into 11 mechanistic domains. Each of the mechanistic domains has been separated into more than 2 mechanistic alerts. The profiling result outcome assigns a target to the corresponding structural alert, mechanistic alerts and domain [10].

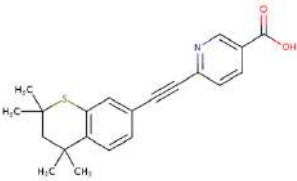
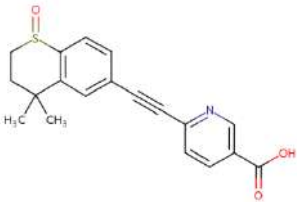
RESULTS AND DISCUSSIONS

The three similar tazarotene structures with a Tanimoto similarity metric of 0.8 (from 0.92 to 0.84) by the CompTox Chemistry Dashboard were predicted for hepatic and skin metabolic activation (*in vivo* and *in vitro* rat) and their DNA and protein binding (mechanism of action) by the OECD QSAR Toolbox software (version 4.3). The parent structures of the three similar compounds (without the third compound) of tazarotene can bind to DNA (Radical mechanism via ROS formation (thiols)) and they can bind to protein (Michael addition on polarised alkynes (polarised alkynes – alkynyl pyridines, pyrazines, pyrimidines, triazines) and Michael addition on polarised alkenes – sulfinyls) and experimental metabolic pathways of activation were not observed for rat *in vivo* and *in vitro*. In the liver metabolism simulator (*in vivo* rat), from eleven to twenty metabolites were predicted. The results of metabolic activation of the three similar compounds of tazarotene (*in vivo* rat metabolism simulator) and their protein and DNA binding are presented in Table 1.

Table 1. Possible hepatic metabolic activation of the similar compounds of tazarotene by QSAR Toolbox (*in vivo* rat metabolism simulator)

Number/Structure/Name of compound	Metabolite/s	DNA binding by OASIS (mechanism of reaction)	Protein binding by OASIS (mechanism of reaction)
1) 	19	No alert found – 9 metabolites; Radical (Radical mechanism via ROS formation (thiols) – 10 metabolites	Michael addition on polarised alkynes (polarised alkynes – alkynyl pyridines, pyrazines, pyrimidines, triazines) – 19 metabolites; Michael addition on polarised alkenes (polarised alkenes – sulfinyl) – 4 metabolites; Nucleophilic addition (Addition to carbon-hetero double bonds (ketones)) – 2 metabolites; Schiff base formation with

6-[(4,4-Dimethyl-3,4-dihydro-2H-1-benzothiopyran-6-yl)ethynyl]pyridine-3-carboxylic acid

2)	11	No alert found – 6 metabolites; Radical (Radical mechanism via ROS formation (thiols) – 5 metabolites)	carbonyl compounds (aldehydes) – 1 metabolite. Michael addition on polarised alkynes (polarised alkynes – alkinyl pyridines, pyrazines, pyrimidines, triazines) – 11 metabolites; Michael addition on polarised alkenes (polarised alkenes – sulfinyl) – 2 metabolites; Nucleophilic addition (Addition to carbon-hetero double bonds (ketones)) – 2 metabolites; Schiff base formation with carbonyl compounds (aldehydes) – 1 metabolite.
			
6-[(2,2,4,4-Tetramethyl-3,4-dihydro-2H-1-benzothiopyran-7-yl)ethynyl]pyridine-3-carboxylic acid			
3)	20	No alert found – 16 metabolites; Radical (Radical mechanism via ROS formation (thiols)) – 4 metabolites	Michael addition on polarised alkynes (polarised alkynes – alkinyl pyridines, pyrazines, pyrimidines, triazines) – 20 metabolites; Michael addition on polarised alkenes (polarised alkenes – sulfinyl) – 8 metabolites; Nucleophilic addition (Addition to carbon-hetero double bonds (ketones)) – 3 metabolites.
			
6-[(4,4-Dimethyl-1-oxo-1,2,3,4-tetrahydro-1-benzothiopyran-6-yl)ethynyl]pyridine-3-carboxylic acid			

Active and inactive DNA binding metabolites were predicted for the three similar tazarotene compounds. Active metabolites have the following mechanism of action (Radical mechanism via ROS formation (thiols)) by DNA binding. Metabolites have the following mechanisms of action (Michael addition on polarised alkynes (polarised alkynes – alkinyl pyridines, pyrazines, pyrimidines, triazines), Michael addition on po-

larised alkenes (polarised alkenes – sulfinyl), Nucleophilic addition (Addition to carbon-hetero double bonds (ketones)), Schiff base formation with carbonyl compounds (aldehydes)) by protein binding.

The results of metabolic activation of the three similar compounds of tazarotene (*in vitro* rat metabolism simulator) and their protein and DNA binding are presented in Table 2.

Table 2. Possible hepatic metabolic activation of the similar compounds of tazarotene by QSAR Toolbox (*in vitro* rat metabolism simulator)

Number/ Name of compound	Metabolite/s	DNA binding by OASIS (mechanism of reaction)	Protein binding by OASIS (mechanism of reaction)
1) 6-[(4,4-Dimethyl-3,4-dihydro-2H-1-benzothiopyran-6-yl)ethynyl]pyridine-3-carboxylic acid	5	No alert found – 6 metabolites; Radical (Radical mechanism via ROS formation (thiols) – 5 metabolites)	Michael addition on polarised alkynes (polarised alkynes – alkinyl pyridines, pyrazines, pyrimidines, triazines) – 11 metabolites;

				Michael addition on polarised alkenes (polarised alkenes – sulfinyl) – 2 metabolites; Nucleophilic addition (Addition to carbon-hetero double bonds (ketones)) – 1 metabolite;
2)	6-[(2,2,4,4-Tetramethyl-3,4-dihydro-2H-1-benzothiopyran-7-yl)ethynyl]pyridine-3-carboxylic acid	9	No alert found – 5 metabolites; Radical (Radical mechanism via ROS formation (thiols) – 4 metabolites	Michael addition on polarised alkynes (polarised alkynes – alkynyl pyridines, pyrazines, pyrimidines, triazines) – 9 metabolites; Michael addition on polarised alkenes (polarised alkenes – sulfinyl) – 2 metabolites; Nucleophilic addition (Addition to carbon-hetero double bonds (ketones)) – 1 metabolite;
3)	6-[(4,4-Dimethyl-1-oxo-1,2,3,4-tetrahydro-1-benzothiopyran-6-yl)ethynyl]pyridine-3-carboxylic acid	9	No alert found	Michael addition on polarised alkynes (polarised alkynes – alkynyl pyridines, pyrazines, pyrimidines, triazines) – 9 metabolites; Michael addition on polarised alkenes (polarised alkenes – sulfinyl) – 4 metabolites; Nucleophilic addition (Addition to carbon-hetero double bonds (ketones)) – 1 metabolite;

Metabolites have the following mechanism of action (Radical mechanism via ROS formation (thiols)) by DNA binding. Metabolites have the following mechanisms of action (Michael addition on polarised alkynes (polarised alkynes – alkynyl pyridines, pyrazines, pyrimidines, triazines), Michael addition on polarised alkenes (polarised alkenes – sulfinyl), Nucleophilic addition

(Addition to carbon-hetero double bonds (ketones)), Schiff base formation with carbonyl compounds (aldehydes)) by protein binding.

The results of metabolic activation of the three similar compounds of tazarotene (skin metabolism simulator) and their protein and DNA binding are presented in Table 3.

Table 3. Probable skin metabolic activation of the similar compounds of tazarotene by QSAR Toolbox

Number/ Name of compound	Metabolite/s	DNA binding by OASIS (mechanism of reaction)	Protein binding by OASIS (mechanism of reaction)
1)6-[(4,4-Dimethyl-3,4-dihydro-2H-1-benzothiopyran-6-yl)ethynyl]pyridine-3-carboxylic acid	2	No alert found	Michael addition on polarised alkynes (polarised alkynes – alkynyl pyridines, pyrazines, pyrimidines, triazines) – 2 metabolites; Michael addition on polarised

2) 6-[(2,2,4,4-Tetramethyl-3,4-dihydro-2H-1-benzothiopyran-7-yl)ethynyl]pyridine-3-carboxylic acid	2	No alert found	alkenes (polarised alkenes – sulfinyl) – 1 metabolite; Michael addition on polarised alkynes (polarised alkynes – alkynyl pyridines, pyrazines, pyrimidines, triazines) – 2 metabolites; Michael addition on polarised alkenes (polarised alkenes – sulfinyl) – 1 metabolite;
3) 6-[(4,4-Dimethyl-1-oxo-1,2,3,4-tetrahydro-1-benzothiopyran-6-yl)ethynyl]pyridine-3-carboxylic acid	1	No alert found	Michael addition on polarised alkynes (polarised alkynes – alkynyl pyridines, pyrazines, pyrimidines, triazines) – 1 metabolite;

Metabolites for the three similar compounds of tazarotene are not active by DNA binding. Metabolites have the following mechanisms of action (Michael addition on polarised alkynes (polarised alkynes – alkynyl pyridines, pyrazines, pyrimidines, triazines) and Michael addition on polarised alkenes (polarised alkenes – sulfinyl)) by protein binding.

CONCLUSIONS

The three similar compounds of tazarotene with a Tanimoto similarity metric of 0.8 by the CompTox Chemistry Dashboard were predicted for hepatic and skin metabolic activation by QSAR Toolbox (*in vivo*, *in vitro* rat metabolism simulator and skin metabolism simulator). Some of predicted metabolites (active) by QSAR Toolbox have electrophilic character and they may react with nucleophilic sites in DNA and also bind to protein. The possible adverse effects of active metabolites on the three similar compounds of tazarotene have the following mechanisms of action (Michael addition on polarised alkynes (polarised alkynes – alkynyl pyridines, pyrazines, pyrimidines, triazines), Michael addition on polarised alkenes (polarised alkenes – sulfinyl), Nucleophilic addition (Addition to carbon-hetero double bonds (ketones)) and Schiff base formation with carbonyl compounds (aldehydes)) by protein binding and Radical mechanism via ROS formation (thiols) by DNA binding.

ACKNOWLEDGEMENTS

This study was financially supported by Burgas University through the Scientific Research Sector – Project number 434/2019.

REFERENCES

1. Ramos-E-Silva, M., D.M. Hexsel, M.S. Rutowitsch, et al. *Clin. Dermatol.*, **19**, 2001, p.460–466.
2. Nagpal, S., J. Athanikar, R.A. Chandraratna. *J. Biol. Chem.*, **270**, 1995, p.923–7.
3. Chandraratna, R.A. *Br. J. Dermatol.*, **135**(49), 1996, p.18–25.
4. DiSepio, D., C. Ghosn, R.L. Eckert, et al. *Proc. Natl. Acad. Sci. U S A*, **95**, 1998, p.14811–15.
5. Roeder, A., M. Schaller, M. Schäfer-Korting, et al. *Skin Pharmacol. Physiol.*, **17**, 2004, 111–18.
6. ChemIDplus Advanced, URL: <https://chem.nlm.nih.gov/chemidplus/>
7. USA EPA, CompTox Chemistry Dashboard, URL: <https://comptox.epa.gov/dashboard/>
8. Williams, A.J., C.M.Grulke, J. Edwards, A.D. McEachran, K. Mansouri, N.C. Baker, G. Patlewicz, I. Shah, J.F. Wambaugh, R.S. Judson & A.M. Richard. *J. Cheminformatics*, **9**, 2017, 61.
9. „Epam“ Bingo PostgreSQL cartridge, URL: <http://lifescience.opensource.epam.com/bingo/bingo-postgres.html>.
10. The OECD (Q)SAR Toolbox: <https://www.oecd.org/chemicalsafety/risk-assessment/oecd-qsar-toolbox.htm>.

OSMOMETER WITH NATURAL AND ARTIFICIAL CYLINDRICAL MEMBRANES

Dimo Hristozov, Zdravka Nikolaeva, Todorka Dimitrova

E-mail: z.v.burieva@gmail.com

ABSTRACT

The present paper describes osmometers with natural and artificial membranes of osmotic cells. The membranes are cylindrical because this form is closest to the shape of the protoplasmic sacs of cells in living organisms. Quantitative results are given for the osmotic pressure depending on the membrane area, which for a cylindrical shape is much larger than the area of the flat membranes in the classical osmometers. An experiment was simulated to find the magnitude of the osmotic pressure when the membrane is healthy and when it is damaged in living organisms, as in some diseases.

Key words: diffusion, osmosis, cell membrane, osmotic pressure, regression analysis, coefficient of determination, Fisher criterion

INTRODUCTION

Let a clean solvent and a solution with a sharp boundary between them be placed in a vessel. Such is, for example, the very popular diffusion experiment, which is easily done with a water solvent and a solution of bluestone and water. The heavier solution is located at the bottom of this vessel and the solvent is above the solution. Over time (several days) this sharp limit is blurred: copper sulphate particles penetrate the solvent (water). This mass transfer, called diffusion [1 - 5], ends when equilibrium is reached, when the solute is distributed evenly over the entire volume of the total vessel. The same happens when two solutions with different concentrations are adjacent – a diffusion of particles of the solute with a higher concentration to a weaker solution takes place.

Fick's law of the diffusion:

$$\Delta m = D \cdot \frac{\Delta C}{\Delta x} \cdot \Delta S \cdot \Delta t \quad (1)$$

where: Δm is the mass of substance transferred for the time interval Δt , through an area ΔS , located perpendicular to the axis Ox , along which there is a change in the concentration C in the solution (g/cm^3), $\Delta C/\Delta x$ is concentration gradient; D is diffusion coefficient.

In diffusion, the volume of the solution increases by analogy with pressurized gas in a cylinder with a piston that can perform work (the piston is movable). The solute must also exert pressure at the interface which separates the pure solvent from the solution or two solutions with different concentrations C . The difference ΔC of

the concentrations in this case plays the same role as the pressure difference in gases. The semi-permeable barrier allows the particles of the solvent (water) to pass and retains the particles of the solute (sugar). If the membrane is fixed to the vessel with the two substances, as with osmometers, then the height h of the solution moves - the solution increases in volume. This penetration of the solvent through the membrane into the solution is unilateral diffusion and is called osmosis. The pressure that the solute exerts on the membrane is called osmotic pressure [6 - 8].

The increase in the level h of the solution continues until a hydrostatic pressure is equal to the established osmotic pressure:

$$p_{osm} = \rho g h \quad (2)$$

where ρ is the density of the solution and $g = 9.81 \text{ m/s}^2$ is the ground acceleration.

Diluted aqueous solutions are considered to have a density $\rho = 1.10^3 \text{ kg/m}^3$ (density of water at room temperature). In formula (2), the quantities ρ and g are constants, and h is the maximum height that the solution has reached and it no longer changes. Therefore, in osmosis experiments, h is measured as a function of time t until a plateau is reached (h constant). It should also be noted that the similarity in the behaviour of the ideal gas and of the dilute solution is most evident from the following:

The equation of state of an ideal gas (Clapeyron-Mendeleev) is a relationship between three variables: pressure p , volume V and temperature T :

$$pV = nRT \quad (3)$$

In (3) R is the universal gas constant and n is the amount of substance. The equation for the state of osmotic pressure, or Van Hoff's law, is:

$$p_{\text{osm}} = CRT \quad (4)$$

with this difference, instead of the n/V ratio, the molar concentration C is introduced in it.

EXPERIMENT

Two experiments were performed: with natural and artificial membranes.

Osmometer with natural membrane

Fig. 1 shows an osmometer with a natural membrane (carrot with a cylindrical shape). This form is closest to the shape of the protoplasmic sacs of cells in living organisms.

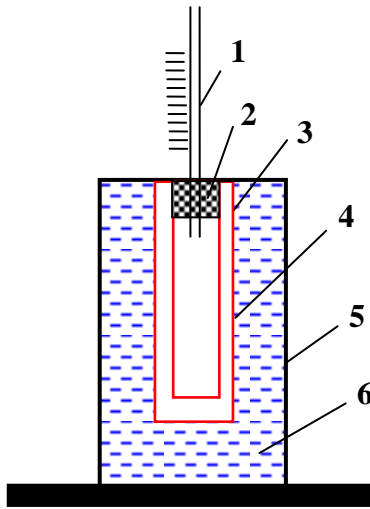


Fig. 1 Vertical projection of an osmometer carrot with a cylindrical cavity in it.

The osmometer has two modules: the first module is the osmotic cell, which consists of a hollowed-out cylindrical cavity 3 in a carrot 4. The second module is a glass tube 1 placed in a stopper 2. The plug-tube module is placed in the mouth of the cylindrical cavity filled with solution. The tube with the cap and the cap to the carrot are additionally strengthened with the help of waterproof plastic glue. Thus assembled together, the two modules are immersed in a common vessel (cup) 5 filled with water 6. The height h of the solution on the glass tube is read by means of a scale. To reduce evaporation, the vessel 5 and the tube - with the opening at the top, are covered. Finally, the "stopper-tube" element is easily separated for the next experiment.

Osmometer with cylindrical artificial (plastic) membrane

This osmometer is analogous to that described in Fig. 1, the carrot being replaced by a thin plastic membrane produced by the Koch company. The first experiment was with a normal, intact osmotic cell membrane. The second experiment was performed after half the area of the plastic membrane had been damaged.

To calculate the height of the solution rise along the capillary tube as a function of time in minutes, regression equations of degree 4 for the natural membrane (carrot) and of degree 6 for the artificial cylindrical membrane are derived:

$$y = b + a_1 \cdot x + a_2 \cdot x^2 + a_3 \cdot x^3 + a_4 \cdot x^4 \quad (5)$$

$$y = b + a_1 \cdot x + a_2 \cdot x^2 + a_3 \cdot x^3 + a_4 \cdot x^4 + a_5 \cdot x^5 + a_6 \cdot x^6 \quad (6)$$

where y is the lifting height of the solution, mm; x is time, min. The coefficients b and a_1, a_2, \dots, a_6 involved in equations (5) and (6) are determined by regression analysis of experimental data [9, 10].

For estimation of the quality of the regression models, the coefficient of determination R^2 was used to determine the degree of linear dependence between the regressors involved in the model and the initial value. The significance of R^2 was checked using the Fisher criterion

$$F = \frac{R^2}{(1 - R^2)} \cdot \frac{(N_1 - k)}{(k - 1)} \quad (7)$$

where: k is the number of the estimated parameters of the model; N_1 is the size of the sample of experimental data. The Fisher criterion has degrees of freedom $v_1 = k - 1$, $v_2 = N_1 - k$.

At $F > F(\alpha, v_1, v_2) = F_{\text{crit}}$, the value of R^2 is considered to be significant and it can be used for estimation of the model adequacy.

The higher the calculated value of R^2 , the more reliable the regression model is.

RESULTS AND DISCUSSION

Osmometers with natural and artificial cylindrical membranes of osmotic cells were described. The following results were obtained:

Osmometer with natural membrane

Table 1 shows the results obtained from the experiment with the described osmometer.

Table 1. Experimental data on lift height h and time t .

h , mm	t , min	h , mm	t , min	h , mm	t , min
1.5	50	24	470	82	685
2.0	100	32	500	87	725
2.5	150	40	525	89	730
5.0	200	52	550	90	770
7.4	250	59	580	90	775
10.0	310	69	640	90	800
15.0	375	77	670	90	825

In the experiment, the radius of the hollow cavity is $r = 5$ mm, its height is $h = 100$ mm, and the thickness of the cylindrical part of the carrot, which acts as a membrane, is 3 mm. The surrounding cylindrical surface of the carrot and the flat lower base (circle) form a total area of 64.6 cm^2 . The concentration of the aqueous sugar solution is 0.25 g/cm^3 .

The type of the derived regression equation is:

$$y = 2.1427 + 0.8963 \cdot x - 0.002892 \cdot x^2 + 6.4 \cdot 10^{-6} \cdot x^3 - 6.456 \cdot 10^{-9} \cdot x^4 \quad (8)$$

OCTOMETER WITH NATURAL MEMBRANE

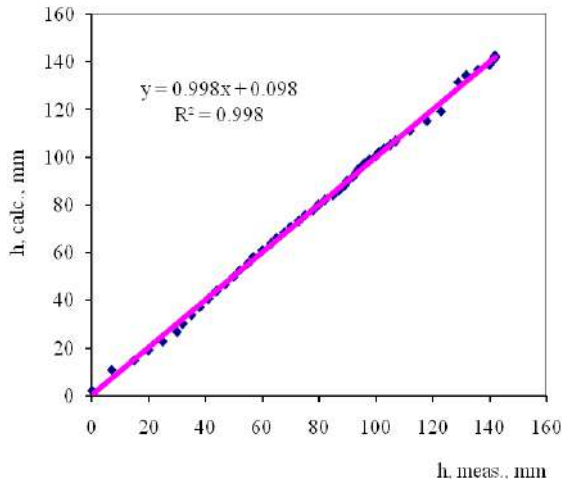


Fig. 2 Measured (h , meas., mm) and predicted (h , calc., mm) by model (8) values of lift height.

The measured (h , meas., mm) and predicted (h , calc., mm) by model (8) values of the height of the liquid rise in the capillary are presented in Fig. 2.

Fig. 2 shows that the value of the coefficient of determination is very close to 1 ($R^2 = 0.95$), in order to assume that the model is characterized by good quality and reliability.

Equation (8) can be used to calculate the lift height for each intermediate time value. Table 1 shows that the maximum height of the liquid in the capillary is 90 mm. An osmotic pressure of 883 Pa corresponds to this height.

Osmometer with cylindrical artificial (plastic) membrane

In this osmometer the carrot has been replaced with a thin plastic membrane from Koch. The cylindrical membrane has a radius $r = 17$ mm and a height of the osmotic cell of 90 mm. The concentration of the sugar solution with water that fills the osmotic cell is $C = 0.019 \text{ g/cm}^3$.

The first experiment carried out with the plastic osmometer was with a normal, intact membrane of the osmotic cell (the first graph in Fig. 3). It was obtained that $h_{\max} = 300$ mm along the glass tube.

Therefore:

$$p_{osm} = \rho gh = 2943 \text{ Pa},$$

which is reached after 40 hours.

The second experiment with the same osmometer was performed after half the area of the plastic membrane was damaged. This damage was achieved with the help of plastic synthetic Bison glue. When the glue dried, the pores of the coated half of the membrane were already clogged. This procedure causes damage to the protoplasmic sacs in diseased living organisms in (second graph in Fig. 3). It was obtained that $h_{\max} = 92$ mm along the glass tube.

Therefore:

$$p_{osm} = \rho gh = 902.5 \text{ Pa},$$

which is reached after 78 hours.

The derived regression equations, respectively for experiments 1 and 2 have the form:

$$y = -0.0175 + 5.9880 \cdot x - 1.2241 \cdot x^2 + 0.1756 \cdot x^3 - 0.01044 \cdot x^4 + \quad (9)$$

$$+ 0.000276 \cdot x^5 - 2.6 \cdot 10^{-6} \cdot x^6$$

$$y = -0.5911 + 2.1317 \cdot x - 0.1267 \cdot x^2 + 0.005083 \cdot x^3 - 9.2 \cdot 10^{-5} \cdot x^4 + \quad (10)$$

$$+ 8.16 \cdot 10^{-7} \cdot x^5 - 2.9 \cdot 10^{-9} \cdot x^6$$

OSMOMETER WITH ARTIFICIAL MEMBRANE

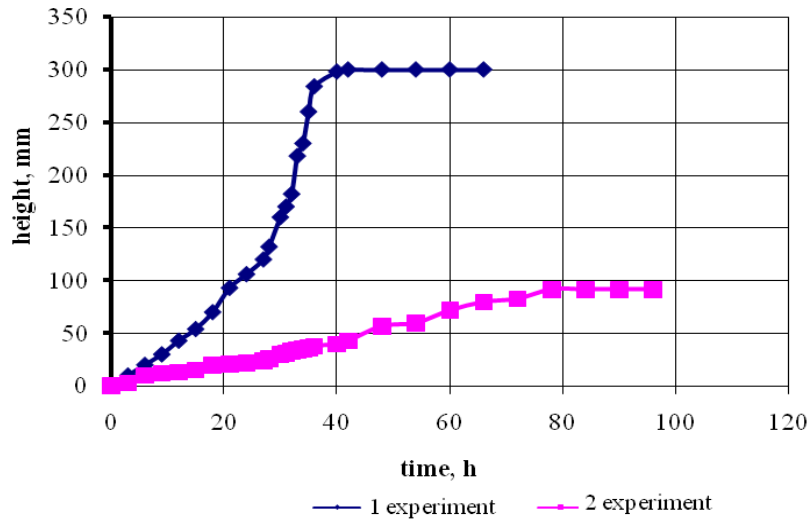


Fig. 3. Height (h , mm) of the liquid in the glass tube as a function of time (t , h) in an experiment with a plastic membrane.

The measured (h , meas., mm) and predicted (h , calc., mm) by models (9) and (10) values of the height of the rise of the liquid in the capillary are presented in Fig. 4 and 5, respectively for plastic membrane experiments 1 and 2.

Equations (9) and (10) can be used to calculate the lift height for each intermediate time value.

1 experiment, ARTIFICIAL MEMBRANE

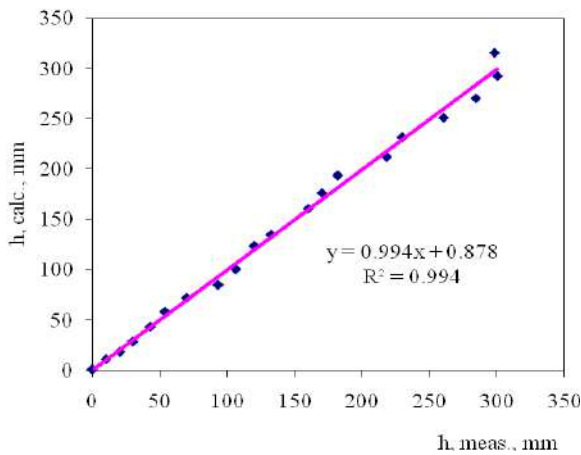


Fig. 4. Height (h , mm) of the liquid in the glass tube as a function of time (t , h) in 1st experiment with a plastic membrane.

The figures show that the value of the coefficient of determination is very close to 1 ($R^2 > 0.99$), in order to assume that the models are characterized by good quality and reliability.

2 experiment, ARTIFICIAL MEMBRANE

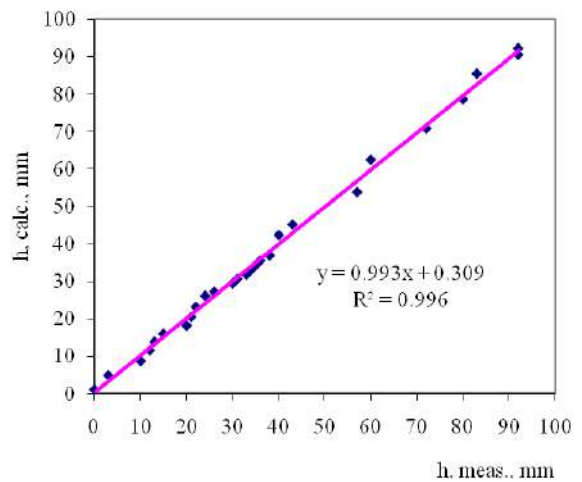


Fig. 5. Height (h , mm) of the liquid in the glass tube as a function of time (t , h) in 2nd experiment with a plastic membrane.

Therefore, damage to the membrane, on the one hand, reduces the magnitude of the osmotic pressure, and on the other, this pressure is obtained after a longer period of time (78 hours).

CONCLUSIONS

From the above results and discussion, it is concluded that:

Osmometers with natural and artificial cylindrical membranes of osmotic cells are described. The cylindrical form is closest to the shape of the protoplasmic sacs of cells in living organisms.

Quantitative results for the osmotic pressure were obtained. In the case of the osmometer with a natural membrane (carrot), the maximum height of lifting of the liquid on the capillary is 90 mm for a time of 550 min and the osmotic pressure of 883 Pa corresponds to this height. The concentration of the aqueous sugar solution is 0.25 g/cm^3 .

Two experiments were performed with an osmometer with an artificial (plastic) membrane. The first experiment with the plastic osmometer was with a normal, intact membrane of the osmotic cell. A maximum lift height of 300 mm is obtained along the glass tube, the osmotic pressure being 2943 Pa, which is reached after 40 hours.

The second experiment with the same osmometer was performed after half the area of the plastic membrane was damaged. This procedure causes damage to the protoplasmic sacs in living organisms during disease. A maximum height of 92 mm is obtained, and an osmotic pressure of 902.5 Pa, which is reached after 78 hours.

To calculate the height of the solution rise along the capillary tube as a function of time in minutes, regression equations of degree 4 for the natural membrane (carrot) and of degree 6 for the artificial cylindrical membrane are derived. The values of the height of the rise of the liquid along the capillary, measured and predicted by the models, are graphically presented. The figures show that the value of the coefficient of determination is very close to 1 ($R^2 > 0.99$), in order to assume that the models are characterized by good quality and reliability. Using the derived regression equations, the elevation height can be calculated for each time value.

The experiments with the artificial membrane show that damage to the membrane, on the one

hand, reduces the magnitude of the osmotic pressure, and on the other, this pressure is obtained after more time (78 hours). And the osmotic pressure is associated with water supply and nutrient solutions in plant and animal organisms!

REFERENCES

1. Serway, R., J. Beicher, J. Jewett. *Physics for Scientists and Engineers*. North Carolina State University and California State Polytechnic University, Pomona, (2000).
2. Nikolaeva, Z., N. Sultanova, St. Kasarova, Z. Dimitrova. *Laboratory Experiments in Physics*. University "Prof. Dr Assen Zlatarov" Publishing House, Burgas, (2015).
3. Plachkova, St., M. Misheva. *Physics with examples from biology*. Kliment Ohridski University Publishing House, Sofia, (2004).
4. Hobson A., *The Physics Teacher*. Vol. **42**, February, (2004).
5. Marinov, M. *Medical Physics*. Union of Physicists in Bulgaria, Sofia, (2007).
6. Arnaudova, P. *A small medical encyclopedia for everyone*. East-West Publishing House, Sofia, (2013).
7. Kasarova, St., N. Sultanova, R. Kasarov, I. Nikolov. *Properties of polymeric materials for optical systems*, Proceedings SPIE, Vol. **11047**, (2019), 110471I-1–110471I-8.
8. Kasarova, St., N. Sultanova, I. Nikolov, R. Kasarov. *Optical polymers in remote imaging devices*, SES 2017 Proceedings, (2017), 354-359.
9. Petrov, N., L. Staneva, Y. Petrov, S. Edrev. *Study on the Determination of the Technical Resources for Toothed Gear Mechanisms of Marine and Aviation Communication Systems*. International Journal of Scientific and Engineering Research (IJSER), **9** (6), June (2018), 1602-1605.
10. Edrev, St., E. Bogoslovov. *Analytical and Experimental Calculation of the Moment of Inertia of the Oberbeck's Pendulum*. Annual Assen Zlatarov University, Burgas, **XLV** (1), (2016), 32-36.

COLOR CHARACTERISTICS OF ZIRCON PIGMENTS SYNTHESIZED FROM AGRICULTURAL WASTE

Irena Markovska, Fila Yovkova, Tsvetan Dimitrov
E-mail: imarkovska@btu.bg

ABSTRACT

The aim of the present paper is to study the possibilities to synthesize zirconium ceramic pigments from pure and waste materials with respect to their possible use as pigments in the silicate industry. Zircon pigments with main phase $ZrSiO_4$ are synthesized by heating a mixture of ZrO_2 , SiO_2 , chromophore ion and mineralizer. The raw materials for the synthesis of pigments are ZrO_2 , Fe_2O_3 , NH_4VO_3 , Co_3O_4 , Cr_2O_3 , MnO_2 , ash from rice husk as a source of SiO_2 , and NH_4Cl as a mineralizer. The following elements have been added as colorants (chromophores): V, Fe, Cr, Co and Mn. The optimal parameters of synthesis are determined and the color characteristics of the synthesized zirconium ceramic pigments are measured with the CIELab system of color measurement.

Key words: zircon pigments, rice husk, solid-state sintering, CIELab color measurement

INTRODUCTION

In recent years the synthesis of new kinds of ceramic pigments has been based on the growing importance of ceramic materials, powders and pigments, as well as the diverse possibilities for obtaining them from both traditional and waste materials, as well as their potentially wide practical use in the ceramic and glass industries, e.g. coloring of ceramic tiles and other articles, mosaic tiles, coloring of glass to obtain various types of colored glasses, etc. Their color palette constantly increases with respect to the production of over-glaze paints and coloring of glazes for the ceramic industry, e.g. for tile production [1].

A number of researchers [2-3] focused their efforts on the mechanism of formation of zircon pigments, the role of the mineralizers, as well as the possibility to use various raw materials in the process. The selenites of the rare earth elements turned out to be quite suitable for the synthesis of zircon pigments.

Rice husks, which are an agricultural waste product, contain high percentage of SiO_2 . The presence of a high content of silica in rice husk ash has been known since 1938, and extensive literature studies have highlighted the high use of ash as a substitute for pure silica [4].

Various studies have shown the effectiveness of using rice husks as a precursor to silica, especially for the production of ceramic materials. Prasad et al. [5] studied the effect of quartz replacement in ceramic vessels and found that

silicon dioxide from the rice husk leads to a decrease in ripening temperature and an increase in strength.

Andreola et al. [4, 6] have investigated the use of silicon dioxide from rice husks for the synthesis of ceramic pigments. They have found more stable pigments and a higher intensity of red color compared to pure quartz pigments, while Sobrosa et al. [7] have reported that glass-ceramics produced with silica from rice husks has higher values of flexural strength and higher Mohs hardness in comparison with commercial glass-ceramics.

The aim of the present work is to synthesize zirconium ceramic pigments from pure and waste materials and study the possibilities for their application in the silicate industry.

EXPERIMENT

Methods

The zircon ceramic pigments were studied mainly by infrared spectroscopy (FT-IR) as well as with the CIELab system of color measurement.

Color Measurement. The color determination of the pigments is carried out spectrally with a tintometer of Lovibond Tintometer RT 100 Color.

The FT-IR studies were performed on a Tensor 27 Fourier infrared spectrophotometer FTIR (Bruker, Germany) in the $400 - 4000 \text{ cm}^{-1}$ interval at a resolution of 1 cm^{-1} . The measurements

were carried out at room temperature. The sample (0.3 mg) was tableted with KBr (100 mg) at a pressure of 2-4 atm. The DTA experiments were performed on an apparatus for complex thermal analysis (STA 449F3 Jupiter), NETZSCH, Germany by heating to 1100°C at a rate of 10°C min⁻¹.

Materials

Zircon pigments with a main crystalline phase zircon ZrO₂.SiO₂ were prepared by the solid phase sintering method. Both pure and waste raw materials were used as raw materials. The basic materials for the synthesis of zircon pigments were very finely ground chemically pure chemicals and waste raw materials. Pure ZrO₂ was used as the source of ZrO₂, and ash from oxidized rice husk was used as the source of SiO₂. The following elements were added as chromophores: V, Fe, Cr, Co and Mn. For this purpose, the following raw materials were used: Fe₂O₃, NH₄VO₃, Co₃O₄, Cr₂O₃ and MnO₂. The mineralizer used was NH₄Cl. The mineralizers play an important role in decreasing the temperature of the process. The compositions are presented in Table 1.

Table 1. Composition of the samples

№ of sample	ZrO ₂	R H A	NH ₄ Cl	Fe	V	Co	Cr	Mn
ZR1	+	+	+	+				
ZR2	+	+	+		+			
ZR3	+	+	+			+		
ZR5	+	+	+				+	
ZR6	+	+	+					+
ZR7	+	+	+	+				
ZR8	+	+	+		+			
ZR9	+	+	+			+		
ZR11	+	+	+				+	
ZR12	+	+	+					+

Compositions of the blends

The pigments were synthesized by the technology of solid phase sintering. A number of mixtures were prepared and a series of samples were synthesized at different combinations of raw materials. Rice husk ash was used as a source of SiO₂. Then 6% mineralizer (NH₄Cl) was added.

An important issue in the synthesis of pigments is the precise dosing of the different components and compliance with the recipe speci-

fied. The quantities of materials from the recipe for 100g blend were weighed with a precision of 0.1g, then they were dry mixed and homogenized in a PULVERISETTE-6 planetary mill, produced by FRITSCH.

The sintering was carried out in a laboratory muffle furnace at heating rate of 300-400°C/h in air, in closed porcelain crucibles with 3 h isothermal period at the final temperature. The pigments were sintered at 1000°C, 1100°C and 1200°C.

RESULTS AND DISCUSSION

Figure 1 presents photos of the starting composition as well as the synthesized pigments.



Fig. 1 Initial mixtures and synthesized pigments: in each composition the mixture is on the left, and the pigment synthesized at 1200°C is on the right

Color measurement

Color is one of the most important indicators of pigment quality. Colored substances absorb and convert light rays of a certain wavelength into the visible portion of the spectrum due to their atomic structure. The CIELab system defines the colors not only of ceramic pigments but also of other materials, which shows that this system is universal and widely used. In the present paper the color determination of the pigments is carried out spectrally with a tintometer of Lovibond Tintometer RT 100 Color. The colour measurements were performed using the CIELab method. This method, which is the standard for analyses in the ceramic industry, especially for ceramic pigments, allows the determination of the whiteness and colour degree of tiles by measuring three parameters: L*, a* and b*, where:

L* (brightness), from absolute white L* = 100 to absolute black L* = 0

a* - green color (-) / red color (+)

b* - blue color (-) / yellow color (+)

The color space of the CIELab system is shown in Figure 2.

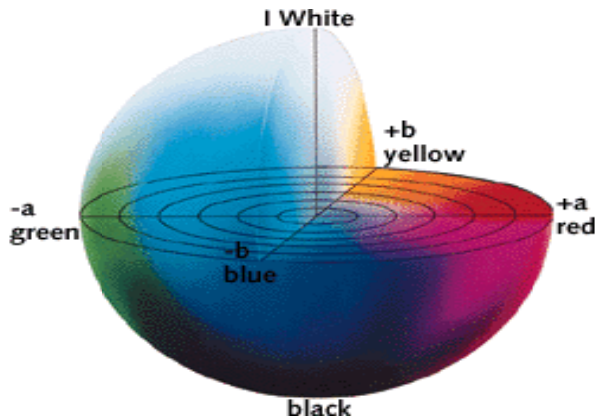


Fig. 2 Colour space of CIELab system

Tables 2 and 3 show the results from the conducted research.

Table 2. Results of color coordinate measurements in the CIELab system of zircon ceramic pigments with rice husks

N _o of sample	T of sintering	Color	L	a *	b *
ZR 1	1000°C	tile red	71.02	17.51	-3.06
	1100°C	color	66.67	12.51	-6.72
	1200°C		68.69	3.13	-14.76
ZR 7	1000°C		48.38	13.77	1.67
	1100°C	tile red	44.22	11.41	8.88
ZR 2	1200°C	color	47.26	7.07	5.32
	1000°C		56.11	-4.08	22.38
ZR 2	1100°C	green	54.52	-3.23	21.26
	1200°C		53.62	-1.09	19.68
ZR 8	1000°C		50.00	7.67	22.2
	1100°C	tobacco	52,38	4.3	25.26
ZR 3	1200°C		54.38	2.77	25.70
	1000°C		74.78	6.61	-12.65
ZR 3	1100°C	light purple	73.07	8.09	-10.04
	1200°C	purple	62.76	9.16	-0.11

Table 3. Results of color coordinate measurements in the CIELab system of zircon ceramic pigments with rice husks

N _o of sample	T of sintering	Color	L	a *	b *

	1200 °C	light purple	62.76	9.16	-0.11
ZR 9	1000°C	purple	75.68	6.17	-11.92
	1100 °C	dark purple	71.36	7.67	-12.27
	1200 °C	purple	63.94	8.62	-1.38
ZR 5	1000°C		68.59	-6.00	7.13
	1100 °C	green	66.84	-5.89	8.06
ZR 11	1200 °C		60.61	-5.76	8.87
	1000°C		67.58	-5.74	7.68
	1100 °C	light green	65.69	-5.63	7.53
ZR 6	1200 °C	green	60.94	-5.51	9.01
	1000°C	dark gray	37.84	0.91	6.16
	1100 °C	gray	55.00	2.23	10.92
ZR 12	1200 °C	gray	49.01	1.85	13.89
	1000°C	dark gray	40.00	1.40	6.89
	1100 °C	gray	51.62	2.73	9.89
	1200 °C	gray	51.92	2.94	16.04

Infrared spectroscopy (FT-IR)

Fourier Transform Infrared spectroscopy (FT-IR) spectra provide information about the functional groups in a sample.

Infrared spectroscopy is based on the interaction of substances with electromagnetic oscillations with a certain frequency. The infrared region of the spectrum includes the interval with wavelengths λ from 1 to 1000 μm but only the interval with wavelengths from 1 to 25 μm is of practical importance.

Molecules contain atoms or groups of atoms that have their own oscillation with a specific frequency. Based on this frequency, the various atomic groups are detected and thus the structure of the molecule is determined [8].

The results of the FT-IR tests are given in Fig. 3 ÷ 6.

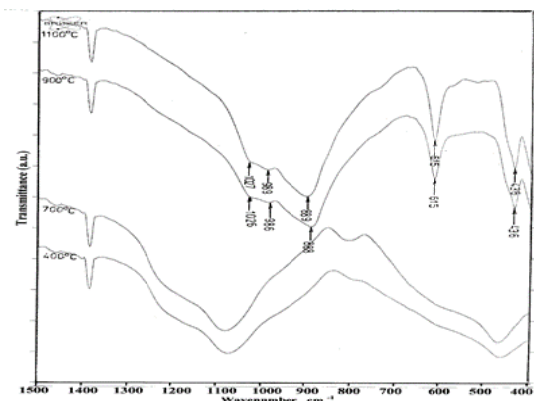
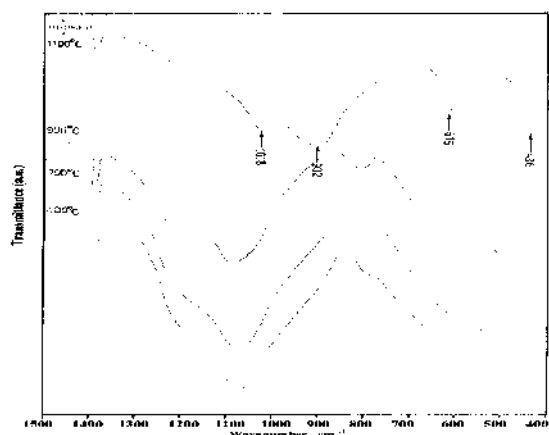


Fig. 3 FT-IR spectra with Co^{2+} chromophore

It was proved by X-ray analysis that at 900°C the main phase $ZrSiO_4$ is completely synthesized. In the case of pigments with a Co^{2+} chromophore, the band of zircon is observed even at 900°C. It is possible that the band at 986 cm^{-1} is due to isomorphic substitution of silicon or zircon atoms by a cobalt atom, as a result of which a Si - O - Co or Zr - O - Co bond is formed (Fig.



3).

Fig. 4 FT-IR spectra with Fe^{3+} chromophore

Fig. 5 FT-IR spectra with Mn^{2+} chromophore

In the systems with chromophores Fe^{3+} and Mn^{2+} the characteristic bands of zircon appear in the samples synthesized at 1100°C (Fig. 4, 5).

In the system with chromophores Cr^{3+} the spectra of the samples are almost identical, which proves the fact that up to 1100°C no zircon phase is synthesized (Fig. 6).

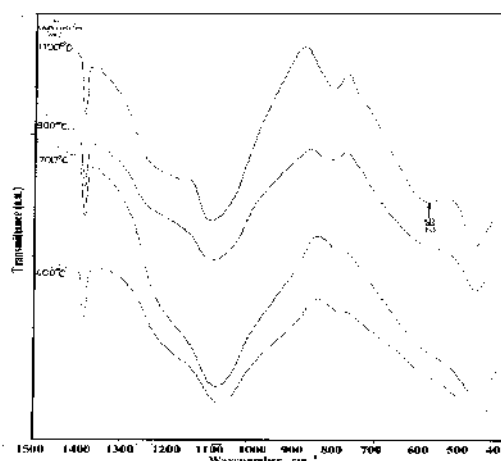
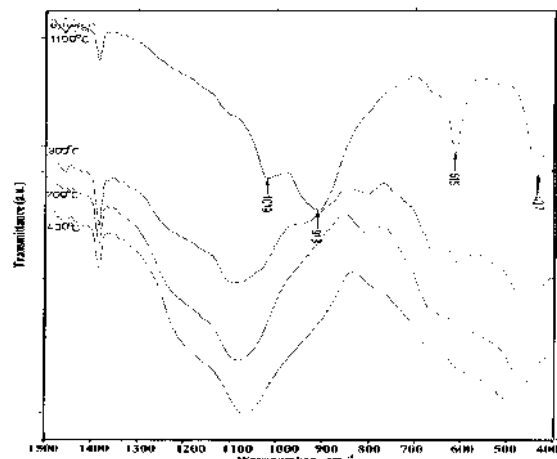


Fig. 6 FT-IR spectra with Cr^{3+} chromophore

The appearance of an absorption region of about 590 cm^{-1} may be related to the formation of the zirconium phase.

CONCLUSIONS

Zirconium ceramic pigments were synthesized by the method of solid state sintering.

The optimal parameters of synthesis of all compositions were determined.

As starting materials for the synthesis of zircon pigments, ZrO_2 , Fe_2O_3 , NH_4VO_3 , Co_3O_4 , Cr_2O_3 , MnO_2 , rice husk ash, and NH_4Cl as a mineralizer were used.

The most intense color appeared in composition ZR1, synthesized at 1000°C with an isothermal delay of 3 hours. This pigment had a tile-red color with a parameter:

$(a^*) = 17.51$, measured by the CIELab system.

In all compositions, with the decrease in synthesis temperature, a decrease in their color intensity was observed.

It has been found out that the synthesized pigments can be successfully used in wall tile glazes.

ACKNOWLEDGEMENTS

This work was supported by the Bulgarian Ministry of Education and Science under the National Research Fund, grant agreement KP-06-H27/14-2018

REFERENCES

1. Gerasimov E., A. Gerasimov, A. Atanasov, V. Toshev, D. Petkov, D. Ivanov, L. Georgieva, L.

- Pavlova, N. Drenska, Vinarov P., Petrov P., Bachvarov S., Panova C., S. Bagarov, S. Serbezov, S. Stefanov., S. Dzhambazov, T. Stojkova, T. Datskova, H. Berlinov, Technology of Ceramic Products and Materials, Ed. S. Bachvarov, Saraswati IC, Sofia, 2003.
2. Eppler R. A., Zirconia-based colours for ceramic glazes, *Am.Cer. Soc. Bul.*, **2**, (1977), pp. 313–315.
 3. Kleinrok D. et. al., Cpracowanie warunkow syntezy I stosowania barwnikow ceramicznych, *Szklo I Ceramika*, **7**, (1980), pp. 239–244.
 4. Andreola F., L. Barbieri, F. Bondioli, Agricultural waste in the synthesis of coral ceramic pigment, *Dyes and Pigments*, **94**, (2), (2012), pp. 207–211.
 5. Prasad C. S., K. N. Maiti, R. Venugopal, Effect of rice husk ash in whiteware compositions, *Ceram. Int.*, **27** (2001), pp. 629–635.
 6. Andreola F., M. I. Martín, A.M. Ferrari, I. Lancellotti, F. Bondioli, J. Ma Rincón, M. Romero, L. Barbieri, Technological properties of glass-ceramic tiles obtained using rice husk ash as silica precursor, *Ceram. Int.*, **39** (2013), pp. 5427–5435.
 7. Sobrosa F. Z., N. P. Stochero, E. Marangon, M. D. Tier, Development of refractory ceramics from residual silica derived from rice husk ash, *Ceram. Int.*, **43**, (9), 15, (2017), pp. 7142–7146.
 8. Bellisola G., C. Sorio, Infrared spectroscopy and microscopy in cancer research and diagnosis, *Am. J. Cancer Res.*, **2**, (1), (2012), pp. 1–21.

ESTIMATION OF NOISE LEVELS ON THE TERRITORY AROUND THE INORGANIC CHEMISTRY BUILDING OF PROF. DR ASSEN ZLATAROV UNIVERSITY

Nikola Todorov, Emiliya Ivanova, Vladilena Deyanova, Violeta Zheleva
E-mail: *steel_nick@yahoo.com*

ABSTRACT

Noise is one of the main factors with adverse effect on the quality of life. Throughout the years, noise pollution has increased and turned into a serious ecological and health problem. In the present study, noise measurements were performed at five different points around the Inorganic Chemistry Building of the Prof. Dr Assen Zlatarov University, Burgas, in the time interval from 9:00 am to 3:00 pm from 9.10.2019 until 6.11.2019. The equivalent noise levels were determined during the breaks and during the academic lectures. It was found out that the noise from the international road E871 increases the noise pollution by 20-25 dB(A) with the equivalent noise levels around the building reaching values of 72 dB(A). These values are significantly bigger than the allowable noise limits in areas of scientific research and lecturing activities. Measures for reducing the noise pollution are suggested.

Key words: *noise level, pollution, traffic, measurement*

INTRODUCTION

Noise is one of the main factors with adverse effect on the quality of life of people [1]. Noise pollution has negative effect on activities such as communication and concentration, especially in educational institutions (schools, educational laboratories, colleges and universities). The noise around educational institutions is of special importance because it affects both the results gained by students and pupils and their health [2].

Shield & Dockrell [3] measured the noise levels around 142 schools in London and studied the types of noise sources aiming to create a general view on the noise environment around the schools in central London. They found out that the predominant noise source around London's schools is the street traffic and the medium sound level for a typical 5 min period during a school day was approximately 57 dB (A).

Ozyonar et al. [3] measured the noise at 9 points of the Cumhuriyet University campus for 5 days in three different periods of the day. They established that the traffic noise is the main source of noise in the university campus. Akintunde et al. [4] measured the noise in Gazi University Engineering Faculty Campus, which is located near a highway. The researchers determined the noise levels at 16 points in three time intervals of the day (9–12, 12–14 and 14–

24) and made two measuring cycles. The noise levels were found to vary from 53.4 to 138.5 dB.

It has been stated in a number of other reports [5-9] that the main noise source in university campuses is the road traffic. In some campuses, noise mapping has already been made [10].

To decrease the noise pollution, certain regulatory documents have been issued in the world and in the Republic of Bulgaria. In Ordinance No 6 from 26.06.2006 [11], it is stated that the allowable noise level in areas of scientific research and educational activities during the daytime is 45 dB(A).

The monitoring of the noise in the Ecology Seminar Room 327 in the Inorganic Chemistry Building of Prof. Dr. Assen Zlatarov University, Burgas established that with open windows the noise level was significantly higher than the allowable limit and reached 63-66 dB(A). This gave us enough grounds to continue our investigation in this direction. The main aims of the present study are:

- ◆ to determine the noise level on the territory of the Inorganic Chemistry Building of Prof. Dr Assen Zlatarov University, Burgas;
- ◆ to estimate the noise pollution;
- ◆ to suggest measures to reduce the noise pollution.

RESEARCH METHOD

Study area

The Inorganic Chemistry Building (ICB) is one of the eleven buildings of Prof. Dr Assen Zlatarov University, Burgas. It has a square shape with a side length of 50 m. It is located in the north-eastern part of the university campus. The international road E871, which coincides with the European road E773, passes north-east of the building. The university campus is situated to the south-west, there is agricultural land to the north-west and the Organic Chemistry Building is to the south-east. The total area of the territory around the ICB is about 12,000 sq. m.

Equipment

◆ Noise meter: two pieces of GM 1356 were used. They are produced according to IEC PUB651 TYPE2 & ANSI S1.4 TYPE2 standards. Range: 30-130 dB A; measurement precision ± 1.5 dB A; range of memory: 1-250 seconds; memory: 4500 records. Outputs: AC, PWM, USB. The USB connector allows downloading the data of both saved in the memory and real-time measurements to a computer for further processing and analysis.

◆ Software: noise meter GM1356 is delivered together with an installation disk containing the necessary software, Sound Lab. It provides opportunity both to monitor the real-time data and download the data recorded in the memory in tabular form for further processing. The data measured by the gauge are: sequential number of the measurement, value measured, hour and date.

◆ Tripod on which the noise meter is fixed.

Sampling

The noise meter is mounted on a tripod and fixed at a height of 160 cm corresponding to the height of students' ears. Parameters of the measurement are:

- frequency – 1 measurement per second
- duration – 59 min (3540 measurements).

The experiment can be terminated earlier than the set period.

The measurements were carried out from 9:00 am until 3:00 pm and lasted for 59 min. The noise level is recorded as L, dB(A). Data download takes usually less than a minute, after that the gauge memory is freed for the next sampling. Each file contains the following information: point of sampling, date, hour and second of the start of measuring. All measurements were carried out in the autumn of 2019.

Computer processing of the results

The data transfer (export) from the noise meter was done using the embedded USB port. The software provides opportunity to export the data in tabular form and they were further processed with software such as MS Excel to visualize the changes in noise level L, dB(A) with time. The values measured were transformed to obtain the equivalent noise level L_{eq} , dB(A). There are possibilities to analyze various time periods, i.e. 45 min (which is the duration of an academic hour), 20 min or 15 min (which is the duration of the break).

RESULTS AND DISCUSSION

Determination of the points of noise measuring

To get an idea about the overall noise distribution, 5 points were selected around the Inorganic chemistry building (P.1; P.2; P.3; P.4 and P.5), where the noise levels were determined. These points were selected as follows:

◆ P.1 is a relaxation place (equipped with benches), where students gather during breaks;

◆ P.2 is positioned south-west of the ICB, at a distance of 10 m from the building facade;

◆ P.3 is positioned south-east from the ICB, at a distance of 10 m from the location of Room 327 where the internal noise was measured earlier;

◆ P.4 and P.5 are positioned north-east and north-west from the ICB, also at a distance of 10 m from the middle points of the building.

Fig. 1 shows a satellite image of the territory of Prof. Dr Assen Zlatarov University, where the ICT is located [12], with the surroundings of the building and the marked positions of the five selected points of noise measuring.



Fig. 1. Satellite image of the ICB and the points where noise measurements were carried out.

Measuring the noise level L, dB(A)

The measurements were taken every Wednesday for 5 consecutive weeks starting from October 6th to November 9th 2019. The measurements lasted 6 hours, from 9 in the morning till 3 in the afternoon.

The data were first obtained in tabular form. Then, using spreadsheet programs like MS Excel, the change of the noise level L, dB(A) with time was visualized (Fig. 2).

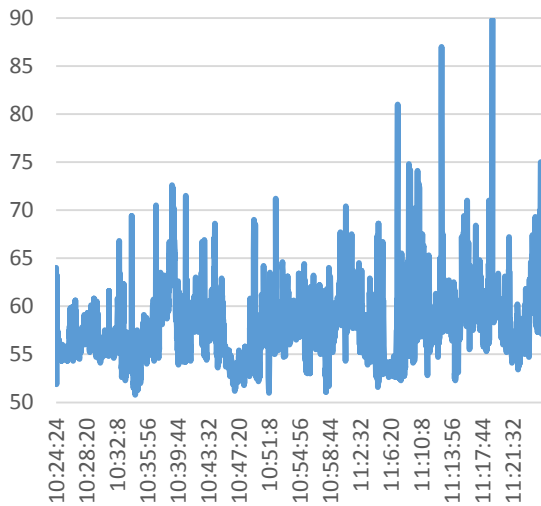


Fig.2. Change of noise level L, dB(A) with time on October 9th 2019 at point P.1

Fig. 2 shows the change of noise level L with time for the period from 10:24 to 11:24 on October 9th, 2019 at P.1. it can be seen from the figure that the noise level varied from 52 to 72 dB(A) from 10:24 till 11:06, then increased and varied in the range from 54 to 90 dB(A). After 11:20, the noise level decreased. These changes can be explained by the presence of students at P.1 during the breaks.

Estimation of the noise pollution

To estimate the noise pollution means to compare the value of the equivalent noise level (Leq) for certain period of time (15 or 20 min) with the allowable limit of noise level according to Ordinance No 6 from 26.06.2006. The equivalent noise levels were determined in the present work for:

- ◆ five selected points: P.1; P.2; P.3; P.4 and P.5;
- ◆ 6 astronomical hours: from 9:00 am to 3:00 pm;
- ◆ during a break: Leq 15 min, dB(A), from 9:00 to 9:15, from 10:00 to 10:15, etc., respectively;
- ◆ during academic hours: Leq 20 min, dB(A).

Despite the fact that the duration of an academic hour is 45 min according to the Regulation of Educational Activities of the University, the equivalent noise levels were measured for 20 min periods from 9:25 to 9:45; from 10:25 to 10:45 and so on for the following reasons: according to a number of studies, [4-7] a duration of 20 min is long enough to describe the noise events taking place. On the other hand, the breaks are sometimes prolonged due to various reasons and the background activity is not well registered about 10 min after the beginning of the academic hour and 10 min before its end.

Fig. 3-7 show changes of the equivalent noise levels at different points of measurement. Fig. 3 presents the obtained results for Leq 15 min dB(A) and Leq 20 min dB(A) in the time interval from 9:00 am to 3:00 pm for students' relaxation spot (P.1).

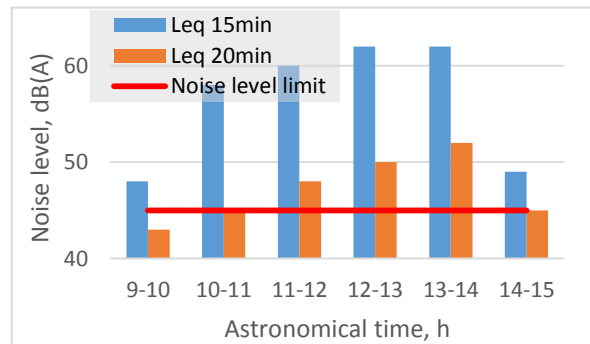


Fig. 3. Change of Leq 15 min dB(A) and Leq 20 min dB(A) in the interval from 9:00 am to 3:00 pm at point P.1.

From Fig. 2 it can be observed that:

- ◆ the noise level during the academic hour is higher than the allowable limits only about noon;
- ◆ the noise levels during breaks are higher than these during the academic hours. Leq 15 min were by 6 to 12 dB(A) higher than Leq 20 min and by 3 to 15 dB(A) higher than the allowable limit for scientific research and educational activity according to the Ordinance No 6/6.06.2006. The increase of noise levels can be explained with conversations between the students.

The obtained results for Leq 15 min dB(A) and Leq 20 min dB(A) in the time interval from 9:00 am to 3:00 pm at the entrance of ICB (P.2) are presented in Fig. 4.

It can be seen from Fig. 4 that:

- ◆ the values of Leq 15 min are by 7-9 dB(A) higher than these at point P.1. This can be explained with the higher number of people (students, lecturers, staff) at the entrance of the ICB.

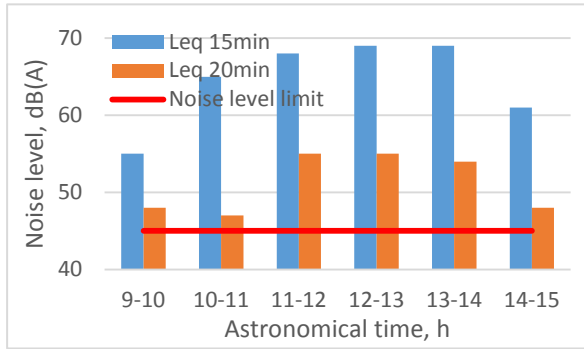


Fig. 4. Change of Leq 15 min dB(A) and Leq 20 min dB(A) during the interval from 9:00 am to 3:00 pm at point P.2.

♦ the values of Leq 20 are lower than these of Leq 15 min but higher than the corresponding ones at point P.1. This can be explained with the presence of people which are not engaged in educational activities, as well as with the existence of another source of noise – cars moving or parking in front of ICB.

♦ all the values for the equivalent noise level at ICB entrance are higher than the allowable limits standardized for the Republic of Bulgaria and the EU.

Fig. 5 shows the results obtained for the noise level on the south-east side of ICB.

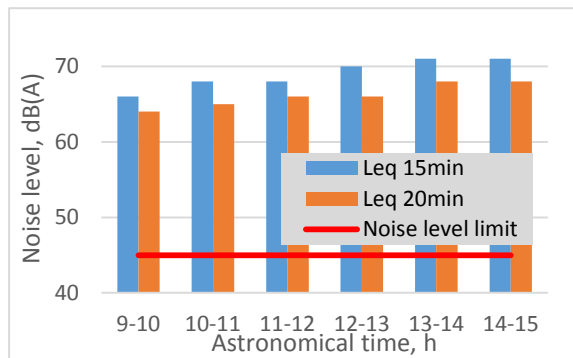


Fig. 5. Change of Leq 15 min dB(A) and Leq 20 min dB(A) for the time interval from 9:00 am to 3:00 pm at point P.3.

As can be seen in Fig. 5, the values of Leq 15 min and Leq 20 min at point P.3 are significantly higher than those at point P.2. The reason for this is the traffic noise on the international road E871, which is the main source of noise at point P.3. The small differences between Leq 15 min and Leq 20 min can be explained with the noise from automobiles on the alleys around the ICB, repair works and green area maintenance around the ICB.

Fig. 6 shows the values of Leq 15 min and Leq 20 min measured at point P.4.

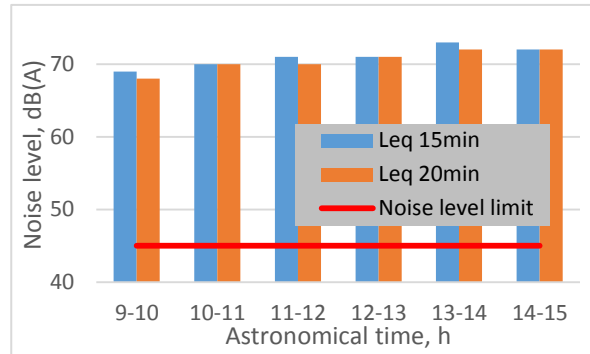


Fig. 6. Change of Leq 15 min dB(A) and Leq 20 min dB(A) for the time interval from 9:00 am to 3:00 pm measured at point P.4.

It can be seen from the data presented in Fig. 6 that:

♦ the values of Leq 15 min and Leq 20 at point P.4 are the highest in the territory around the ICB. The noise level reached values as high as 73 dB(A) which is by 28 dB(A) higher than the allowable limit for noise in areas of scientific research and educational activities according to Ordinance No 6/6.06.2006. The reason for this is the proximity of point P.4 with the international road E871, on which large amount of light and heavy vehicles pass day and night and their number is increasing every year, hence the increasing noise pollution on the territory of ICB.

♦ the values of Leq 15 min and Leq 20 are almost equal because there are no alleys built on the north-eastern side of the ICB and this is the reason why the noise generated by students, lecturers and staff has a small effect on the noise level.

The values of Leq 15 min and Leq 20, measured at point P.5 are presented in Fig. 7.

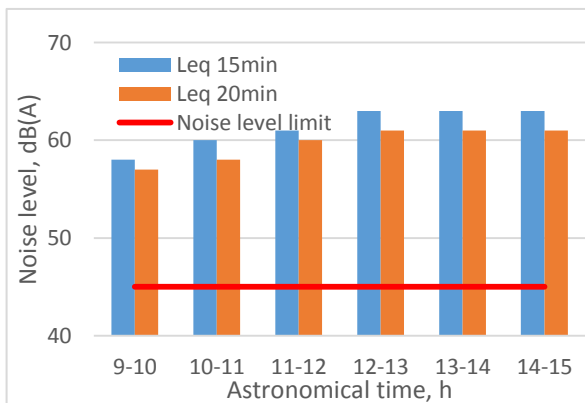


Fig.7. Change of Leq 15 min dB(A) and Leq 20 min dB(A) for the time interval from 9:00 am to 3:00 pm measured at point P.5.

Fig. 7 reveals that the influence of the noise generated by students is weak. The high noise level is caused by the international road E871.

Possibilities for reduction of noise pollution

It becomes clear from the data presented that the main sources of noise pollution around the Inorganic Chemistry Building are the automotive transport and the noise from student communication. We recommend the following measures to be taken to reduce the noise pollution in the area around the ICB:

- ♦ creation of a green belt between the international road E871 and Inorganic Chemistry building. For this purpose, noise reducing shrubs and trees should be planted in a checkerboard pattern. The green belt will reduce the exposition to the automotive transport. The expected noise reduction is by 20 – 25 dB and, simultaneously, it will reduce the exposition to harmful gases and particulate matter in the region;

- ♦ a sensor for registration of the noise level should be placed at the entrance of the Inorganic Chemistry building which should emit a light signal when the allowable limit for noise is exceeded;

- ♦ certain activities should be carried out to inform students and lecturers about the harm caused by high noise levels on human health and increase the sensitivity of the campus community to the effects of noise pollution.

CONCLUSION

Studies were carried out to determine the noise level on the territory of the Inorganic Chemistry Building of Prof. Dr Assen Zlatarov University. The noise level was measured at five points around the Inorganic Chemistry Building in the time interval from 9:00 am to 3:00 pm in the autumn of 2019. The equivalent noise levels were recorded for 15 min intervals during the breaks and 20 min intervals during the academic hours. An estimation of the noise pollution was made. It was confirmed that the main sources of noise pollution are the automotive traffic on the international road E871 and the noise from student communication. It was established that the noise at the 5 points studied exceeds the allowable limits for noise level for areas of scientific research and educational activities. To reduce the noise pollution, the planting of a green belt between the international road E871 and the ICB

was proposed, as well as placing a light emitting noise sensor at the entrance of the ICB and informing the students and lecturers about the harm caused by the high noise levels.

REFERENCES

1. <http://eea.government.bg/bg/soer/2018/noise/index>, National report on the state and protection of the environment in the Republic of Bulgaria, 2018
2. Shield, B and J Dockrell, External and internal noise surveys of London primary schools, *J Acoust Soc Am.*, 2004 Feb; 115(2):730-8
3. Ozyonar, F., O. Gokkus, H. Muratcobanoglu and O. Gursoy, Assessment of on-Campus Noise Levels at Cumhuriyet University, *Fresenius Environmental Bulletin*, 27(5A/2018)
4. Akintunde E., J. Bayei and J. Akintunde, Analysis of Noise Level in a Campus Area: Case Study for Gazi University Maltepe Campus, *Ergonomics Int J*, 2019, 3(4): 000211
5. Balila, A. and A. Siddiqi, *Critical Evaluation of the Noise Environment with Respect to Academic Activities: A Case Study of some Buildings in the Faculty of Engineering at King Abdulaziz University*, *Journal of King Abdulaziz University: Engineering Sciences*, 1999, 2,1, 193-210
6. Phukan, B. and K. Kalita, An Experimental Study of Noise Pollution in Guwahati, Assam, India, *International Journal of Environmental Sciences*, 2013, 3, 5.
7. Ozer, S., M. Zengin and H. Yilmaz, Determination of the Noise Pollution on University (Education) Campuses: a Case Study of Ataturk University), *Ekologi*, 2014, 23, 90, 49-54.
8. El-Sharkawy, M. and A. Alsubaie, Study of Environmental Noise Pollution in the University of Dammam Campus, *Saudi Journal of Medicine & Medical Sciences*, 2014, 2, 3, 178-184
9. Olaosun, A. and O. Ogundiran, Noise Levels in a Nigerian Tertiary Institution, *International Journal of Recent Scientific Research*, 2014, 5, 4, 720-723.
10. Akintunde, E., J. Bayei and J. Akintunde, Noise level mapping in University of Jos, Nigeria, *GeoJournal*, 2020, DOI: 10.1007/s10708-019-10135-w
11. Ordinance № 6/26.06.2006.
12. maps.google.com

REMOVAL OF SULFUR COMPOUNDS BY ADSORPTION

Yordanka Tasheva, Aleksandar Dimitrov, Milena Dimitrova

E-mail: jtasheva_2006@abv.bg

ABSTRACT

*The adsorption process of thiophenic sulfur compounds, thiophene(T), benzothiophene(BT), and dibenzothiophene(DBT), from their binary model mixtures in *i*-octane and ternary model mixtures in *i*-octane and toluene, on sorbents (Al_2O_3 , silica gel) were investigated. The presence of toluene in ternary model mixtures significantly reduced the desulfurization performance of the sorbents.*

Key words: sulfur compounds, ecology, adsorption, advanced technologies, purification

INTRODUCTION

High-sulfur fuel poses increased environmental risks because its combustion in automobiles and industrial operations releases noxious sulfur oxides into the atmosphere.

Sulfur oxides are known as precursors of acid rain, and are reported to cause fuel refining problems, such as catalyst deactivation during oil processing and corrosion problems in pipeline, pumping, and refining equipment. Furthermore, sulfur compounds poison the catalysts for carbon monoxide oxidation and nitrogen oxide reduction in vehicle exhaust catalytic converters. Because of these considerations, environmental regulations worldwide have imposed ultra-low sulfur concentrations in liquid fossil fuels at 10 mg/kg for diesel. Stricter policies that will require zero sulfur emissions are even foreseen, giving rise to the need for further development of advanced sulfur removal technologies [1].

The removal of sulfur containing compounds from transportation fuels is an important operation in petroleum refining, and is achieved by catalytic processes operated at high pressures and elevated temperatures. Deep desulfurization has attracted increasing interests due to increasingly stringent environmental regulations on sulfur content as well as the possible use of liquid fuels for fuel cell applications (where sulfur is a poison for catalysts). Today, refineries rely on hydrodesulfurization (HDS) processes to reduce sulfur levels, but achieving deep-desulfurization levels would require enlargement of existing reactor sizes and increasing hydrogen consumption. There has been much recent interest in desulfurization of liquid fuels at ambient temperature and pressure using a variety of adsorb-

ents for selective sulfur removal, such as activated carbon, modified carbons, NaY and other type-Y zeolites, and Ag-doped on mesoporous supports.

Liquid transportation fuels (gasoline, diesel and jet fuel) contain mainly aliphatics and aromatics plus small amounts of thiophenic sulfur. In adsorptive desulfurization, the aromatics compete with thiophenic sulfur for adsorption sites, while aliphatics are not competitive. The contents of aromatics are about 20% by volume in diesel and jet fuel, and about 30% in gasoline. The sulfur compounds are mainly thiophene and alkylated thiophenes in gasoline, benzothiophene and alkylated derivatives in jet fuel, and dibenzothiophene and its derivatives in diesel [2].

Previous studies have explored the utilization of various solid adsorbents on the removal of sulfur from fuel and nearly 100% sulfur removal was achieved by using alumina adsorbents.

Adsorptive desulfurization can supplement HDS process as a polishing step and offers an alternative solution to the high cost of production of ultra-clean fuels [3, 4].

In this study, the removal of sulfur compounds from model mixtures by adsorption onto commercial alumina and silica gel was investigated.

EXPERIMENT

Thiophene (T), benzothiophene (BT), dibenzothiophene (DBT), *i*-octane and toluene were purchased from Sigma-Aldrich by Valerus, Sofia.

The adsorbents used in this study were commercial standard Al_2O_3 90, neutral and standard silica gel 60. The adsorbents thus selected were

activated according to the methods described in a previous work [5].

Binary model mixtures and ternary model mixture were used. Binary model mixtures contain *i*-octane and a sulfur compound or toluene of various concentrations (ranging from 500 to 850 mg/kg sulfur or toluene). A ternary model mixture contains *i*-octane, toluene (600 mg/kg or 25 % toluene) and a sulfur compound of various concentrations (ranging from 500 to 850 mg/kg sulfur). The solution (ranging from 10 to 30 ml) and the corresponding adsorbent (50–100mg) were mixed in a column at ambient temperature (25°C). The sulfur content after adsorption was investigated by BSS 20846 and the toluene content was investigated by BSS 2977.

The obtained experimental results are presented in the next section.

RESULTS AND DISCUSSION

The following tables show the results of adsorption purification of binary model mixtures and the ternary model mixture of sulfur thiophene compounds and toluene.

Table 1. Results of adsorption purification of binary model mixture (thiophene – *i*-octane) with silica gel

initial sulfur content: 750 mg/kg

№	Contact time, min	Sulfur content, mg/kg
	ratio	1:10
1.	10	650
2.	20	612
3.	30	588
4.	60	554
5.	90	541
6.	120	522
7.	150	510
8.	180	460
9.	210	430
10.	240	410
11.	270	381
12.	300	334
13.	330	310
14.	360	285
	ratio	1:15
15.	10	598
16.	20	562
17.	30	524
18.	60	498
19.	90	486
20.	120	476

21.	150	444
22.	180	432
23.	210	410
24.	240	390
25.	270	356
26.	300	315
27.	330	268
28.	360	235
	ratio	1:20
29.	10	582
30.	20	564
31.	30	510
32.	60	486
33.	90	452
34.	120	422
35.	150	388
36.	180	366
37.	210	345
38.	240	318
39.	270	276
40.	300	253
41.	330	232
42.	360	218

Table 2. Results of adsorption purification of binary model mixtures (thiophene – *i*-octane) with alumina

initial sulfur content: 750 mg/kg

№	Contact time, min	Sulfur content, mg/kg
	ratio	1:10
1.	10	666
2.	20	624
3.	30	598
4.	60	574
5.	90	560
6.	120	525
7.	150	495
8.	180	476
9.	210	452
10.	240	433
11.	270	412
12.	300	382
13.	330	368
14.	360	341
	ratio	1:15
15.	10	620
16.	20	572
17.	30	546
18.	60	522
19.	90	500
20.	120	482
21.	150	458

22.	180	436	23.	210	424
23.	210	420	24.	240	404
24.	240	394	25.	270	382
25.	270	377	26.	300	364
26.	300	355	27.	330	345
27.	330	334	28.	360	326
28.	360	310		ratio	1:20
	ratio	1:20	29.	10	528
29.	10	588	30.	20	473
30.	20	548	31.	30	455
31.	30	530	32.	60	410
32.	60	488	33.	90	394
33.	90	465	34.	120	366
34.	120	426	35.	150	348
35.	150	408	36.	180	320
36.	180	378	37.	210	304
37.	210	356	38.	240	286
38.	240	336	39.	270	268
39.	270	314	40.	300	244
40.	300	288	41.	330	222
41.	330	265	42.	360	208
42.	360	246			

Table 3. Results of adsorption purification of binary model mixture (benzothiophene – *i*-octane) with silica gel

initial sulfur content: 650 mg/kg

№	Contact time, min	Sulfur content, mg/kg
	ratio	1:10
1.	10	610
2.	20	592
3.	30	576
4.	60	558
5.	90	540
6.	120	527
7.	150	498
8.	180	476
9.	210	461
10.	240	443
11.	270	418
12.	300	400
13.	330	385
14.	360	364
	ratio	1:15
15.	10	602
16.	20	578
17.	30	551
18.	60	527
19.	90	504
20.	120	488
21.	150	463
22.	180	440

Table 4. Results of adsorption purification of binary model mixture (benzothiophene – *i*-octane) with alumina

initial sulfur content: 650 mg/kg

№	Contact time, min	Sulfur content, mg/kg
	ratio	1:10
1.	10	618
2.	20	589
3.	30	574
4.	60	550
5.	90	536
6.	120	522
7.	150	492
8.	180	474
9.	210	458
10.	240	439
11.	270	410
12.	300	385
13.	330	368
14.	360	346
	ratio	1:15
15.	10	588
16.	20	570
17.	30	552
18.	60	530
19.	90	513
20.	120	483
21.	150	462
22.	180	430
23.	210	405

24.	240	386	25.	270	298
25.	270	368	26.	300	276
26.	300	340	27.	330	254
27.	330	322	28.	360	232
28.	360	304		ratio	1:20
	ratio	1:20	29.	10	508
29.	10	482	30.	20	475
30.	20	444	31.	30	458
31.	30	424	32.	60	438
32.	60	407	33.	90	420
33.	90	392	34.	120	403
34.	120	369	35.	150	382
35.	150	344	36.	180	355
36.	180	338	37.	210	334
37.	210	320	38.	240	318
38.	240	289	39.	270	284
39.	270	270	40.	300	261
40.	300	248	41.	330	243
41.	330	226	42.	360	222
42.	360	204			

Table 5. Results of adsorption purification of binary model mixture (dibenzothiophene – *i*-octane) with silica gel

initial sulfur content:550 mg/kg

№	Contact time, min	Sulfur content, mg/kg
	ratio	1:10
1.	10	532
2.	20	510
3.	30	490
4.	60	468
5.	90	445
6.	120	422
7.	150	402
8.	180	380
9.	210	364
10.	240	347
11.	270	328
12.	300	312
13.	330	298
14.	360	282
	ratio	1:15
15.	10	523
16.	20	502
17.	30	482
18.	60	463
19.	90	438
20.	120	419
21.	150	401
22.	180	377
23.	210	348
24.	240	319

Table 6. Results of adsorption purification of binary model mixtures (dibenzothiophene – *i*-octane) with alumina

initial sulfur content:550 mg/kg

№	Contact time, min	Sulfur content, mg/kg
	ratio	1:10
1.	10	526
2.	20	504
3.	30	486
4.	60	464
5.	90	442
6.	120	418
7.	150	386
8.	180	366
9.	210	348
10.	240	331
11.	270	310
12.	300	290
13.	330	272
14.	360	250
	ratio	1:15
15.	10	520
16.	20	488
17.	30	472
18.	60	450
19.	90	433
20.	120	418
21.	150	398
22.	180	378
23.	210	352
24.	240	336
25.	270	319

26.	300	296
27.	330	274
28.	360	256
ratio		1:20
29.	10	484
30.	20	453
31.	30	425
32.	60	409
33.	90	381
34.	120	362
35.	150	334
36.	180	316
37.	210	298
38.	240	280
39.	270	261
40.	300	245
41.	330	227
42.	360	218

Table 7. Results of adsorption purification of ternary model mixture with silica gel

initial sulfur content:850 mg/kg; initial toluene content:25 %

№	Contact time, min	Sulfur com- pounds, mg/kg	Toluene, %
ratio		1:10	
1.	10	801	24
2.	20	778	22
3.	30	752	22
4.	60	712	22
5.	90	688	22
6.	120	656	22
7.	150	634	21
8.	180	610	21
9.	210	582	21
10.	240	560	21
11.	270	546	21
12.	300	525	20
13.	330	508	20
14.	360	482	20
ratio		1:15	
15.	10	784	23
16.	20	763	22
17.	30	751	22
18.	60	736	21
19.	90	710	21
20.	120	691	21
21.	150	677	20
22.	180	658	20
23.	210	625	20
24.	240	588	20
25.	270	560	20
26.	300	528	19
27.	330	489	18
28.	360	462	18

ratio		1:20	
29.	10	768	22
30.	20	740	22
31.	30	715	22
32.	60	685	21
33.	90	670	21
34.	120	654	21
35.	150	623	21
36.	180	590	20
37.	210	568	20
38.	240	544	19
39.	270	521	19
40.	300	498	18
41.	330	472	18
42.	360	450	18

Table 8. Results of adsorption purification of ternary model mixture with alumina

initial sulfur content:850 mg/kg; initial toluene content: 25%

№	Contact time, min	Sulfur compounds, mg/kg	Toluene, %
ratio		1:10	
1.	10	773	23
2.	20	745	22
3.	30	722	22
4.	60	690	21
5.	90	666	21
6.	120	642	21
7.	150	618	21
8.	180	592	20
9.	210	570	20
10.	240	555	20
11.	270	538	20
12.	300	520	19
13.	330	488	18
14.	360	464	17
ratio		1:15	
15.	10	774	22
16.	20	751	22
17.	30	730	22
18.	60	712	22
19.	90	698	22
20.	120	676	21
21.	150	654	21
22.	180	638	20
23.	210	612	20
24.	240	587	20
25.	270	553	19
26.	300	530	19
27.	330	514	18
28.	360	508	18
ratio		1:20	

29.	10	764	22
30.	20	750	21
31.	30	737	21
32.	60	720	21
33.	90	682	21
34.	120	658	20
35.	150	637	20
36.	180	614	20
37.	210	598	19
38.	240	573	18
39.	270	555	18
40.	300	522	18
41.	330	488	18
42.	360	462	18

The results presented in Tables 1 to 8 show that by using the adsorption method sulfur and arene hydrocarbons are removed from the model systems prepared by us, resembling the composition of the middle distillate fractions.

It is noteworthy that the adsorbent aluminium trioxide that we used removes both sulfur compounds and toluene to a greater extent.

From the three ratios of raw material used (adsorbent = 1:10, 1:15 and 1:20), the expected greatest reduction in sulfur compounds and toluene was obtained by applying the adsorbent = 1:20 ratio of raw material.

The presented experimental results prove that alumina is a better adsorbent compared to silica gel when used to remove sulfur compounds and toluene from model mixtures resembling middle distillate fractions.

It should be noted that the reduction of sulfur compounds by adsorption in binary model systems is the greatest with process duration of 10 to 60 min., and subsequently the removal of sulfur compounds is in the range of 18 to 24 mg/kg.

It is observed that upon adsorption of the quaternary mixture the reduction of sulfur compounds is in a higher percentage, which is most probably due to the presence of toluene.

REFERENCES

1. Wang L., S. Baode, Fr. Yang et al. *Chemical Engineering Science*, **73**, (2012), p. 208.
2. Wang F., Zh. Zhang, J. Yang et al. *Fuel*, **107**, (2013), p. 394.
3. De Luna M., M. Samaniego, D. Ong et al. *Journal of Cleaner Production*, **178**, (2018), p. 468.
4. Fallah R., S. Azizian, G. Reggers et al. *Fuel Processing Technology*, **119**, (2014), p. 278.

COUNTING OF CD45+ CELLS WITH EASYCOUNTER BC AUTOMATIC FLUORESCENCE MICROSCOPE USING ANTI-CD45 ANTIBODY CONJUGATE

Dimitrina Krasteva, Yavor Ivanov, Katya Gabrovska
E-mail: dida_burgas@mail.bg

ABSTRACT

Fluorescent conjugate between monoclonal CD45 antibody and fluorescent dye dR110(6-carboxy-4, 7-dichlororhodamine 110) were prepared. Purification of the obtained conjugate was carried out by gel filtration chromatography through Sephadex G-25 column. The emission maximums of the obtained conjugate and initial fluorescent dye dR110 were measured. A single-step method for leukocyte isolation from human blood was performed. The isolated cells were proved by Giemsa-Eosin staining using an optical microscope. Then the isolated leukocyte was counted by EasyCounter automatic fluorescent device and by Olympus optical microscopy. Staining of all white blood cells (WBCs) was carried out by the obtained conjugate anti-CD45 antibody – fluorescent dye dR110, and the dead WBCs were stained with Sofia-Green fluorescent dye. The leukocyte count in six apheresis samples was measured. The coefficients of variation of the obtained results with EasyCounter were compared to these obtained with the Olympus optic microscope.

. Key words: CD45+ cells, antibody, dR110, conjugate, cell counting

INTRODUCTION

Leukocytes or white blood cells (WBCs) are immune cells that fight infection, neoplasms and other inflammatory conditions, and mediate allergic responses. The normal number of WBCs in the blood is 4,500 to 11,000 WBCs per microliter. Both elevated and low leukocyte counts can be markers of infection and malignancy. Different kinds of WBCs express different count of CD45 glycoprotein. The expression of CD45 is the highest on lymphocytes (279,369±101,409), intermediate on monocytes (52,398±15,192), and the lowest on granulocytes (26,890 ±7,856). Counting of leukocytes can be performed by automatic fluorescence microscope using the biomarker expression of CD45. Staining for the expression of CD45, a common leukocyte biomarker and fluorescent intercalating reagent that stains dead cells, can distinguish healthy leukocytes from dead cells. White blood cells (WBCs), also called leukocytes, are the cells of the immune system. All white blood cells are nucleated. The number of leukocytes in the blood is often an indicator of a disease, and thus the white blood cell count is an important subset of the complete blood count.

Determination of leukocytes and their viability is very important. Based on the expression of CD 45 antigen onto the cell surface, a screening

could be made for the number of mature leukocytes. The determination of cell viability of leukocytes has been performed by several methods, including methylene blue dye exclusion (optical microscopy), propidium iodide and 7- amino-actinomycin D using fluorescence microscopy [1–3]. Flow cytometry is the other effective method for cell counting [4–10]. Optimization of the flow cytometric analysis requires the use of one fluorescent dye to select nucleated cells and another to determine viability. The determination of cell concentration using a flow cytometer has been well established [11]. The immunofluorescence method using conjugate of antibody specific to CD 45 cells with different fluorescent dyes is a perspective method for this purpose.

MATERIALS AND METHODS

Reagents

Sephadex G25 Medium was purchased from Pharmacia Fine Chemicals, Sweden. Giemsa; Eosin yellowish (Eosin Y, for Microscopy); methylene blue; dR110(6-carboxy-4, 7-dichlororhodamine 110); bovine serum albumin (BSA); anti-CD 45 antibody; methanol; glycerine; dimethyl formamide, N-hydroxysuccinimide, N-(3- Dimethylaminopropyl)-N'-ethylcarbodiimide hydrochloride (EDC);

PBS; Ethylenediaminetetraacetic acid (EDTA); Triton X-100 were delivered by Sigma-Aldrich, Germany. Human peripheral blood was taken from healthy volunteer donors.

Leukocyte isolation from human peripheral blood

Fresh human blood diluted 1:1 with BSS, pH 7.2, was used for analysis. A mixture containing 15 ml of Ficoll and 25 ml of diluted blood was carefully placed in a plastic tube with a conical bottom.

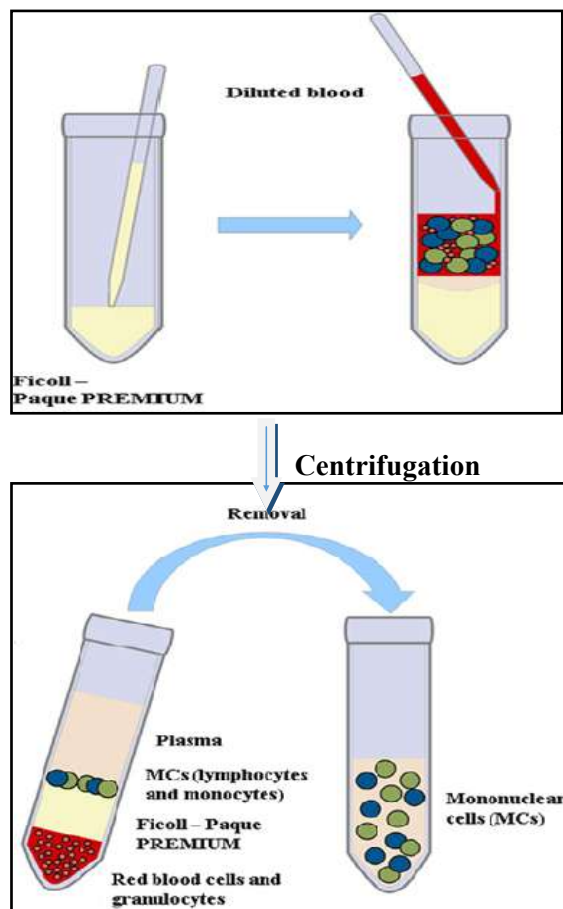


Fig. 1. Separation of blood with a density gradient Ficoll – Paque PREMIUM and isolation of mononuclear cells

Subsequent centrifugation (400 x g) for 40 min at 20°C was used to obtain four layers (plasma, mononuclear cells, Ficoll and red blood cells with granulocytes). Each layer was placed in a separate tube. To the mononuclear cell layer, BSS, pH 7.2, was added and centrifuged to separate the cells from Ficoll. Erythrocytes and granulocytes were then lysed from mononuclear cells using 0.87% NH₄Cl. A white pellet of white blood cells was obtained, which was resuspended

in 1 ml BSS, pH 7.2 and 0.01% EDTA (Fig. 1). The isolated leukocytes were observed with Giemsa-Eosin staining with an Olympus BX51 microscope [15].

Preparation and purification of anti-CD45 antibody - dR110 conjugate

A conjugate between monoclonal CD45 antibody and fluorescent dye dR110 (6-carboxy-4, 7-dichlororhodamine 110) was prepared by the carbodiimide method. DR110 in dimethylformamide DMF (5 mg/mL), N-hydroxysuccinimide (10 mg/mL, 10 mM PBS pH 6.0) and EDC (10 mg/mL, 10 mM PBS pH 6.0) was shaken at 7 000 rpm for 1.5 h. Then it was mixed with 100 µl (1mg/ml, PBS pH 7.4) anti-CD45 antibody and was incubated in a shaker for 60 min at room temperature. The tube was wrapped in foil. Then it was left to react at 4°C, overnight. Finally, the conjugate was isolated from uncoupled reagents.

Sephadex G25 Medium column was used (11 x 1 cm). Flow rate was 0.3 mL/min and fractions were 1.7 mL each. Elution was performed with storage buffer (10 mM PBS, pH 7.4). Fractions were analyzed at 280 nm and 491 nm wavelength for protein and DR110, respectively. The conjugate was in fractions 2.

Counting of leukocytes with EasyCounter BC new image cytometer and Olympus optic microscope

First, the total leukocyte concentration was determined with EasyCounter and Sofia Green DNA fluorescent dye. Dye solution (0.1mg/mL Sofia Green and 1% Triton X-100) was added to 50 µL sample from isolated leukocytes.

The solution of Triton X-100 turns impermeable (live) cells into permeable (dead) cells. The DNA dye penetrated all dead cells and this allowed the measurement of total cell count. Then the sample was mixed and 8 µL of it was placed in a chip and the count of leukocytes was determined by EasyCounter. The total count of leukocytes (CD45 cells) was also measured by using obtained conjugate anti-CD45-dR110 and EasyCounter. To 50 µL isolated leukocytes in 10 mM PBS, pH 7.4 were added 2 µL anti-CD45-dR110 (5µg/mL). The sample was mixed and incubated at 37°C for 20 min in a shaker. After the incubation, 8 µL of it was placed in a chip and the count of leukocytes was determined in a minute by EasyCounter.

The parallel experiment was performed for counting of leukocytes with Olympus optic microscope. For this purpose, the same staining sample of isolated leukocytes was diluted 20 times with 10 mM PBS, pH 7.4. 20 μ L of the sample was placed in a Thomas camera and the cells were counted with Olympus microscope.

Sofia Green fluorescent dye with concentration 0.1 mg/ml and EasyCounter BC were used for determination of dead leucocytes.

EasyCounter BC device

The fluorescently stained cells were examined using the new EasyCounter BC instrument (Milkotronic Ltd, Bulgaria) with image-acquisition and associated software for image analysis and data management. The sample was loaded into the microfluidic camera (Cellchip) with 4 channels. Each channel had 16 fields. The average cell count from the 16 fields was calculated. The EasyCounter BC system automatically focuses on the cellchip and the stained cells are captured by a sensitive CMOS camera. The algorithm for the analysis of digital images determines the number and the size of fluorescent cells and calculates their total concentration and viability in percent. The results are automatically presented on the display of the device.

RESULTS AND DISCUSSIONS

1. *Preparation of conjugate dR110-CD45 antibody*

A conjugate between monoclonal CD45 antibody and fluorescent dye dR110 (6-carboxy-4, 7-dichlororhodamine 110) was prepared by the carbodiimide method. The conjugating mixture had antibody fluorescent dye conjugate, free antibody and unconjugated dye. The mixture was filtrated by size-exclusion chromatography with Sephadex G25 Medium (Fig. 2).

The conjugate had the highest molecular weight in the mixture and exited the column first. Flow rate was 0.3 mL/min. Anti-CD45 antibody – DR110 conjugate was in fractions 2 (Fig. 2).

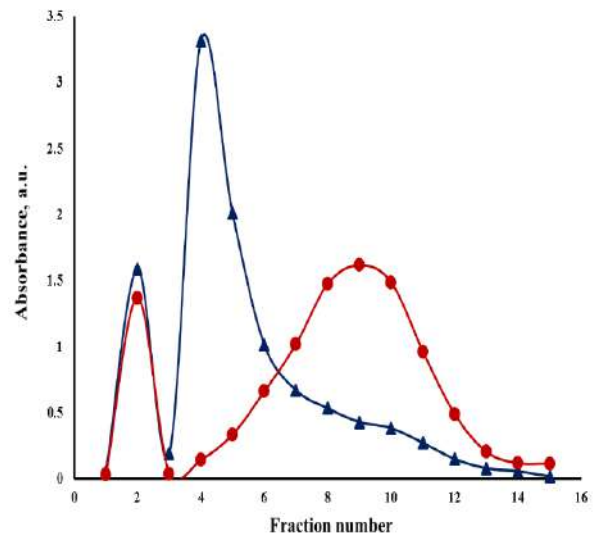


Fig. 2. Sephadex G 25 size exclusion chromatography of conjugate mixture contains anti-CD45 antibody – dR110 conjugate: Absorbance at 491 nm (●) and 280 nm (▲).

Fluorescent dye: protein ratio (F/P) was in optimal values (3–10). This ratio was found to be preferable due to obtained signal-to-noise results (not shown). In this case, the conjugate provided high enough fluorescent signal and negligible background.

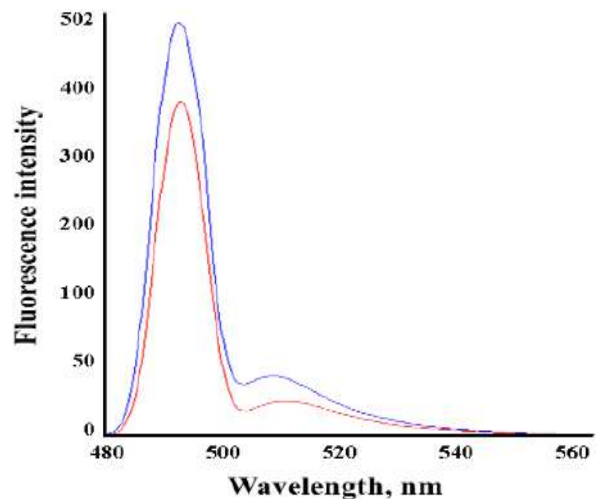
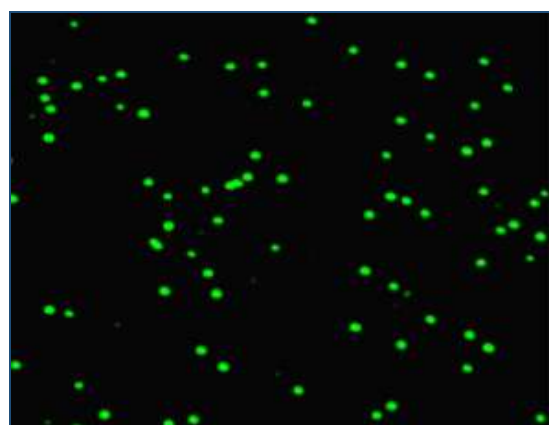


Fig. 3 Fluorescence spectra of the free fluorescent dye dR110 (blue) and fluorescent conjugate anti-CD45 antibody – dR110 (red).

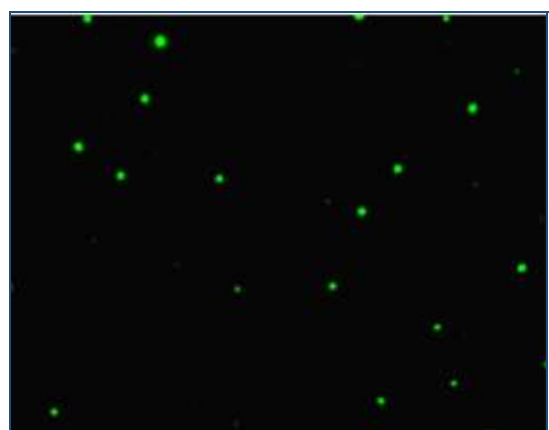
Fig. 3 shows fluorescence spectrophotometric assays of the obtained conjugate (fraction 2). The analysis was performed with Perkin Elmer LS45 fluorescent spectrophotometer. The characteristic maximum at 491 nm for free DR110 was observed and at anti-CD45 antibody - DR110 conjugate, too and showed the successful binding between the antibody and the fluorescent dye. The slight change of conjugate emission maximum proved the formation of conjugate anti-CD45antibody – dR110.

2. Staining of isolated leukocytes from human peripheral blood

Human blood leukocytes from healthy patients were isolated by Ficoll reagent and proved microscopically through standard Giemsa-Eosin staining.



a)



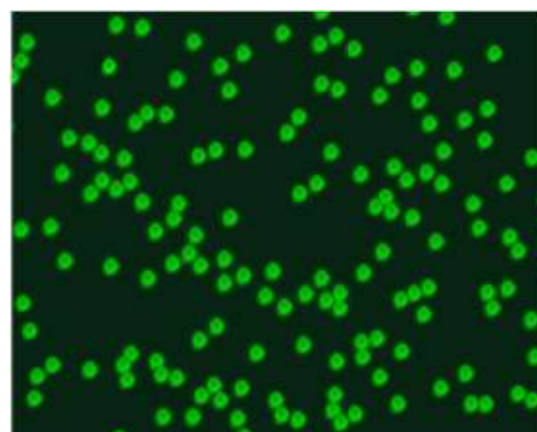
b)

Fig. 4. Fluorescence images of WBCs with EasyCounter BC automatic fluorescence microscope: a) Total count of WBCs with fluorescent conjugate anti-CD45 antibody – dR110; b) Dead WBCs count with Sofia Green fluorescent dye

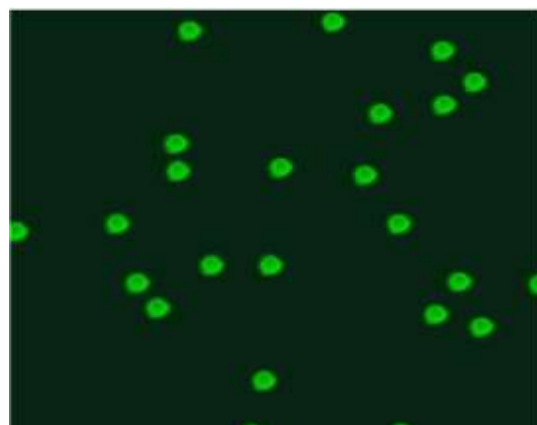
The total count of isolated leukocytes was measured by using EasyCounter BC automatic

fluorescence microscope and by obtained fluorescent conjugate anti-CD45antibody – dR110 (Fig. 4a). The dead cells were counted with EasyCounter BC and with Sofia Green fluorescent dye (Fig. 4b). For counting of dead isolated leukocytes, the cells were stained with Sofia Green fluorescent dye with concentration 0.1µg/ml.

A parallel experiment was performed to count leukocytes with Olympus optic microscope. The total count of isolated leukocytes was measured by using Olympus microscope and by obtained fluorescent conjugate anti-CD45antibody – dR110 (Fig. 5a). The dead cells were counted with Olympus microscope and with Sofia Green fluorescent dye (Fig. 5b).



a)



b)

Fig. 5. Fluorescent images of WBCs with Olympus optic microscope: a) Total WBCs count with fluorescent conjugate anti-CD45 antibody – dR110; b) Dead WBCs count with Sofia Green fluorescent dye

The obtained results show that the new EasyCounter BC is an alternative device for rapid cell counting.

3. Determination of variation coefficients

The coefficients of variation (CV) of the results obtained by EasyCounter BC and Olympus optical microscope were determined.

Table 1. Coefficients of variation of the results obtained with EasyCounter BC

№	Total, EasyCounter, Sofia Green	Total cells count using anti-CD45-dR110 cells/mL	
		Cells/mL	CV, %
1	65 283	63 472	3.0
2	82 311	80 102	5.4
3	103 475	99 634	5.8
4	58 834	55 728	5.2
5	73 452	71 905	4.8
6	92 148	87 524	6.0

A comparison of the coefficients of variation obtained by the two methods shows that the data obtained by EasyCounter BC were three times lower than the results obtained with an Olympus optical microscope. The coefficients of variation of the results obtained by EasyCounter BC automatic fluorescence varied in the range of 3-6% (Table 1).

Table 2. Coefficients of variation of the results obtained with Olympus optic microscope

№	Total cells count using anti-CD45-dR110 cells/mL	
	Cells/mL	CV, %
1	55 325	14.2
2	74 521	15.7
3	92 638	18.4
4	43 234	16.8
5	58 954	19.1
6	80 388	16.2

The coefficients of variation of Olympus optic microscope are in the range of 14-19%. This shows the better reproducibility and accuracy of the EasyCounter automatic fluorescent device.

The results were obtained on the basis of six samples. Each sample was measured 10 times.

CONCLUSION

The conjugate anti – CD45 antibody - fluorescent dye dR110 was prepared. The new method for total WBCs count and dead WBCs count was developed by using the new EasyCounter BC fluorescence automatic microscope. Staining of all WBCs was carried out by the obtained conjugate anti-CD45 antibody - fluorescent dye dR110 and the dead WBCs were stained with Sofia-Green fluorescent dye. The viability of cells was calculated on the basis of the total and dead WBCs count. The new method ensures precise and accurate analysis. The obtained coefficients of variation with EasyCounter BC were three times lower than those obtained with the Olympus optic microscope.

REFERENCES

1. Dyson JED. Fluorescent dyes for studying cell death. *App Fluores Technol* 1990, 2, 1–9.
2. Juneja S, Lukeis R, Tan L, Cooper I, Szelag G, Parkin JD, Ironside P, Garson OM. Cytogenetic analysis of 147 cases of non-Hodgkin lymphoma: Non-random chromosomal abnormalities and histological correlations. *Br J Haematol* 1990, 76, 231–237.
3. Zelenin AV, Poletaev AI, Stepanova NG, Barksy VE, Kolesnikov VA, Nikitin SM, Zhuze AL, Gnutchchev NV. 7-amino-actinomycin D as a specific fluorophore for DNA content analysis by laser flow cytometry. *Cytometry* 1984, 5, 348–354.
4. Darzynkiewicz Z, Bruno S, Del Bino G, Gorczyca W, Hotz MA, Lassota P, Traganos F. Features of apoptotic cells measured by flow cytometry. *Cytometry* 1992, 13, 795–808.
5. Harrison CJ. The lymphomas and chronic lymphoid leukaemias. In: Rooney DE, editor. *Human Cytogenetics: Malignancy and Acquired Abnormalities*, 3rd ed. Oxford: Oxford University Press, 2001.
6. Philpott N, Turner A, Scopes J, Westby M, Marsh J, Gordon-Smith E, Dalgleish A, Gibson F. The use of 7-amino actinomycin D in identifying apoptosis: Simplicity of use and broad spectrum of application compared with other techniques. *Blood* 1996, 87, 2244–2251.
7. Schmid I, Ferbas J, Uittenbogaart CH, Giorgi JV. Flow cytometric analysis of live cell

83 proliferation and phenotype in populations with low viability. *Cytometry* 1999, 35, 64–74.

8. Schmid I, Krall WJ, Uittenbogaart CH, Braun J, Giorgi JV. Dead cell discrimination with 7-amino-actinomycin D in combination with dual color immunofluorescence in single laser flow cytometry. *Cytometry* 1992, 13, 204–208.

9. Schmid I, Uittenbogaart CH, Giorgi JV. Sensitive method for measuring apoptosis and cell surface phenotype in human thymocytes by flow cytometry. *Cytometry* 1994, 15, 12–20.

10. Schlenke P, Frohn C, Klüter H, Saballus M, Hammers HJ, Zajac SR, Kirchner H. Evaluation of a flow cytometric method for simultaneous leukocyte phenotyping and quantification by fluorescent microspheres. *Cytometry* 1998, 33, 310–317.

11. Zlatina Becheva, Katya Gabrovska & Tzonka Godjevargova. Immunofluorescence microscope assay of neutrophils and somatic cells in bovine milk. *Food and Agricultural Immunology*, 2017,28, 6, 1196-1210.

DETERMINATION OF TOTAL CELL COUNT AND VIABILITY OF LEUKOCYTES IN BLOOD BY DOUBLE FLUORESCENT STAINING

Milka Atanasova, Yavor Ivanov, Katya Gabrovska
E-mail: milka_88@abv.bg

ABSTRACT

White blood cell (WBC) count is a crucial laboratory test for basic diagnostic practices. A method has been developed to determine the total cell number and viability of white blood cells in fresh capillary and venous blood by a new EASYCOUNTER BC fluorescence microscope (produced by Milko-tronic LTD). The method enables leukocyte counting without any sample pre-treatment. A new DNA – binding dye, TO-DAM-3, is used in combination with acridine orange. Acridine orange is used for staining of the total cell population, whereas TO-DAM-3 is used for dead cells staining. The dye permeates only in dead cells because their cell membrane is compromised. This double staining enables WBCs counting in a single sample, which minimizes the standard error and increases stain-to-stain precision. The optimal working range for measuring WBCs with the EASYCOUNTER BC was determined. The coefficient of variation (CV, %) of the results obtained with EASYCOUNTER BC in the optimal working range varied between 2.85% and 5.7%. This shows that the EASYCOUNTER BC automated fluorescence microscope in combination with double fluorescence staining could be used for rapid clinical diagnostics.

Key words: white blood cells, TO-DAM-3, acridine orange, cell counting

INTRODUCTION

Determination of the number of white blood cells (WBCs) as well as their viability in capillary or venous blood is an important indicator for clinical diagnostics and patient treatment. This analysis is necessary to diagnose infections, allergic reactions, inflammation, blood cancers such as leukaemia or lymphoma, side effects caused by drugs and monitoring of treatment. In some cases, it is crucial to obtain the results as soon as possible in order to accelerate diagnostics and treatment. Determining the number of white blood cells is one of the most common tests that are carried out with patients when their diagnosis is established. Leukocytes are found throughout the body, including the blood and lymph system, and are far fewer than red blood cells [5]. They protect the body against infectious diseases, other foreign agents, and altered body cells [2, 6-8]. As a reference or quantitative limits in adults and adolescents (over 15 years of age), values between 3.5 and 10.3×10^9 G / l are considered normal. Increased leucocyte level is present in various infections, mainly bacterial. The values can reach 30.0×10^9 G / l. All white blood cells have a nucleus that distinguishes them from red blood cells (RBCs) and platelets

and can therefore be coloured when mixed with DNA dyes.

During the 1950s, laboratory technicians counted each individual blood cell underneath a microscope. Generally, the number of white blood cells is obtained by manual microscopic counting procedure, by colouring the blood sample with Giemsa stain (methylviolet, gentian violet) and microscopic examination of the sample in a haemocytometer (for example Burker's Chamber). The method has high standard error due to the human factor. Tedious and inconsistent, this method was later replaced with haematology analyzers.

Fluorescence techniques, which were introduced at the beginning of the century, are now widely used as a research tool in cytology. Blood has been studied by several fluorochromes, including auramine and acridine. Acridine orange is the most popular fluorochrome for studies on whole blood, reticulocyte counting and identification of nucleic acids. It has also been used in cell culture, blood parasites, and certain automated techniques [9, 11]. Furthermore, when such a fluorescence technique is combined with an automated device, a very quick and precise analysis could be developed.

The introduction of automated cell counting devices to quantify the viable number of cells is a much more convenient method due to the removal of the human factor [1, 3, 4]. Replacing the Giemsa dye with a fluorescent dye increases the sensitivity of the analysis. In the present work we used a combination of the well-known fluorescent dye acridine orange and the newly synthesized dye TO-DAM-3.

Acridine orange (AO) is an amphipathic, vital dye that intercalates leukocyte nucleic acids and acidic vesicles. AO has a 450 nm excitation wavelength and has emission peak wavelength at 525 nm (green). TO-DAM-3 has a 627 nm excitation wavelength and has emission peak wavelength at 655 nm (red). Acrid orange is used to stain the entire cell population, while TO-DAM-3 is used to stain dead cells. The dye only penetrates dead cells because their cell membrane is damaged. Thus, living cells can be successfully distinguished from dead cells.

Thus, the number of dead cells is determined, and by the difference of the total number of cells and the listed dead cells the number of living cells is determined and the cell viability is estimated. Therefore, there is a great need for a quick and simple method for white blood cells counting. In addition, devices that can be seamlessly mounted in a variety of clinical applications and even in remote field clinics are needed to provide a quick and accurate analysis.

MATERIALS AND METHODS

Materials

Capillary or venous blood sample was taken from volunteers. Acetic acid, gentian violet, acridine orange, sodium phosphate monobasic monohydrate, sodium phosphate dibasic, sodium chloride from Sigma Aldrich were used. DNA fluorescent dye TO-DAM-3, produced by Milkotronic LTD, was also used.

Apparatus

Easycounter BC Automatic fluorescent microscope equipped with special software, two different light sources (470 and 627) and two separate fluorescent filters. Microfluid camera (cellchip) for sample loading and analysing (Milkotronic, LTD, Bulgaria), Olympus BX51 Microscope.

Methods

Determination of the total count of WBCs using light microscope and lysis of the red blood cells

RBCs affect the correct count of WBCs due to their high count in blood. Therefore, before counting leukocytes, erythrocytes must be lysed. For this purpose, 180 μ l of Turk's reagent were added to 20 μ l of capillary or venous blood sample, the mixture was placed in a haemocytometer (Bürker counting chamber), and WBCs were counted under low magnification [10]. The number of white blood cells was obtained by bright field microscopic examination of the sample.

Determination of total cell count and viability of WBCs in capillary and venous blood using EASYCOUNTER BC and double fluorescent staining procedure

Fresh whole blood was diluted with PBS in a ratio of 1: 4 (Dilution factor 5). 100 μ l of the diluted blood were pipetted in an Eppendorf tube containing lyophilized mixture of the fluorescent dyes acridine orange and TO-DAM-3 (10 μ g/ml). The sample was incubated for 10 minutes at room temperature. The prepared sample was used for determination of WBCs total count and viability.

8 μ l from the samples were placed in one of the channels of the microfluidic camera (cellchip).

Counting and analyzing the total number of WBCs, the number of dead WBCs and the WBCs viability was measured and calculated using EASYCOUNTER BC.

RESULTS AND DISCUSSION

1. Determination of the viability of WBCs in capillary and venous blood using EASYCOUNTER BC

Measurement of the concentration and viability of nucleated cells in clinical samples is difficult to achieve due to the presence of red blood cells (RBCs), platelets and cellular debris. To remove interfering red blood cells, clinical samples are usually pre-treated in order to lyse red blood cells [12]. But even these methods are not always successful in removing all the red blood cells and lead to significant errors in determining white blood cells concentration. Furthermore, when performing this step, a great dilution of the sample is necessary, which additionally complicates microscopic counting.



a)

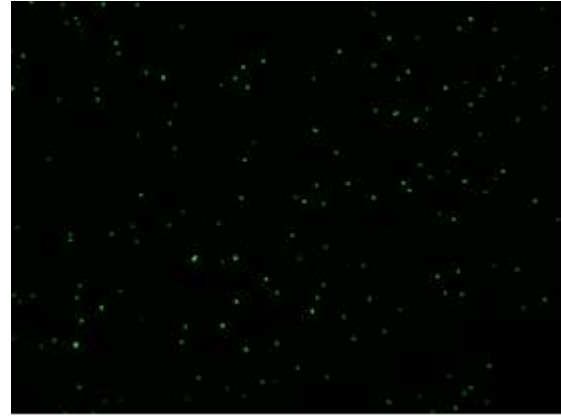


b)

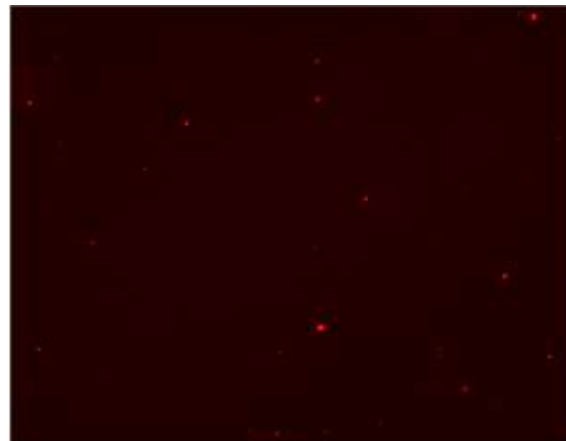
Fig. 1. Bright field images from light microscope of: (a) diluted blood sample (without RBCs lysis), (b) diluted blood sample with lysed RBCs (x 40).

Fig. 1 shows images of blood sample under microscope. On the left, the blood sample is diluted 10 times with PBS, and is not treated in order to remove the RBCs. Their count in the sample is much higher than the WBCs count, which greatly hinders the WBCs observation and makes their correct and accurate counting impossible. Obviously, at high red cells count, the number of observed and counted WBCs is decreased. That is why, the RBCs lysis before WBCs microscopic counting is a must.

On the right, the blood sample is diluted 10 times with 2 % aqueous solution of acetic acid in order to remove the RBCs. The image shows that there is a great decrease in the number of RBCs, which allows the WBCs counting. Nevertheless, there are residual RBCs that could still interfere with the correct WBCs counting.



a)



b)

Fig. 2. Images of stained WBCs: total count (a) and stained dead WBCs (b) obtained by the Easycounter BC automatic fluorescence microscope

Using the fluorescence cell staining method, the need for red blood cells lysis is eliminated. Thus, the concentration and viability of WBCs in capillary and venous blood can be measured without the removal of red blood cells from the sample. Measurement is performed directly with the EASYCOUNTER BC automatic fluorescence microscope. The blood sample is diluted with PBS and stained simultaneously with both the AO and TO-DAM-3 dyes. The DNA dye AO stains the nuclei of all the leukocytes present in the sample, as it is able to penetrate through their membranes (Fig. 2(a)). The other dye, TO-DAM-3 stains only the dead leukocytes in the cell population because their cell membrane is compromised and permeable to the dye (Fig. 2(b)). Live cells do not stain because their cell membrane is intact and impermeable to the dye. In this way, a clear distinction can be made between living and dead cells. Based on these two

results and the built-in software, the viability of the leukocytes is calculated as a percentage.

The automated fluorescent microscope performs the assay automatically as it shoots sixteen pictures with the blue light source and the green filter and after that it shoots the same fields with the red light source and the red filter. Accordingly, all cells in the sample are counted (stained with AO) and only dead cells (stained with TO-DAM-3) are counted. This allows averaging of the results and achieving high precision.

Viability of 10 venous blood samples was determined. Each sample was diluted 5 times with PBS and stained with the mixture of the dyes. After that each stained sample was automatically measured (10 times) using EASYCOUNTER BC and the viability was calculated. All the samples showed viability between 90-98 % which is quite usual considering that the blood samples were obtained and tested in the same day. With such viability ratio the 5-fold dilution was very appropriate as it provides a good number of cells per image for both the total number of cells and for the dead cells. The results were averaged, the standard deviation and the coefficient of variation were calculated. The CV, % varied from 2.2% to 5%, which showed a high accuracy and good correlation.

2. Validation of automatic fluorescence microscopic method for total WBCs count using EASYCOUNTER BC

The total number of WBCs in a sample of venous blood, diluted in PBS at different ratios was determined. After the respective incubation, counting and analyzing the total number of WBCs using EASYCOUNTER BC was performed. In order to validate the method, the same samples of venous blood were treated in order to lyse the RBCs. Then a visual microscopic examination was performed using Bürker counting chamber.

Fig. 3 shows that the results obtained by the two methods are comparable only at some of the dilutions. At the low dilutions the microscopic method is not very reliable due to the interference of the red blood cells, which at such dilutions could not be satisfactorily removed. At dilutions 6, 8 and 10 times both methods showed very close and correlating results. At the high dilutions again a deviation in the results was observed due to the excessively reduced number of cells, which is unsuitable for counting at this scale of the microscope.

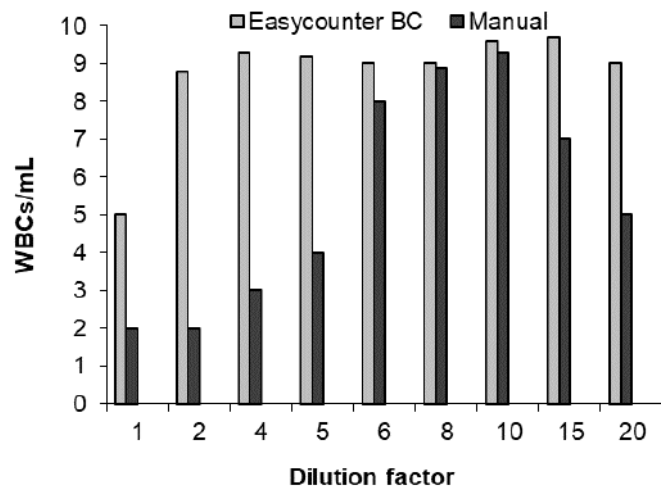


Fig. 3. Total number of WBCs determined by EASYCOUNTER BC and manual light microscopic counting at different sample dilutions

For comparison the developed automatic fluorescence method showed correlating results at almost all dilutions. Only for the first sample (dilution 1 – concentrated whole blood) the obtained results were not reliable. For all the rest of the dilutions the method showed a good correlation and reproducibility.

Furthermore, the developed method has a number of advantages: it does not require red blood cells lysis, takes less time and has lower standard error. Due to the bigger sample volume that is loaded in the cellchip, thousands of leukocytes are counted by the automated techniques in order to obtain more accurate results, whereas in visual examination using a haemocytometer only 100-200 white blood cells are typically tested.

Stain to stain precision of the method was determined. For this purpose, a series of diluted capillary blood was prepared using PBS.

Each dilution aimed to reach a certain concentration range. Each diluted sample was separately stained three times with the DNA fluorescent dye AO and measured 10 times. The results were averaged and plotted in Table 1.

The table shows that at the low number of cells tested (0-10 cells per microliter), the results obtained are either invalid or with a very high deviation. As the number of cells increases, the coefficient of variation decreases, reaching the lowest levels at 500-1000 cells per microliter. Almost all tested concentrations showed good reproducibility of the results and low coefficients of variation. This shows that samples with different cell numbers can be successfully tested and

different dilutions can be applied according to the needs and specificity of the sample, achieving high measurement accuracy.

Table 1. Stain to stain precision of the method considering total leukocyte count

WBCs/ μ l target	Stain N	Mean	SD	Total CV, %
0-1	1	<1	0,43	NA
	2	<1	0,6	NA
	3	1	0,2	NA
5-10	1	7	1,03	14
	2	5	1,2	24
	3	6	1,1	18
20-30	1	26	2,8	10,8
	2	25	1,98	7,9
	3	21	1,3	6,2
50-60	1	48	5,5	11
	2	55	7,3	13
	3	47	4,4	9
80-100	1	82	4,7	5,7
	2	99	6,3	6,3
	3	79	5,5	6,9
200-500	1	318	15	4,7
	2	300	13	4,3
	3	342	12	3,5
500-1000	1	630	18	2,85
	2	665	20	3
	3	672	20	2,9

CONCLUSION

The proposed method for WBCs counting using fluorescent double staining method with AO and TO-DAM-3 and the automatic fluorescent microscope provides fast, accurate and precise results. Using the cell fluorescence method, the need for red blood cells lysis is eliminated. Thus, the concentration and viability of WBCs in capillary and venous blood can be measured without the removal of red blood cells from the sample. The application of these two fluorescent dyes allows the counting of cells to be performed in a single sample, with single dilution step, the total number of cells and the number of dead cells is counted from the same fields, which further increases the accuracy of the analysis. The ready to use lyophilized reagents and the specific software make the assay very easy to perform. The assay allows the elimination of human error and presents the results in a very accessible form. The method could be successfully incorporated in different aspect of clinical diagnostics.

REFERENCES

1. Elhanan, T. and Yelin, D., "Measuring blood velocity using correlative spectrally encoded flow cytometry". *Optics Letters*, 39, 4424–4426, 2014.
2. Fleur-Brooks, M. 2008. "Exploring Medical Language: A Student-Directed Approach" (7th ed.). St. Louis, Missouri, US: Mosby Elsevier. p. 398
3. Golan, L. and Yelin, D., "Flow cytometry using spectrally encoded confocal microscopy". *Optics Letters*, 35, 2218–2220, 2010.
4. Golan, L., Yeheskely-Hayon, D., Minai, L., Dann, E. J. and Yelin, D., "Noninvasive imaging of flowing blood cells using label-free spectrally encoded flow cytometry". *Biomedical Optics Express*, 3, 1455–1464, 2012.
5. Guyton, A. C. and Hall, J. E., *Textbook of medical physiology*. Elsevier, 2010.
6. Houwen, B., "The differential cell count". *Laboratory Hematology*, 7, 89–100, 2001.
7. Illoh, O. C., Current applications of flow cytometry in the diagnosis of primary immunodeficiency diseases. *Archives of pathology&laboratory medicine* 128, 23-31, 2004.
8. O'Gorman, M. R., Zollett, J. and Bensen, N., "Flow cytometry assays in primary immunodeficiency diseases". *Methods in molecular biology*, (Clifton, N.J.) 699, 317–335, 2011.
9. Seligman, P.A., Allen R., Kirkchanski S., Natale P., "Automated analysis of reticulocytes using fluorescent staining with both acridine orange and an immunofluorescence technique", *American Journal of Hematology*. 14:57-66, 1983.
10. Sugiuchi, H., Ando, Y., Manabe, M., Nakamura, E., Mizuta, H., Nagata, S., Okabe, H., "Measurement of total and differential white blood cell counts in synovial fluid by means of an automated hematology analyzer". *Journal of Laboratory and Clinical Medicine*, 146,1, July, 36-42, 2005.
11. Wearne A., Robin H., Joshua D.E., Kronenberg H., "Automated enumeration of reticulocytes using acridine orange". *Pathology*. 17:75-7, 1985.
12. Yeo, C., Saunders, N., Locca, D., Flett A., Preston, M., Brookman, P., et al., "Ficoll-Paque versus Lymphoprep: a comparative study of two density gradient media for therapeutic bone marrow mononuclear cell preparations". *Regenerative Medicine*, 4, 689–96, 2009.

A SUSTAINABLE APPROACH TO CREATING A BIODIESEL SUPPLY CHAIN FROM DAIRY WASTE SCUM

Desislava Nikolova

E-mail: desislava_nikolova@btu.bg

ABSTRACT

Biodiesel is practically an inexhaustible, clean fossil fuel substitute. It can be produced from various substances, including animal or agricultural fats. The growing need for plant oils for biodiesel production has increased the need for alternative sustainable strategies based either on non-food crops or agro-industrial wastes that do not compete with food and feed production. In this study the opportunity for biodiesel production from dairy waste scum has been analyzed. The creation of a sustainable supply chain is a topical area which is continuously developing and that is why the main focus of this study is to create an efficient, sustainable supply chain that minimizes the overall costs for its operation and provides the best scenario for reducing environmental impact throughout the supply chain.

Key words: *biodiesel, supply chain, dairy waste scum, sustainable*

INTRODUCTION

Biofuels are gaining importance as alternative renewable fuels that can cope with major problems caused by the usage of conventional fuels, such as deterioration of the energy supply worldwide, environmental pollution and energy security [1]. The application of biodiesel offers several advantages, such as reduced greenhouse emissions, gaseous pollutants and particulate matter and still biodiesel is usually reported as being costlier than traditional diesel fuel [2]. The high cost of biodiesel is the reason for the continuing work on reducing its production cost in order to make the new biodiesel competitive, because the cost of biodiesel is the main stumbling block to its commercialization [3].

The present work examines biodiesel from dairy waste scum as a suitable alternative for petroleum diesel. A large part of the world population consumes milk and various dairy products on a daily basis. Every day, dairies generate a great percentage of waste scum which is difficult to dispose. In addition, waste oils are a very serious challenge to the environment due to their disposal problems. Biodiesel production from waste milk scum has been analyzed in terms of the process of transesterification by converting waste milk scum into methyl ester and glycerol [4]. One acceptable scenario is transesterification of waste milk scum and its inclusion in the dairy supply chain. The classical dairy supply chain is

a combination of processes, including agriculture, livestock farming, manufacturing, packaging, distribution, retail and consumption [5].

The role of the strategic approach is to provide a solution that addresses sustainability through the Triple Bottom Line Plus method. The TBL β method implements economic optimization, in terms of profit and environmental optimization (with regards to the harmful emissions generated throughout the chain); social optimization, in terms of social aspects; political optimization, in terms of government investment and government support; and technological optimization, in terms of minimizing the total amount of raw materials.

The main asset of the present work is the creation of an efficient, sustainable supply chain in order to minimize the total operating costs of the chain, aiming to provide the best option for reducing the environmental impact of the entire supply chain.

PROBLEM DESCRIPTION

Dairy waste scum as a raw material for biodiesel production

When cleaning the equipment in large dairy vessels, there are specific residues left such as residual butter and fats, which are leached and collected in an effluent treatment plant as dairy waste scum. The dairy waste scum is collected in

a fresh state in the scum removing area of the effluent treatment plant. The scum is a non-solid, dense, floating substance, white in texture and colour because it is usually formed by a mixture of fats, proteins, lipids and others [6]. The following are four basic methods for biodiesel production: blending, micro emulsification, pyrolysis, and transesterification, amongst which transesterification is a well-established and the most common method for biodiesel production.

The chemical composition of dairy scum oil is presented in Table 1 [3].

Table 1. Chemical composition of dairy scum oil

Component	Carbons	Fatty acid%
Butyric	4:0	1.3634
Caproic	8:0	1.4987
Capric	10:0	0.9444
Lauric acid	12:0	2.7176
Myristic acid	14:0	14.3526
Palmitic acid	16:0	42.1390
Steric	18:0	15.7632
Oleic acid	18:1	19.2093
Linoleic acid	18:2	0.4822
Linolenic acid	18:3	0.2509

The high proportions of saturated and mono saturated fatty acids in dairy waste scum oil are considered optimal for fuel production. Polymerization in the combustion of such a fuel would be substantially lower than in the combustion of a fuel derived from polyunsaturated fatty acids.

Properties of scum biodiesel

Viscosity is the most significant factor that influences the fluidity of biodiesel. Viscosity is 3.75 mm²/s at 40 °C, which makes it easier to pump, atomize and achieve finer droplets in the fuel injection system [7]. The flash point is 157°C, which is greater than traditional petroleum diesel. The higher flash point makes storage and transport issues less important. Specific gravity is 0.876; this lower value indicates the completion of a reaction and effective removal of glycerine [8]. Due to the longer fatty acid carbon chain and the more saturated fatty acid, the cetane number is 60 min, which is higher compared to vegetable oils methyl esters [9]. The pour point and cloud point must be considered when biodiesel is to be used in a cold climate. The cloud and pour points, 5°C and 2°C, indicate that scum biodiesel is less suitable for cold

weather conditions. This is due to the high percentage of saturated fatty acid methyl ester.

Biodiesel supply chain from dairy waste scum

The following diagram (Fig. 1) describes the biodiesel supply chain from dairy waste. It includes milk production farms as the supplier of the raw material, dairy plants, customer areas and biorefineries for utilization of the obtained waste products through biodiesel production.

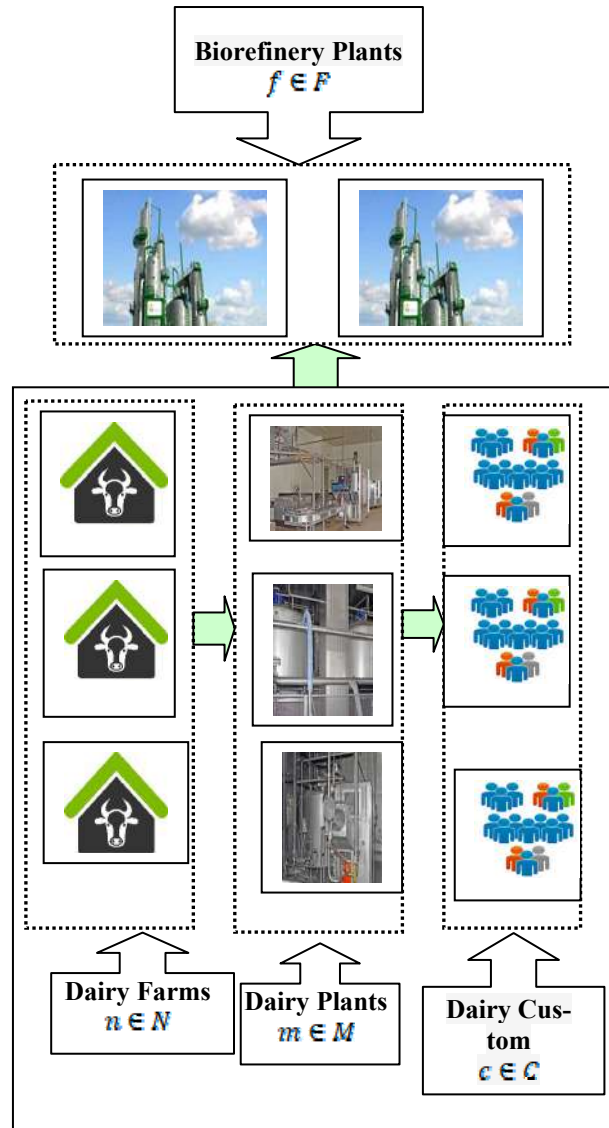


Fig. 1 Structure of biodiesel supply chain from dairy waste scum

where F is a set of candidate regions for biodiesel production;

N is a set of the dairy farms producing milk as a raw material used in dairy plants;

M is a set of the regions in which dairy plants are installed;

C is a set of the regions that use ready-made dairy products (dairy customers).

The problem studied in this paper can be formulated as follows: There are different types of milk products which can be used as raw material for the production of different dairy products. These raw materials can be produced from dairy farms located in different places. Each of these farms has limited productivity and a nomenclature that is known in advance, such as price and the type of transport that can be used for the transportation of milk. On the other hand, it is assumed that there is a set of dairy plants in different places in the current area. For each of these plants, the possibilities for producing the respective final products and the technologies for their production are known, as well as the generated waste products which can be used for biodiesel production. The potential places where biodiesel plants can be installed are various. Biorefineries are amongst the eligible sites for this purpose. At the same time, the places for delivery of the final products, their type and admissible quantity are known. The transport logistics for each type of raw material, final product and waste raw materials is set and the transport capacity, available types of transport, distance and released emissions are known for each of them. With all this information, the task is to determine the optimal operating conditions of the system as a whole.

The evaluation of the operation of the biodiesel supply chain from dairy waste scum system includes all costs for the supply of raw materials, production and transport costs, as well as costs for the construction of the necessary biorefineries. Regarding this, the task is to determine the optimal operating conditions of the system which provide a minimum of the aim function while observing the technological, environmental and time constraints. The environmental impact of the supply chain is measured in terms of total greenhouse gas emissions ($kgCO_2 - eq.$) resulting from the life-cycle activity. They are converted into carbon credits multiplied by the market price of carbon emissions ($kgCO_2 - eq.$). This task can be formulated as a task of Mixed Integer Linear Programming (MILP).

CONCLUSION

The necessity of a good, sustainable substitute for conventional fuels leads to increasing biodiesel popularity. The ongoing humanitarian, economic and environmental crises in different parts of the world are the reason for the high demand for alternative fuels, but the question with the cost of the raw material for biodiesel still remains unsolved.

The article considers dairy waste scum as an alternative raw material for biodiesel production and its inclusion in a sustainable supply chain. This study provides the characterizations of dairy waste scum as a potential raw material for biodiesel production as well as the qualities of the scum biodiesel. The paper presents a model of sustainable supply chain from dairy waste scum.

ACKNOWLEDGEMENT

The study has been carried out with the financial support of the National Science Fund, Ministry of Education and Science of the Republic of Bulgaria, Contract No KII-06-H37/5/06.12.19.

REFERENCES

1. Dutta, K., A. Daverey, J. G. Lin, *Renew. Energy*, **69**, (2014), p. 114-122
2. Demirbas A.H, *Energy Educ Sci Technol*, Part A, **23**, (2009), p. 1-13
3. Sivakumar P., K. Anbarasu, S. Renganathan, *Fuel*, **90**, (2011), p. 147-151
4. Ramalingam S., S. Sudagar, R. Balamurugan, R. Naveen, *Energy Sources*, Part A, (2019)
5. Kirilova E.G., N.G. Vaklieva-Bancheva, *J. of Cl. Prod.*, **167**, (2017), p. 493-504
6. Koley A., T. Samanta, D. K. Singha, *Int. J. for Res. in Appl. Sc. & Eng. Tech.*, **7**, (2019)
7. Islam MN, Islam MN, Beg MRA, *Bioresour Technol.*, **92**, (2004), p. 181-6
8. Sharma YC, B. Singh, SA Upadhyay, *Fuel*, **87**, (2008); (12):2355-73
9. Bala BK., *Energy Educ Sci Technol*, Part A **15**, (2005) p.1-45

STUDY OF THE MACRONUTRIENT COMPOSITION OF CONFECTIONERY OFFERED ON THE MARKET AND ITS PHYSIOLOGICAL INFLUENCE

Galina Grigorova
E-mail: galinakirova@abv.bg

ABSTRACT

A study of the physicochemical composition of 20 assortments of confectionery products, comprising the protein and total fat content, has been carried out. Calculations have, furthermore, determined their total carbohydrates content and energy value. The results show a relatively low protein content of 1.02 g to 9.9 g, high carbohydrate content of 30.85 g to 60.68 g, and fat content of 3.94 g to 31.57 g. Confectionery products are ready-to-eat foods with high "energy density"; they are a source of fast carbohydrates and high-fat content. The data obtained by conducting this study can be used both for labelling confectionery and designing menus in order to reduce the risk of overweight and obesity among a wide range of consumers of this type of food.

Key words: carbohydrates, fats, proteins, rational nutrition

INTRODUCTION

Food has a strong and varied effect on the human body. Both nutritionists and the population get acquainted with the main energy sources in food: fats, carbohydrates and proteins from the information about the energy value of food products. Control over them is important with respect to the healthy nutrition of the population. The World Health Organization identifies obesity as a global epidemic and a significant public health problem. Overweight and obesity among children and adolescents are gaining momentum, especially in developed countries. Various confectionery products are the subject of the present study. The energy value of food is determined in kcal (kilocalories) or kJ (kilojoules), where 1 kcal = 4.1841 kJ. The main energy sources for the body are proteins, fats and carbohydrates. The energy equivalents of the nutrients are as follows: 1g protein is 17 kJ (4 kcal); 1g carbohydrates is 17 kJ (4 kcal); 1g fat is 38 kJ (9 kcal) [1]. The energy balance is positive when the amount of received energy exceeds the amount of consumed energy. In the human body, excess energy is converted into reserve adipose tissue. Under systemic energy intake and overfeeding, body weight increases, and this leads to obesity. The energy received with food by the body must correspond to the consumed energy, therefore it is necessary for consumers to be familiar with

the energy composition of food. Energy demand is the amount of energy a person needs to get from food in order to remain healthy and active [1]. People's energy demands vary from person to person, depending on their body weight, body composition, age, gender, and physical activity. Carbohydrates and fats represent these very important macronutrients that confections carry. Moreover, they are important for the additional energy intake and the risk of unbalanced diets. Carbohydrates are a major source of energy for the body and play an important role in the proper functioning of the immune system, blood clotting, and overall human growth [2].

The aim of the present study is to determine the content of the main macronutrients, proteins and fats in different types of confectionery and to present the carbohydrate and energy content of the studied confectionery in order to properly inform consumers about their nutritional values. The data can be used for correct labelling of products and shaping a daily diet associated with limiting the risk of overweight and obesity among the population.

EXPERIMENT

Materials and methods:

The study was conducted in 2019-2020. Twenty types of confectionery, such as cakes, pastry, cookies, etc. were analyzed for protein

content and total fat. The following verified test methods were used to reach the results: proteins according to BDS 3412 article 3.9: 1979 [4] and total fats according to BDS 5439: 1985 [9].

The carbohydrate content as well as the energy content of each of the studied types of confectionery were calculated.

RESULTS AND DISCUSSION

Food is vital for structuring and development of the human body, for ensuring the maintenance of a constant set of conditions in metabolic processes and physical activity. The normal functioning of the human body depends on the energy received from food, which varies for each individual. Age, health and physical activity play a central role and require different amounts of energy. Energy value is one of the basic indicators for determining scientifically based physiological norms for proper nutrition of the population. The European Commission considers that it is appropriate to provide the mandatory information on the nutrition facts label per 100g or 100ml.

A study analyzing the content of the main macronutrients in different varieties of confectionery has been conducted. Carbohydrate and energy content of confectionery products has been presented in order to correctly inform consumers about the nutritional value. The obtained information can be useful for correct labelling of products and for the preparation of daily diets with the purpose of limiting the risk of overweight and obesity among the population. Various kinds of confectionery products with high carbohydrate content have been analyzed during the course of this study. Carbohydrates play a central role in a person's diet. Their main function is to provide energy. They provide more than half of the energy value of a daily ration of the human body. Carbohydrates are building blocks which are important for the correct operation of the intestines. They are a source of energy for the normal function of intestinal microflora.

Sweet carbohydrates, mono- and disaccharides improve the taste of food. Some important sources of carbohydrates are: cereals, flour, pasta, sugar and confectionery, kitchen desserts, etc. But confectionery, such as cakes, pastries, cookies, along with the carbohydrates in flour and sugar, also contains large amounts of fats. Fats, which are present in many foods, are found in large quantities mainly in products of animal origin, such as meat and dairy. The results obtained from the physicochemical analysis of macronutrients in pastries, confectionery rolls, cookies, and cakes are presented in Table 1. Confectionery is not the main source of protein. The results show that it contains small amounts of protein, as the highest protein values however belong to the confectionery known as meringue, which still depends on the recipe. Carbohydrates predominate, ranging from 30.85 g to 60.68 g. The fat content in different confectionery products ranges from 8.3g to 31.57g, and varies depending on the recipes. It strongly affects the energy content of different types of products. Fats have the greatest possible effect if the ration contains almost equal amounts of vegetable, milk and other animal fats. The recommended balanced ratio of protein and fat in grams is 1:1 for students. Fat is the source of energy with the highest energy equivalent. Foods high in fat (20-40 g) include caramel cake 26.42 g, Garash cake 27.32 g, truffle cake 30.32 g, cheesecake with caramel 24.22 g. Products with moderate fat content (10-19g) include cake 11.03 g, cookies 11.85 g, éclair 16.39 g, cherry paste 18.81 g, chocolate paste 13.24 g, butter cream cake 14.4 g, sweets with sugar syrup 14.29g. Low fat products (3-9 g) include meringue 3.94 g and cake with vegetable oil cream 8.30 g. Food products with very low fat content (<3g) include the sweet beverage *boza* with 0.2 g (this product also has the lowest protein content of 1.02 g). A study conducted on similar indicators in confectionery shows a fat content of 16 to 30% and a carbohydrate content of 62 to 75% [3].

Table 1. Macronutrient content and energy in 100 g net weight of confectionery

No	Types of confectionery	Proteins (g)	Fats (g)	Carbohydrates (g)	Energy value kcal / 100g	Energy value kJ / 100g
1	Caramel Cake	5.50	26.42	53.79	474.9	1985.47
2	Cupcake	7.24	11.03	51.94	336.0	1414.17

3	Cookies	6.12	11.85	42.43	300.9	1263.80
4	Meringue	9.9	3.94	60.68	314.5	133.9
5	Small sweets	5.49	31.57	53.32	519.4	2167.86
6	Chocolate roll	2.76	20.47	53.19	404.0	1708.54
7	Eclair	7.22	16.39	30.9	300.0	1254.47
8	Boza	1.02	0.2	10.11	46.32	196.61
9	Fondant mini cake	3.81	9.15	52.48	307.5	1295.48
10	Cherry mini cake	3.20	18.81	47.42	371.8	1556.51
11	Chocolate mini cake	2.59	13.24	52.76	340.6	1430.83
12	Revane	4.64	6.79	54.05	295.5	1248.96
13	Garash Cake	5.67	27.32	34.79	401.7	1698.7
14	Butter Cream Cake	2.94	14.4	53.58	355.7	1493.6
15	Cake with vegetable oil cream	4.33	8.30	49.98	291.9	1230.4
16	Truffle Cake	2.84	30.35	34.61	423.0	1759.6
17	Cheesecake	5.52	19.58	30.85	321.7	1342.8
18	Cheesecake with caramel	4.07	24.22	23.95	329.9	1372.0
19	Tulumba	2.61	14.27	53.0	350.9	1473.4
20	Caprice mini cake	4.28	12.5	52.41	335.2	1409.58

Nutrition, as a basic life process, is related to the reception, processing and digestion of food from the environment, necessary for the construction and renewal of cells and tissues, implementation and regulation of vital functions. Prolonged nutrient deficiency or excess often leads to disease. In medicine, a rational diet is defined as a healthy and optimal diet, which adequately meets the body's needs for energy and nutrients with a certain quantitative and qualitative composition. This satisfies the needs for growing up, helps maintain optimal body weight and well-being, increases the body's resistance to diseases and adverse environmental factors, maintains the optimal level of life processes in a variety of working and living conditions, ensures physical and mental health and the creation and development of a healthy and viable generation. In order for nutrition to be rational, it must meet certain requirements and principles. Nutrition must meet the body's energy needs to maintain metabolism and physical activity and satisfy the processes of growing up, pregnancy, lactation and muscle mass accumulation. The basis of rational nutrition is the principle of balance, which ensures optimal satisfaction of the body with nutrients and biologically active substances in strictly defined quantitative and qualitative

ratios. The food should contain balanced proportions of basic nutrients: Proteins (P), fats (F), carbohydrates (C). When feeding adults, the quantitative ratio P: F: C is recommended to be 1: 1: 4. When performing heavy physical work, the relative proportion of carbohydrates can increase to 1: 1: 5 (6). Intensified growth can increase protein, and the diet of the elderly can reduce fat to 1: 0.8: 4, while increasing the relative proportion of vegetable fat, fish oil and milk fat (containing short-chain fatty acids that are absorbed directly into the blood [7]).

The energy value of the studied confectionery products is high and is a result of the high carbohydrate and fat content. The performed physicochemical analyses of the content of macronutrients in the various confectionery products show that this type of ready-to-eat foods are high-energy holders of carbohydrates and fats.

REFERENCES

1. Nesterova V., Food Hygiene and Food Legislation, 2014
2. USDA National Nutrient Database for Standard Reference, Release 2010, Top 10 Foods Highest in Carbohydrates (To Limit or Avoid), 2010, www.healthaliciousness.com.

3. Gyurova D., Enikova R., Science Dietetics, 1-2 (17), VI, "Study of the macronutrient composition of 18 types of confectionery offered on the Bulgarian market." (2014). p.42-46
4. BDS 3412 Bread and bakery products. Sampling rules and test methods
5. Ordinance No 1 of 2018 of the Ministry of Health on the physiological norms for nutrition of the population.
6. Regulation (EU) No 1169 / 2011 of the European Parliament and of the Council of 25.10.2011 on the provision of food information to consumers.
7. Garchev R., Guide for practical exercises in Physiology, Medical Publishing House, 2015
8. Gogov, J., S. Chomakova., D. Popova, Lillova., Yurukov, Labeling of the nutritional value of meat products, 2015
9. BDS 5439: 1985 Confectionery. Physico-chemical tests. Method for determination of sugar and oil content.

ULTRASONIC DISTANCE MEASUREMENT SYSTEM

Ivaylo Belovski
E-mail: ivbel@abv.bg

ABSTRACT

Ultrasonic sensors are widely used in modern sensor systems. They can discover objects made from various materials regardless of their colour, shape, size or the disturbances present in the atmosphere. Their work is based on the principle of echolocation. The high particulate matter content and small depositions on sensor surface have practically no effect on the serviceability. In the present paper, a technical solution for such a sensor system for registration of objects and measuring the distance to them in the range from 2 cm to 400 cm is presented.

Key words: *ultrasonic, Arduino, sensor system*

INTRODUCTION

The registration of objects in the processes of industrial automation is realized by contact and contactless sensors. Mechanical switches can be used as contact sensors for the presence of an object. They generate an on/off type signal caused by mechanical contact with the object. When the pressure exerted by the object disappears, the switch goes back to its initial state.

Contactless sensors do not need to touch the moving object. Their output signal is a function of the mutual position of the sensor and the object. Among the advantages of these sensors are their high reliability as there are no mechanical contacts between the object and the converter, no friction, wearing down, noise or change of the transitional resistance.

One disadvantage, however, is the non-linear conversion function. These converters can work in analogue or discrete mode. In analogue mode, the output signal is a continuous function of the distance between the converter and the object. In discrete mode, there are two discrete levels of the output signal – high and low. The high output level indicates the presence of an object located within certain distance from the converter. The low level indicates the absence of objects if the object is too far away from the converter. Proximity converters are usually used in discrete mode of operation. Depending on the physical principle used, they can be: inductive, eddy current, ultrasonic, optic, etc.

Ultrasonic sensors can discover objects made from any material reflecting the sound waves despite its colour, shape, size or the presence of disturbances in the environment [1-3]. High dust

content in the air and small depositions on the sensor surface have practically no effect on their serviceability.

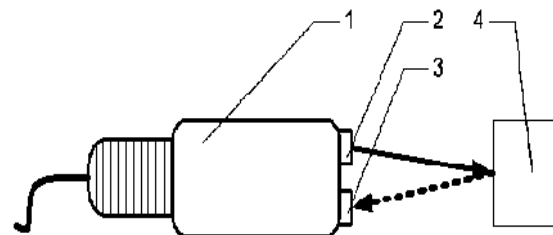


Fig. 1. Ultrasonic converter of proximity: 1 – sensor body; 2 – ultrasonic emitter; 3 – ultrasonic receiver; 4 – object

In this type of sensors, an ultrasonic emitter and a receiver are used (Fig.1). The ultrasound emitted is reflected by the object and travels back to the receiver. They are characterized by high noise resistance, fire and explosion safety, simple design, resistance to shock and vibrations, a wide range of temperature and pressure, high accuracy and speed. For these reasons they are widely used in the industry.

Another type of widely spread sensors for measuring distances is the optical ones (Fig. 2). Their operation is based on the interaction (interruption, passing through or reflection) of the generated light beam with the object [4-5]. The beam is generated by electron circuitry. The receiver is usually a photodiode or a photoresistor with the same spectral characteristics as the emitter. To limit the operation of the receiver to register only the light generated by the emitter, two solutions are commonly used: pulse operation or

synchronous detector which reacts only to pulses with the frequency used by the emitter. For many kinds of optical sensors, the beam is generated by a light emitting diode working in the visible or infrared spectrum.

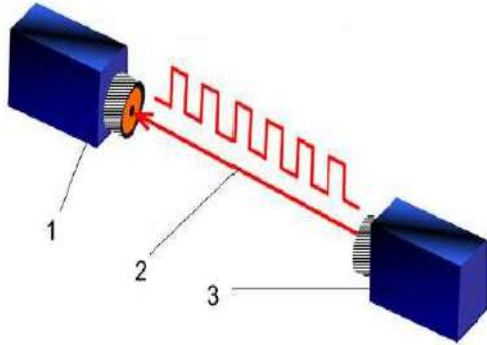


Fig. 2. Optical sensor for registration of objects

Besides IR LED, laser diodes are also used in optical sensors. One such sensor is the sensor type **ST VL53L0X**. It detects the presence of objects located at distances from 1 cm to 200 cm with 1 mm resolution. It has an I2C digital interface and is not affected by the colour or the surface of the detected object (Fig.3). It is powered by 2.6V – 5.5V voltage through an embedded voltage regulator. To the digital interface, a logical level converter was added allowing connection with microcontrollers with working voltage in the range of 2.6V - 5V.

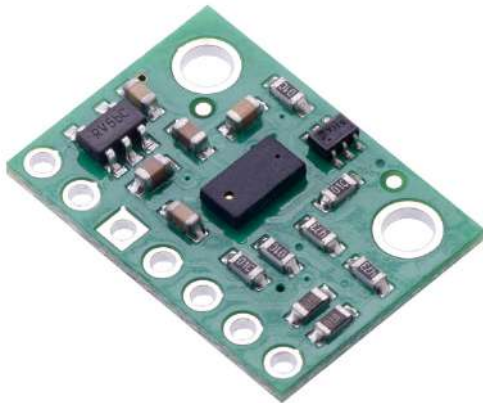


Fig. 3. Distance sensor - ST VL53L0X, I2C

Another popular module for measuring distances is **Benewake TFmini LiDAR, UART** [6]. The module detects the presence of objects at distances up to 7 m (up to 12 m indoors) with resolution of 0.5 cm and frequency of measurement 100Hz. It contains UART TTL interface and is powered by voltage of 5 V. The common

current consumption is 25mA (up to 800 mA in peak performance). The working voltage of the interface is 3.3 V (Fig. 4).



Fig. 4. Distance sensor - Benewake TFmini LiDAR, UART

The aim of the present paper is to present a technical solution for registration of objects of any type and measuring the distance to them in the range from 2 cm to 400 cm.

PRESENTATION

The block diagram of the sensor system designed is presented in Fig. 5.

Block Arduino – This is the main unit of the sensor system which receives and processes the information gathered by the sensors, sends it by Bluetooth connection to the mobile device and initiates the indication. Version Arduino Pro Mini was selected (Fig. 6). It is based on Atmega 328 microcontroller.

The LED indication unit is used to visualize the distance measured to the object. It has the shape of an arrow (Fig. 7), on which there is a LED matrix of 8 bi-colour LEDs.

LEDs emit solid green (when no object is detected). When an object is detected, voltage is supplied to the LED corresponding to the distance and it changes its colour to red. Eight pins are used to control the LEDs.

The Ultrasonic Sensor unit is based on sensor type HC – SR04.

The ultrasonic sensor for distance HC-SR04 ensures contactless measurement of distances from 2 cm to 400 cm at a resolution of 3 mm.

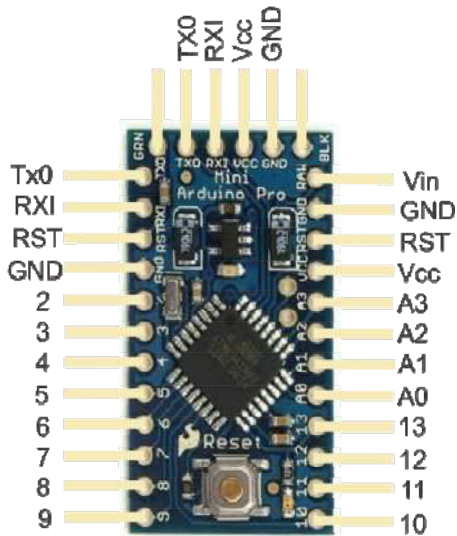
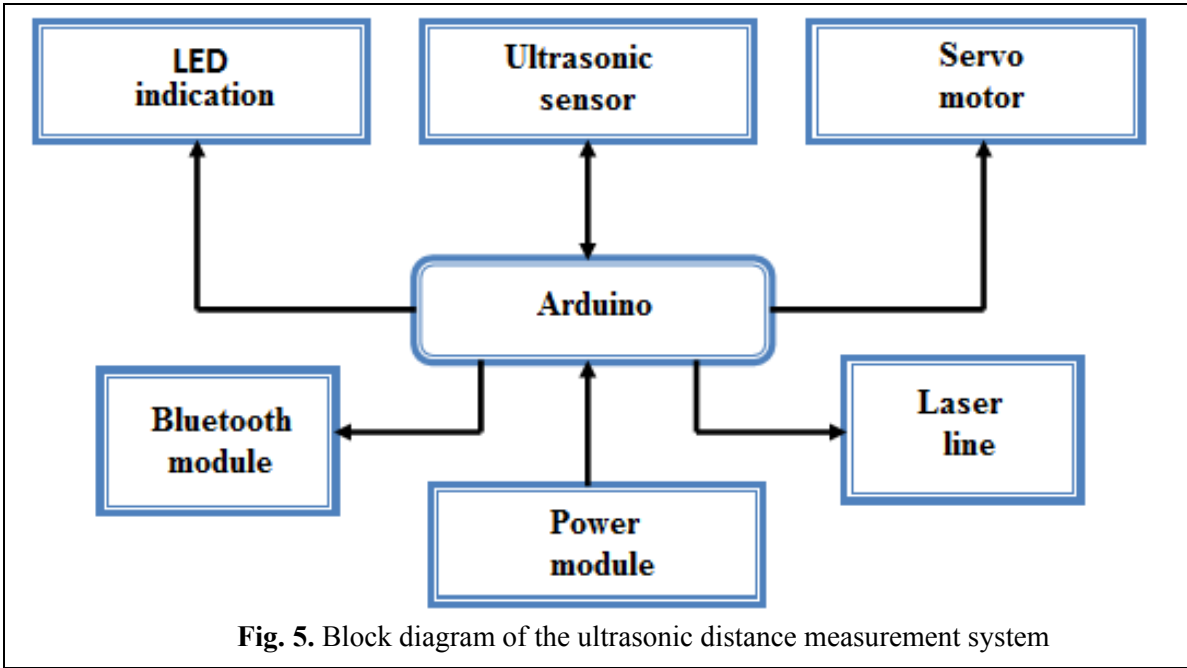


Fig. 6. Microcontroller circuit board Arduino ProMini

The sensor comprises an ultrasonic emitter, a receiver and a circuit for measurement and control. The appearance of the sensor is presented in Fig. 8. The sensor operation is based on the principle of echolocation. The module sends an ultrasonic signal and receives its reflected signal from the object. Measuring the time from the moment of emitting of the pulse to the moment of receiving the reflected signal, it is possible to calculate the distance to the object. The pins Vcc and Gnd are used for the power supply while the pins Trig and Echo are used for emitting and receiving the pulsed sequences. [7].



Fig. 7. LED indicator arrow



Fig. 8. Ultrasonic sensor for distance HC-SR04

Servomotor unit: it is built on the basis of servomotor type – MICRO R/C Servo, which is used to control the direction of movement of the ultrasonic sensor.

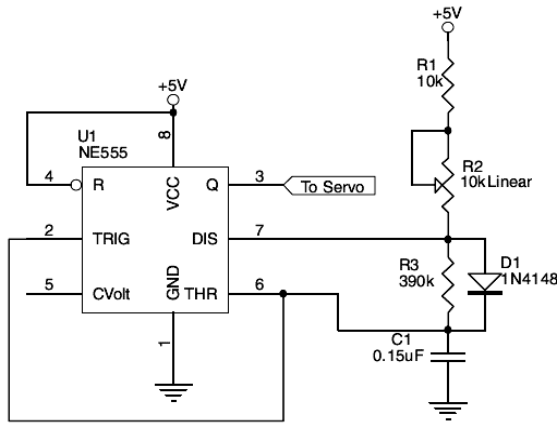


Fig. 9. Circuit of the control pulses sent to the servomotor.

The control pulses to the servomotor can be generated by a comparatively simple electronic circuit composed on the basis of timer 555 (Fig. 9).

The length of the pulses generated is calculated as follows:

$$T_H = 0,693 \cdot (R_1 + R_2) \cdot C, \quad T_L = 0,693 R_3 \cdot C \quad (1)$$

Since R_2 is a variable resistor, then the high level signal will vary in the range:

$$0.693(10k + 10k)0.15e^{-6} = 2.079mS \quad (2)$$

$$0.693(10k + 0)0.15e^{-6} = 1.039mS \quad (3)$$

Bluetooth module unit: this unit is realized on the basis of module HC – 06 and its aim is to send wirelessly information to a mobile device (Fig. 10).

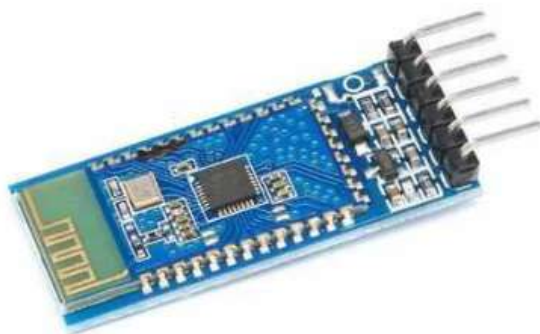


Fig. 10. General view of the Bluetooth module HC – 06

HC – 06 is composed of a serial Bluetooth 4.0 BLE HM 10 module. It is powered and operates with voltage of 3V – 5V, and it also has a TTL

interface, embedded antenna and one LED. It is configured by default with pair code 000000 and exchange rate of 9600 bps.

Laser line unit: this unit is realized with a module based of solid state laser (light emitting diode). Power - 5 mW, wave length - 650 nm, power supply - 5 V. Red coloured light in the visible spectrum. This unit is used for better visualization of device operation as it shows the direction of the ultrasonic sensor.

Power supply unit: the unit provides power supply to the microcontroller circuit with voltage of $U=5V$. It is realized with a standard power supply unit (a mobile phone charger) with output voltage of 5V and nominal current of 1A. The power consumption of the device does of exceed 500mA.

Fig. 11 shows the fully assembled sensor system.

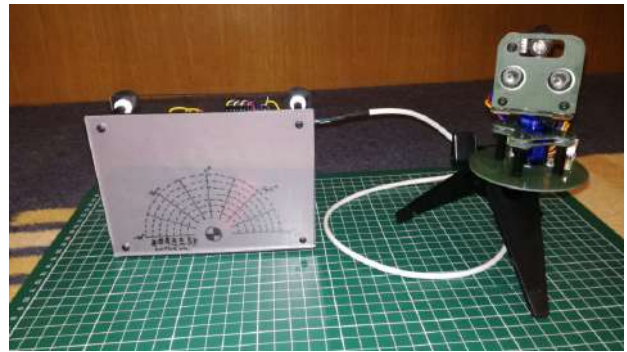


Fig. 11. General view of the ultrasonic system

CONCLUSION

A project has been designed and a prototype of an ultrasonic system for the detection of objects of any kind and measuring the distance to them in the range from 2 cm to 400 cm has been prepared. The information obtained from the measurement is transmitted to a mobile device and simultaneously indicated by the system. Complete software for the individual modules has been made.

ACNOWLEDGMENTS

This work was supported by the Bulgarian Ministry of Education and Science under the National Research Programme “Young scientists and postdoctoral students”, approved with DCM #577/17.08.2018.

REFERENCES

1. Zou Yi, Ho Yeong Khing, Chua Chin Seng and Zhou Xiao Wei, 2000, *Multi-ultrasonic sensor fusion for mobile robots*, Proc. of 2000 IEEE Int. Symposium on Intelligent Vehicles, pp. 387-391.
2. Heale A., L. Kleeman, 2001, *Fast Target Classification Using Sonar*, Proc. of 2001 IEEE/RSJ Int. Conf. on Intelligent Robots and Systems, pp. 1446-1451.
3. Kai-Tai Song; Chih-Hao Chen ; Cheng-Hsien Chiu Huang, 2004, *Design and experimental study of an ultrasonic sensor system for lateral collision avoidance at low speeds*, IEEE Intelligent Vehicles Symposium, DOI: 10.1109/IVS.2004.1336460
4. Tamiya N., H. Mandai, T. Fukae, 1996, *Optical spread spectrum radar for lateral detection in vehicles*, Proc. of 1996 IEEE Int. Symposium on Spread Spectrum Techniques and Applications, pp. 195-198.
5. Fukae T., N. Tamiya, H. Mandai, 1996, *Lateral distance measurement using optical spread spectrum radar*, Proc. of 1996 IEEE Int. Symposium on Intelligent Vehicles, pp. 1-6.
6. <https://lightwarelidar.com>
7. <https://cdn.sparkfun.com/datasheets/Sensors/Proximity/HCSR04.pdf>

SELECTION OF IMMERSION TRANSDUCERS FOR INVESTIGATION OF PELTIER MODULE

Radostin Kasarov

E-mail: diagnostika.kasarov@abv.bg

ABSTRACT

Six different notches on one penetrometer have been examined by ultrasonic immersion technique. Ten types of transducers with frequencies from 1 to 10 MHz have been used. A comparison of the acoustic signals reflected from the investigated penetrometer has been carried out. Measurements of Ultrasound path and wave attenuation have been accomplished. Based on ultrasonic investigations, proper transducers for characterizing the thermoelectrical properties of Peltier Modules are selected.

Key words: *immersion ultrasonic method, ultrasonic attenuation, sensitivity, screen resolution, Peltier module*

INTRODUCTION

Ultrasonic testing is a non-destructive technique for examination of solid (typically metallic or ceramic) components and materials. It can be used for detection of cracks and flaws as well as for material characterization [1, 2, 3]. The ultrasonic test method operates on the principle of injecting a very short pulse of ultrasound from a transducer into a component, and then receiving and analyzing any reflected sound pulses. The frequency of ultrasound pulses must be carefully selected to provide a proper balance between image detail and depth of penetration. In general, high frequency pulses produce higher quality images but cannot penetrate very far into the test material.

The major element in the transducer is a crystal size or diameter size designed to vibrate with the desired frequency. A given transducer is often designed to vibrate with only one frequency, which is its resonant frequency. Therefore, the only way to change ultrasound frequency is to change transducers. This is a factor that must be considered when selecting a transducer for a specific experimental procedure. Certain frequencies are more appropriate for certain types of examinations than others. The ability to conduct and interpret the results of an ultrasound

examination depends on a thorough understanding and practical experimentation of these ultrasound interactions.

Typically, a researcher scans a transducer on the surface of the component in such a way as to check the entire area to be tested by scanning motion. One way to couple the sound from a transducer to a test object is to apply a liquid, usually water, which conducts the sound between the probe and the test material. This technique is known as immersion testing. In immersion testing, the transducer is placed in the water, above the test object, and a beam of sound is projected.

EQUIPMENT

A typical experimental equipment consists of ten immersion transducers, a Krautkramer-Branson ultrasonic flaw detector and a special specimen – penetrometer, controlled by UV-radiation [4]. The transducers are selected to transmit compression waves of 1, 2, 4, 5 and 10 MHz into the material at a chosen focal distance shown in Table 1.

The penetrometer is made from titanium with a thickness of 3.94 mm as a Peltier Module [5] and size of 50 mm in length and 15 mm width and has six notches (steps) with sizes shown in Table 2.

Table 1. Transducers characteristics, focal distance and frequency range

Transducer	Element Size [mm]	Focal distance [mm]	Ultrasonic wave shape	Frequency range [MHz]
Z1N	Ø 20	64 *	detachable collar	0.5 - 4
Z2K	Ø 10	32 *	detachable collar	0.5 - 4
Z4K	Ø 10	64 *	detachable collar	0.8 - 8
Z5K	Ø 10	80 *	detachable collar	0.8 - 8
Z5M	Ø 5	20 *	detachable collar	0.8 - 8
Z10K	Ø 10	160 *	detachable collar	2 - 20
Z4KL20	Ø 10	20	detachable collar line focus	0.8 - 8
Z4KP20	Ø 10	20	detachable collar point focus	0.8 - 8
Z10ML15	Ø 5	15	line focus	2 - 20
Z10MP15	Ø 5	15	point focus	2 - 20

*Near field length – Fresnel zone

Table 2. Notches (Steps) characteristics

Size	Step No.1	Step No.2	Step No.3	Step No.4	Step No.5	Step No.6
Length [mm]	15	15	15	15	15	15
Depth [mm]	2.55	2.08	1.45	1.09	0.85	0.69
Width [mm]	2.7	2.05	1.48	1.08	0.76	0.41

EXPERIMENT

The test penetrometer is positioned in a small water-filled tank. An ultrasound probe is then moved on a horizontal axis at constant distance to the penetrometer (Fig. 1). The sound travels through the water and into the penetrometer. Following the sound's interaction with the exterior and interior microstructure, any flaws that may exist, or with the inner surface of the component, the echoed sound wave returns to the probe.

RESULTS

When using the immersion method, the image of soundwave peaks is slightly different from the contact technique. In this case there is an additional peak between the initial pulse and the back wall peaks caused by the sound wave going from the water to the test material. The arrival time of the echo and its amplitude enable interpretation of where and what it is originating from in the material. Some energy is lost when the waves hit

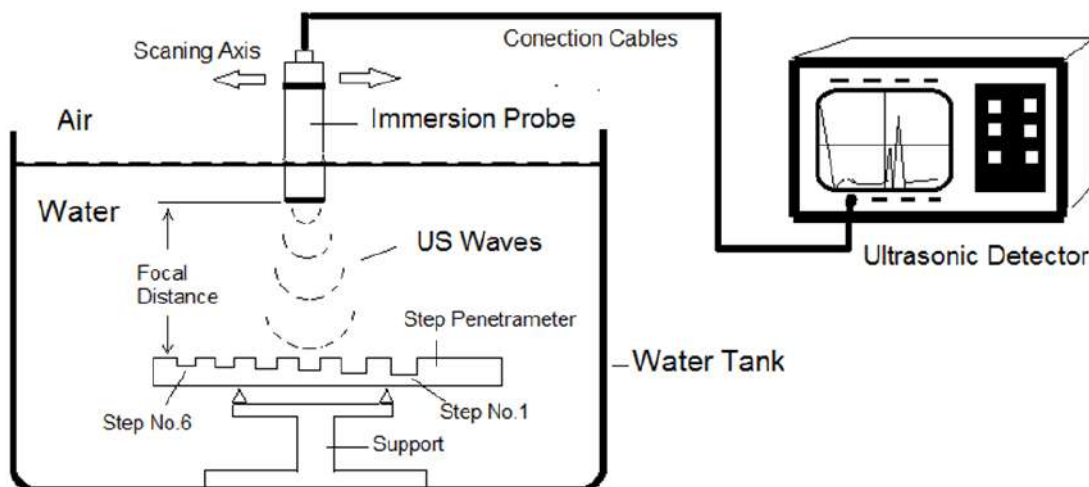


Fig. 1. Experimental set-up

the test material, so the front wall peak is slightly lower than the peak of the initial pulse. The rate at which an ultrasound pulse is absorbed generally depends on two factors: the material through which it is passing and the frequency of the ultrasound. The attenuation rate is specified in terms of an attenuation coefficient. Its value for water is 0.002 dB/cm.

The ultrasonic detector USM35XS is adjusted to ignore the initial pulse peak, so the first peak it will show is from the front wall of the penetrameter (from notches side).

The data obtained for the all penetrameter steps show different signal amplitude from transducers in respect to the screen position shown in Table 3, but only the data obtained for the Z4KL20, Z4KP20, Z10ML15 and Z10MP15 transducers show a good signal resolution, as can be seen in Fig. 2. In this case we get a higher amplitude with transducers Z4KL20 (4MHz) and Z4KP20 (4MHz) than that with transducers Z10ML15 (10MHz) and Z10MP15.

Table 3. Adjusting the sensitivity in dB for different types of transducers in respect of the registered back pulse echoes from penetrameter steps

Transducer	Step No.1	Step No.2	Step No.3	Step No.4	Step No.5	Step No.6
Z1N	24	23.5	23	23	23	23
Z2K	25	25	24	24	24	24
Z4K	29	28.5	28	28	28	28
Z5K	31	31	31	31	30.5	31
Z5M	31	31	31	31	31	31
Z10K	43	42.5	42	42	42	42
Z4KL20	32.5	32	31	29.5	29	28.5
Z4KP20	33	32.5	32.5	31	31	31
Z10ML15	47	46	45	45.5	45	45
Z10MP15	46	45	45	45	44	44

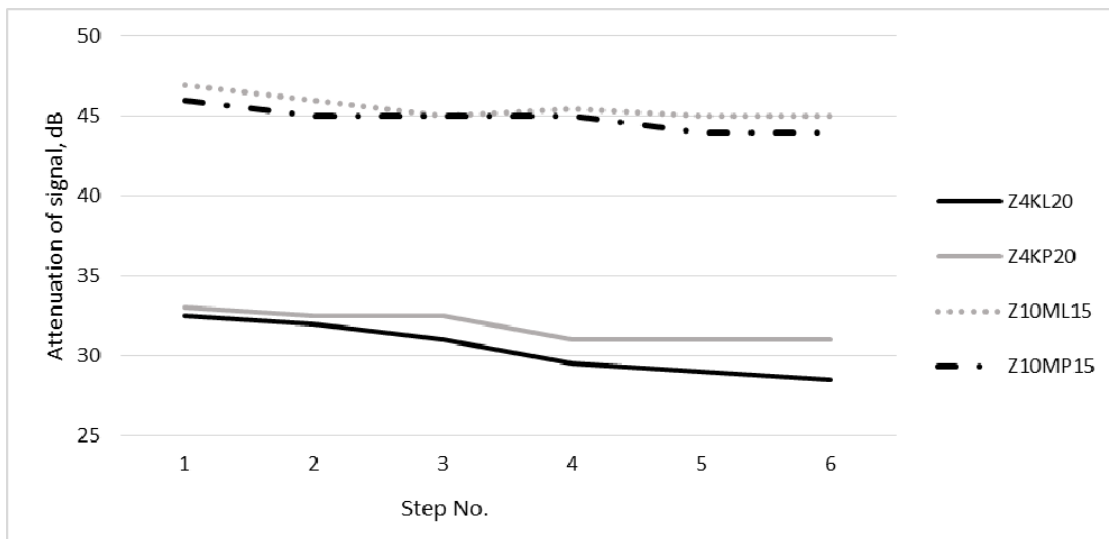


Fig. 2. Signal attenuation for selected transducers

CONCLUSIONS

The conducted experiments show that the applied non-destructive testing method can serve as a comparison between the different materials in

terms of structure and homogeneity, as well as for quality control without disturbing their integrity.

The results of the research conducted with the immersion method show that we can confidently

distinguish the steps with a different depth and width.

In ultrasound imaging the significance of wavelength is that short wavelengths are required to produce short pulses for good detail (in the depth direction) and this requires higher frequencies. The data obtained for all steps unambiguously show a good signal resolution and amplitude with respect to the screen position of the Z4KL20, Z4KP20, Z10ML15 and Z10MP15.

The results are obtained with the optimal adjustment mode: sensitivity of 29-33 dB in frequency range at 5-10MHz. With the same parameters for transducers Z4KL20 and Z4KP20 with detachable collar line and point focus we get a higher amplitude than that of the transducers Z10ML15 and Z10MP15.

The observations during the experiment show minimal but sufficiently distinct and well reproducible differences in a sample of the same thickness as a Peltier Modules, which may be a criterion for characterizing the electrical and thermal properties of Peltier Modules. The co-application of this method with electrical measurements ensure a better study and correct selection of Peltier Modules regarding their appli-

cations in various electronic devices.

REFERENCES

1. Hübschen, G. *Ultrasonic techniques for materials characterization*, In: *Materials Characterization Using Nondestructive Evaluation (NDE) Methods*, pp. 177-224.
2. Ramzi, R., M. F. Mahmud and E. Bakar. *Immersion ultrasonic inspection system for small scaled composite specimen*, *Journal of Engineering and Applied Sciences* 10 (22), 2015, 17146-17150.
3. Kasarov, R. *Investigation of Polymeric Materials by Means of Electro Acoustic Methods*, *Assen Zlatarov University Annual*, Vol. XLVII, Book 1, 2018, p.97.
4. Nikolaeva, Z. and T. Mihalev, *Modeling ultraviolet radiation for Burgas Municipality*, *International Scientific on-line Journal Science & Technologies*, Stara Zagora, Bulgaria, IV (3), 2014, pp. 15-19.
5. Belovski I., A. Aleksandrov, K. Teodosios. *Study of operation of Peltier modules in cascade*, *International Scientific Conference UNITECH 2017 - Gabrovo, Proceedings*, vol. 1, 2017, 207 – 211.

RADIOLOGICAL MONITORING OF THE WORKING ENVIRONMENT

Radostin Kasarov, Plamena Atanasova, Sabina Nedkova
E-mail: *diagnostika.kasarov@abv.bg*

ABSTRACT

Background radiation is all around us and forms the environment in which everyone lives and works. Depending on the main source that provides it, background radiation sources can be natural, artificial and technologically modified. Monitoring of the background radiation of the environment, or radiological monitoring is the process of measuring the dose rate of ionizing radiation due to radioactive substances in the environment, or measuring the concentration of radionuclides in the components of the environment (air, water, soil, vegetation). This type of monitoring is part of the assessment of the working environment, whose main task is to provide protection and safety at work, by identifying radioactive hazard as part of the working space.

Key words: radiological monitoring, working factors assessment

INTRODUCTION

Ionizing rays from natural or artificial radioactive sources are extremely dangerous to living organisms because they have no senses to recognize and avoid them. The biological effect of ionizing radiation is due to its high energy, the lack of any sensation at the time of irradiation, as there are no receptors for this type of energy in living organisms and the large discrepancy between the absorbed energy and the radiobiological effect. For example, exposure to a lethal dose of 10 Gray (1000 R) will increase the body temperature by 0.01° C.

The monitoring of the radiation background of the environment in which people live and work is part of the monitoring of the physical factors of the environment and is a very important part of ensuring healthy and safe working conditions. By order of the Minister of the Environment and Water, a program for continuous and periodic monitoring of radiation parameters has been approved, and implemented by the National System for Radiological Monitoring of the Environment. Its aim is to detect deviations from permissible values in the main components of the environment: atmospheric air, water and soil. The permissible values of the radiation background, or the so-called dose rate of the equivalent dose of gamma radiation, are measured in $\mu\text{Sv/h}$ (microsieverts per hour), and the safe values of the natural radiation gamma background are in the range 0.06-0.40 $\mu\text{Sv/h}$.

EXPERIMENT

The objects of the present study is the assessment of the background radiation of an outdoor work environment in the campus of University Prof. Dr Assen Zlatarov University in Burgas with coordinates: 42° 527936 N and 27° 446122 E and the manner and accuracy of operation of three dosimetric instruments. The measurement of gamma radiation background (gamma radiation dose rate) and measurement of volumetric activity of natural and man-made radionuclides in atmospheric air on the chosen day, 7th of July 2020, was carried out with dosimetric control devices from three different manufacturers: SEIFERT - FAG, Bella and Graetz (Fig. 1).



Fig. 1. Dosimetric control devices used in the experiment for background radiation assessment

Together with the background radiation, other indicators of the environment were assessed too, namely illuminance (Lux) and humidity (%) with M1156 device, amount of O₂ with DRAEGER gas analyzer), wind speed and direction with HUGER anemometer and temperature. For ob-

jectivity of the results, the tests during the three parts of the day, morning, noon and evening, were summarized and presented with the letters A, B, C, and the dosimeters used were marked with: D₁ (FAG), D₂ (Bella) and D₃ (Graetz).

RESULTS AND DISCUSSION

The results summarized by hours and measuring devices are shown in Fig. 2 - 4.

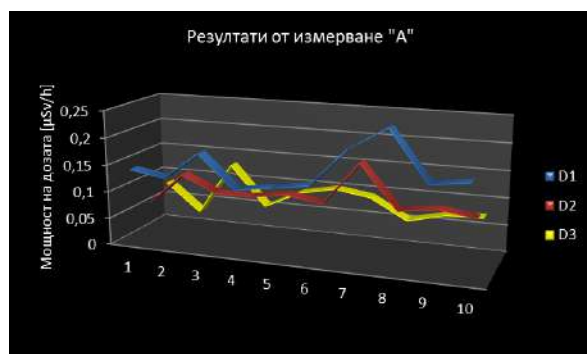


Fig. 2. Results from experiment, part A

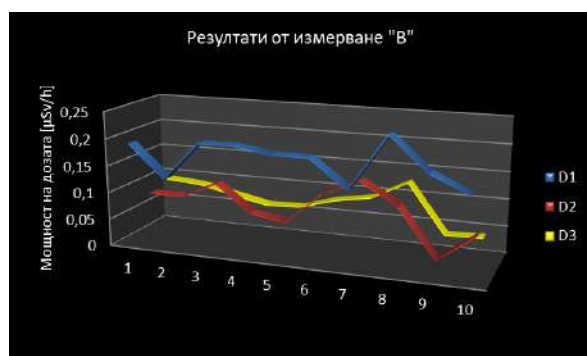


Fig. 3. Results from experiment, part B

When analyzing the graphs shown, it can be noted that in the measurements made at the experiment point with coordinates 42° 527936 N. and 27° 446122 E at different times, values in the range of 0.24-0.25 $\mu\text{Sv/h}$ were reported from the D₁ dosimeter, which were relatively higher than the readings of the other two dosimeters. Therefore, it can be assumed that the average values (Fig. 4) and the interval between the maximum and minimum values (Fig. 5) for each of the three dosimeters are a function of their design capabilities and element base, including the ionization detector itself.

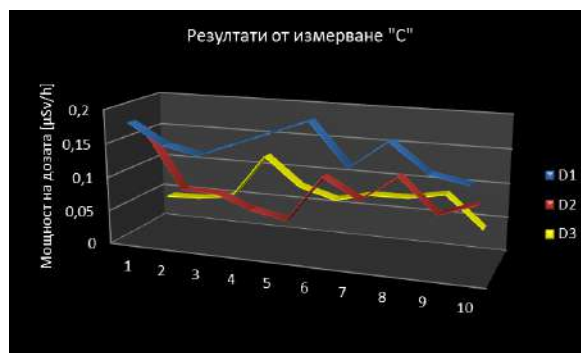


Fig. 4. Results from experiment, part C

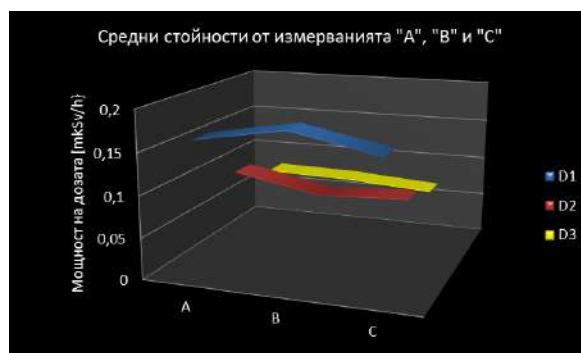


Fig. 5. Average results, from all experiment, parts A, B, C

It is noteworthy that when measuring C (the third part of the experiment, in the afternoon), the readings of dosimeter D₁ do not exceed 0.20 $\mu\text{Sv/h}$, which indicates its higher measurement sensitivity to the surrounding environment. In support of this conclusion is the trend shown in Fig. 5, which shows a difference of 0.07 $\mu\text{Sv/h}$ between max/min reported value by the same dosimeter.

On the other hand, when analyzing the data shown in Fig. 2 to Fig. 5, a relative stability is observed in all measurements of all three dosimeters: they are limited in small intervals, and thus the obtained values can claim representativeness depending on the location and the averaged atmospheric conditions described in Table 1.

The average values of temperature, humidity, illumination and wind direction show that the day chosen for the study is a typical summer day with an average temperature of over 30° C, average velocity of a wind with NE/E (northeast/east) direction and humidity around 40%, usual for the town of Burgas.

Table 1. Average atmospheric conditions for measuring the gamma background of the environment, 07.07.2020

Time interval	T, °C	Illumination Lux	Wind/velocity m/s	Humidity %
9.30-10.30	33	1320*10	ne	42
12.30-13.30	34	697*10	0,81 ne/	39
15.30-16.00	33	671*10	0,89 e/ 1,15	44

From the measurements of the radiation background, it is noticed that it has the highest values in the time interval 12.30-13.30 (second part of the experiment B), when the average temperature is the highest, but not the illumination. In this connection, no definite connection can be made between the light intensity and the radiation background of the environment.

CONCLUSIONS

1. The D₁ FAG dosimeter from SEIFERT turned out to be the most sensitive in this case and the specific study of the surrounding environment.

2. The measured background gamma radiation (gamma radiation dose rate) in the open air on 07.07.2020 has safe values for humans, with average values for devices A, B and C in the range of 0.07 μSv/h to 0.13 μSv/h.

3. A definite connection cannot be made between the light intensity (illumination) and the radiation background of the area.

REFERENCES

1. Naredba za radiatsionna zashtita (obn. DV br. 16 ot 20.02.2018)
2. Naredba za normi za tselite na radiatsionnata zashtita i bezopasnost pri likvidirane na posledstviyata ot uranovata promishlenost v R Bulgaria (Naredba No 1/15.11.1999)

REHABILITATION OF BICYCLE LANE LIGHTING

Mladen Proykov
E-mail: m_proykov@abv.bg

ABSTRACT

The paper presents a complete solution for rehabilitation of the lighting of the pedestrian area and the constructed bicycle lane on the road from Burgas to Lozovo. Comparative analyses of several solutions with different types of outdoor LED luminaires are presented. The comparative analyses are made on the basis of the achieved lighting indicators and energy efficiency. A method for automated control of the lighting system and dimming of the lighting fixtures in the dark part of the day is proposed.

Key words: street lighting; bicycle lanes; LED light.

INTRODUCTION

Street lighting is an important factor in the life of modern people. Artificial lighting creates conditions for activity practically around the clock. Good street lighting is an important prerequisite for the safe movement of motor vehicles in the evening and at night, increasing the capacity of the street network and reducing crime.

The total duration of the dark part of the day, when artificial lighting is needed, is about 4012 hours. Studies show that during this period the number of accidents has increased 1.5 times. According to statistics, with the improvement of street lighting, accidents are reduced by up to 30%. The number of criminal acts in the dark hours of the day is significantly reduced (up to 50%). According to statistical observations, when 50% of the street lighting is turned off, criminal acts increase by 65%, hooliganism increases by 25%, and the thefts of motor vehicles grows by 13%.

The dependence of the ratio of the number of accidents, criminal and hooligan acts during the dark hours and during the day as a function of the realized average luminance of the roadway decreases almost linearly.

Based on the results of research, it has been established that the costs of the reconstruction of the lighting systems are from five to ten times lower in comparison with the damages caused by criminal or traffic accidents for a year. Therefore, the main problem today is to increase traffic safety and to reduce the number of criminal acts and traffic accidents [1].

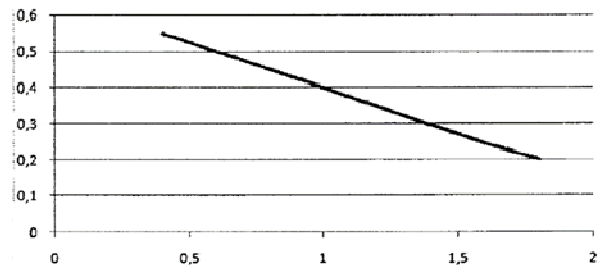


Fig. 1. Ratio of the number of accidents night / day, depending on the degree of illumination

In order to do this, the following requirements need to be met [4 ,5]:

- To observe the European standards for street lighting EN 13201: 2016;
- Light sources to be ecological and energy efficient;
- To use light sources with colour temperature between 3000 and 4500 K;
- To use light sources with a high colour rendering index ($R_a > 70$);
- To use luminaires with low overall luminance and “cut off” or “semi cut off” light distribution;
- To use modern systems for adaptive street lighting.

ELECTRICAL ENERGY RESEARCH

According to the European standard for street lighting EN 13201-1: 2016 “Street lighting. Part 1: Guide to the selection of lighting classes”, streets are divided into four light classes, which are listed in Table 1 [5].

The standard states that “Lighting classes P are intended primarily for areas for pedestrians and cyclists using footpaths and cycle paths located separately or along the traffic lane, or neighbourhood streets, etc.”

Table 1. Lighting Standard EN 13201-1:2016

Definition	Lighting classes
City or suburban streets, with main traffic	M
Streets with conflict zones or where luminance values cannot be calculated	C
Streets for pedestrians and slow - moving vehicles	P + HS
Additional classes for which it is necessary to calculate semi-cylindrical or vertical illuminance	SC + EV

The lighting class sets the minimum, sufficient, normal, lighting indicators that must be realized.

The number of the lighting class P (P1 ÷ P6) is determined by formula (1):

$$P = 6 - VWS \quad (1)$$

where: (VWS) is the sum of the weighted values which are determined according to the EN 13201-1: 2016 standard and the corresponding instructions in it.

The parameters (VW) determining the choice of lighting class for the considered bike lane are:

- Movement speed – VW1 = 1;
- Traffic intensity – VW2 = 0;
- Traffic composition – VW3 = 1;
- Parked vehicles – VW4 = 0;
- Luminance of the surrounding space – VW5 = 0;
- number of lanes – VW6 = 0;
- road crossing frequency – VW7 = 0;
- visual guidance – VW8 = 0.

The sum of the weighted values for the bicycle lane is $VWS = 2$.

According to formula (1), the lighting class for the considered bike lane is P4.

The standard values of lighting indicators for classes P4 and P1 according to BDS EN 3201: 2016 are shown in Table 2.

An “Energy efficiency” section has been introduced in the new European standard, defining how to calculate the energy efficiency indicators

of street lighting systems, using the calculated power density indicator (PDI) DP and the calculated indicator for annual energy consumption (AECI). DE - source.

Table 2. Normal values of lighting indicators for class P4 according to EN 3201:2016

Lighting classes	Additional requirements				
	Horizontal illumination		Vertical illumination	Semi - cylindrical illumination	
	Eh av [lx]	Emin [lx]	Ev min [lx]	Esc min [lx]	TI [%]
P4	5.0	1.0	1.5	1.0	30
P1	15	3	5	5	20

Indicator Dp has a dimension reciprocal to the dimension of light output:

$$D_p = \frac{P}{\sum_{i=1}^n E_{i\ av} \cdot A_i}, \quad [W/Lx.m^2] \quad (2)$$

The annual energy consumption indicator D_E integrates the power during the year, in accordance with the lighting load schedule:

$$D_E = \frac{\sum_{j=1}^m P_j \cdot t_j}{A}, \quad [Wh/m^2] \quad (3)$$

where: P is power of the lighting system [W], A is area of the illuminated element [m^2], n is total number of illuminated elements.

The studied bike lane (Fig. 2) is two-way, located on the one side of the road from Slaveykov to Lozovo (Burgas).



Fig. 2. Overview of the entire route

The new solution for the bicycle lane is a central, direct route, which can be divided into four sections, with the following parameters:

- section 1: sidewalk width 1.9 m. and bike lane width 2.5 m;
- section 2: sidewalk width 3 m and bike lane width 2.5 m.;
- section 3: shared bike lane with a width of 3 m;
- section 4: sidewalk width 1.9 m and bike lane width 3 m.

The calculations were made for several street LED lighting fixtures (Fig. 3), with different power and type, with an asymmetric light distribution curve.



Fig. 3. LED street light fixtures

Fig. 4 shows the light distribution curve of a LED street luminaire.

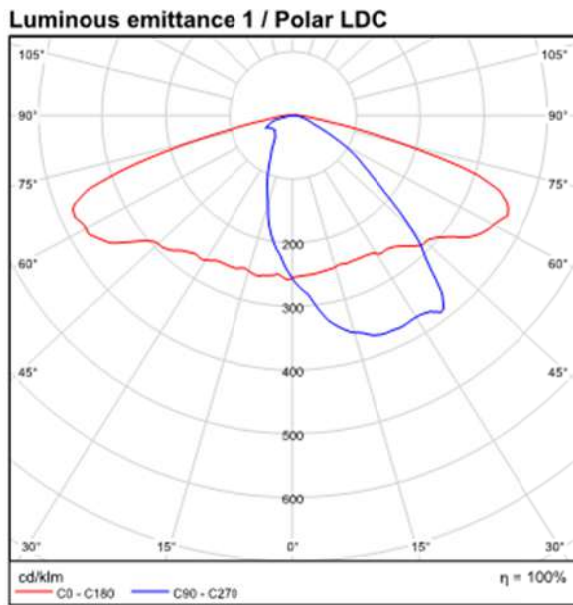


Fig. 4. Light distribution curve of a LED street luminaire.

Table 3 shows the lighting parameters of the luminaires used.

Table 3. Technical parameters of LED luminaires

Power	Light angle	Luminous flux	R _a
[W]	[deg]	[Lm]	[CRI]
7	67°	1023	>70
9	67°	1364	>70
12	67°	1542	>70
14	67°	2000	>70

17	67°	2046	>70
20	67°	2400	>70
26	67°	3190	>70
35	67°	3950	>70

The calculations were made with Dialux evo software, with different types of street LED lighting fixtures. Figures 5 and 6 show the 2D and 3D results of the calculation simulations for a luminaire with a power of 20W, for section 2.

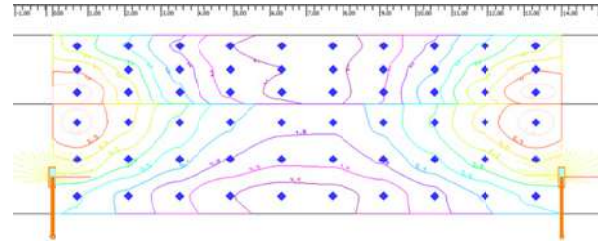


Fig. 5. 2D simulation with the Dialux software

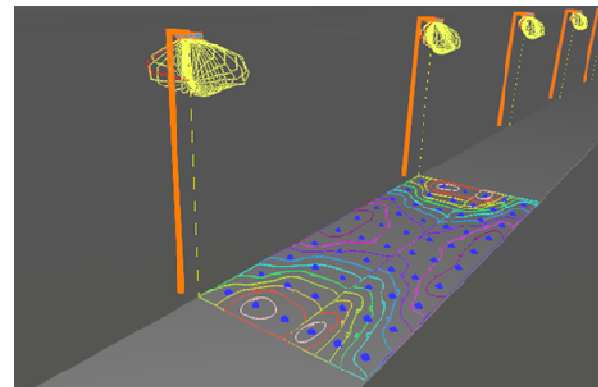


Fig. 6. 2D simulation with the Dialux software

The results of the calculations for each section are shown in Table 4, in compliance with the EN13201: 2016 standard. The tables show only the most optimal results for each luminaire.

Table 4. Results for the different types of luminaires for each section

Power	Additional requirements					
	Horizontal illumination		Vertical illumination	Semi - cylindrical illumination	Energy efficiency indicators	
P	E _h av	E _h min	E _v min	E _{sc} min	D _p	D _E
W	lx	lx	lx	lx	W/Lx.m ²	Wh/m ²
Section 1						
7	5.4	5.5	1.6	1.16	0.022	0.5
9	5.6	4.4	1.66	1.11	0.026	0.57

12	5.9	4.5	1.61	1.08	0.031	0.73
14	5.2	3.8	1.53	1.05	0.029	0.71
17	5.7	3.6	1.59	1.07	0.038	0.86
20	5.3	4.2	1.59	1.54	0.043	0.91
26	6.3	4.6	1.54	1.31	0.043	1.07
35	5.8	3.7	1.5	1.36	0.049	1.33
Section 2						
7	5.2	3.8	1.58	1.01	0.019	0.4
9	5.5	4.1	1.62	1.03	0.021	0.46
12	5.2	4.1	1.63	1.07	0.028	0.58
14	5.1	3.7	1.52	1.02	0.025	0.56
17	5.2	3.6	1.59	1.07	0.032	0.68
20	5.2	3.9	1.62	1.06	0.035	0.72
26	5.4	3.6	1.54	1.04	0.036	0.86
35	6.5	4.3	1.58	1.03	0.039	1.06
Section 3						
7	5.4	3.9	1.57	1.09	0.020	0.45
9	5.4	4.1	1.63	1.11	0.024	0.51
12	5.1	4.0	1.60	1.02	0.031	0.65
14	5.2	4.1	1.51	1.00	0.029	0.59
17	5.3	3.8	1.66	1.11	0.037	0.77
20	5.3	3.9	1.62	1.07	0.039	0.81
26	5.3	3.5	1.52	1.00	0.043	0.96
35	6.9	4.6	1.6	1.02	0.042	1.19
Section 4						
7	5.5	4.2	1.66	1.17	0.033	0.73
9	6.3	4.5	1.51	1.06	0.033	0.83
12	5.1	4	1.60	1.02	0.052	1.07
14	5.2	1.1	1.51	1.00	0.047	0.97
17	5.3	3.6	1.60	1.06	0.059	1.26
20	5.1	3.7	1.60	1.02	0.064	1.33
26	5.6	3.5	1.58	1.00	0.070	1.58
35	7.2	4.9	1.64	1.09	0.067	1.94

Table 5 shows the distribution, installation method and power of the different types of LED luminaires for the individual sections of the bike lane.

Table 5. Distribution of LED luminaires for each of the sections

Power	Bicycle lane width	Sidewalk width	Pole distance	Light centre height	Boom angle	Boom length
W	m	m	m	m	deg	m
Section 1						
7	2.5	1.9	12	6	0	0.5
9	2.5	1.9	14	7	0	0.5
12	2.5	1.9	15	7	0	0.5

14	2.5	1.9	17	8	0	1.5
17	2.5	1.9	18	8	0	1
20	2.5	1.9	20	9	0	0.5
26	2.5	1.9	22	9	0	1.5
35	2.5	1.9	24	9	5	1.5
Section 2						
7	2.5	3	12	6	5	1
9	2.5	3	14	7	0	1.1
12	2.5	3	15	8	0	0.6
14	2.5	3	17	8	5	1.6
17	2.5	3	18	8	0	1.6
20	2.5	3	20	9	0	0.6
26	2.5	3	22	9	0	2.1
35	2.5	3	24	9	10	0.6
Section 3						
7	3	1.9	12	6	0	1.6
9	3	1.9	14	7	5	0.6
12	3	1.9	15	8	0	1.1
14	3	1.9	18	9	0	0.6
17	3	1.9	18	8	5	1.6
20	3	1.9	20	9	0	0.6
26	3	1.9	22	9	5	1.6
35	3	1.9	24	9	5	1.1
Section 4						
7	3	12	6	5	0.6	7
9	3	14	6	0	0.6	9
12	3	15	8	0	1.1	12
14	3	18	9	0	0.6	14
17	3	18	8	0	1.6	17
20	3	20	9	0	1.1	20
26	3	22	9	5	1.1	26
35	3	24	9	5	0.6	35

The efficiency of the lighting system is proved by the newly introduced indicators for energy efficiency in EN 13201: 2016: D_p (power density, $W/lux.m^2$) and D_E (annual energy consumption for street lighting, %). For a bicycle or pedestrian lane, D_p must not exceed $0.054W/lux.m^2$ at an illumination of $E \leq 15lux$.

From the presented lighting calculations it is evident that the lighting of the bike lane meets the requirements for energy efficiency: $D_p = (0.029 \div 0.033)W/lux.m^2$ [3].

From the lighting calculations, a comparison can be made between the different options with different types of lighting fixtures and the most energy efficient option can be determined. The total installed capacity P_Σ is calculated by formula 4.

$$P_\Sigma = \frac{L}{lm} \cdot P_1 \quad (4)$$

where: L is length of the section; L_M is pole distance; P_l is lamp power.

It has been experimentally proved that the average annual working time T_{year} for street light luminaires is 4760h. Therefore, the annual electricity consumption P_{year} for the bike lane can be calculated by the formula:

$$P_{year} = P_{\Sigma} \cdot T_{year} \quad (5)$$

The results of the calculations for the annual electricity consumption for the individual sections are given in Table 6.

Table 6. Electricity consumption for different luminaires

Luminaires	Number of poles	$P_{inst.}$	$P_{year.}$
W	pcs.	kW	kWh
7	333	2.32	11106
9	286	2.56	12240
12	267	3.2	15231
14	229	3.2	15265
17	222	3.76	17981
20	200	4	19040
26	182	4.72	22500
35	168	5.82	27765

The calculations in Table 6 show that lamps with a power of 7W achieve the required normal illumination with the lowest annual electricity consumption.

Table 7 presents the calculations made for the cost of the construction and installation works for the whole route, for each option. The results show that the lowest cost of construction is achieved with 35W power lamps.

Table 7. Calculated cost

Luminaires	Total cost of construction and installation works for the entire route
P, W	(BGN)
7	610 536
9	543 274
12	516 649
14	464 802
17	454 993
20	424 164
26	397 540
35	376 520

In order to make the most accurate technical and economic assessment, both the annual electricity consumption (Table 6) and the initial capital investments (Table 6, 7) must be taken into account.

Using the the price of electricity for street lighting (0.0024 BGN/ kWh), the cost of electricity which will be paid annually can be calculated, for the whole section and for each option (Table 8).

Table 8. Comparative analysis of consumed electricity

Luminaires	Electrical energy	Cost of electrical energy (annually)	Cost of electrical energy (for 10 years)
P, W	kWh/y	(BGN)	(BGN)
7	11106	2666	26656
9	12240	2938	29376
12	15232	3656	36556
14	15266	3664	36638
17	17982	4316	43157
20	19040	4570	45696
26	22501	5400	54004
35	27766	6664	66640

From the analysis (Table 7 and Table 8), it is clear that the most profitable option is with lamps with a power of 35W, due to the fact that the amount of initial investment (BGN 376,520) and the price of electricity consumed for a period of 10 years (BGN 66,640) is the lowest (as mentioned, the average lifespan of a street LED luminaire is about 10 years).

RESULTS AND DISCUSSION

Lighting calculations were made with the DIALux evo software product for luminaires with different power.

The initial investments and annual electricity consumption for each luminaire are calculated.

An energy efficient evaluation of the lighting installation for each luminaire has been made. A summary of the initial costs and the costs of electricity consumption for a period of 10 years has been made.

Based on the obtained results, the most economically appropriate option for the lighting of the bicycle lane is proposed.

ACKNOWLEDGMENTS:

The author is grateful to the Scientific and Research Sector, Scientific and Artistic-Creative Activities Program of Prof. Assen Zlatarov University, Burgas, for funding the present study through contract No NIH - 427/2019.

REFERENCES

1. Tzankov P., M. Jovchev, H. Ibrishimov, Tz. Petkov, E. Stanev and L. Dimitrov, *Electrical energy research of street lighting in Gabrovo*, Proceedings of the National Lighting Conference for Young Scientists, Lighting 2016, 21 – 23 October, Sofia, Bulgaria.
2. Ashryatov A., *Improving the efficiency of existing lighting systems*, Proceedings of the National Lighting Conference for Young Scientists, Lighting 2016, 21 – 23 October, Sofia, Bulgaria.
3. Van Tichelen P., T. Geerken, J. Bosch, M. Laborelec, V. Van Hoof, L. Vanhooydonck, A. Vercalsteren, *City of San Josse Public Streetlight Design Guide, USA, 2011, "Final Report Lot 9: Public street lighting"*, 2007/ETE/R/021.
4. Buyukkinaci B., S. Onaygil, O. Guler, B. Yurtseven, Y. Dursun, *Road lighting control according to EN 13201-1*, Proceedings VII BalkanLight, Sofia 2018.
5. BS EN 13201:2016. Street lighting. Part 1-5.

ENERGY EFFICIENCY IN THE MODERN HOME

Mladen Proykov
E-mail: m_proykov@abv.bg

ABSTRACT

A study of the achieved electricity efficiency in a single-family, two-storey residential building was made with the introduction of a "smart home" system. The relevant technical and economic analyses and conclusions are presented.

Key words: smart home.

INTRODUCTION

In recent years, dictionaries have added words such as intelligent building, smart house and so on. These concepts involve a healthy and comfortable microclimate with minimal consumption of energy resources. The construction of such buildings is provoked by the desire to reduce energy costs, which is easily explained by the constant rise in energy prices.

The intelligent building should be equipped with systems for automatic control of all its elements and installations. These systems have the task of providing a favourable living environment. A key element of the intelligent building is the automatic control system, which is a set of software and hardware solutions, whose main task is to ensure reliable and secure management of all installations of the building.

Smart buildings should be able to change according to the changing needs of their occupants. The intelligent building that manages all installations and meets the needs of its occupants as much as possible can ensure optimal operation of all its subsystems, such as: climate control, disaster protection systems, emergency situations, detection of unauthorized access, achieving rational use of energy and communal resources, etc.

The development of building automation technologies paves the way for new systems and applications characterized by intuitiveness, flexibility and more autonomous behaviour. In this way, the human - computer interaction environment will become a human - computer collaboration. Technological development logically leads to the creation of new opportunities to make people's lives easier.

Currently, several standards are used in the implementation of projects for intelligent build-

ings, namely: EIB (European Installation Bus), KNX, LON (Local Operating Network), X10 and BACnet.

The main regulations setting the requirements to the designers in the "Electrical" area are Ordinance No 7/2010, Ordinance No RD 16-1058/2009 and LTP [1, 2, 3]. They specify the mandatory requirements for designers to make the necessary decisions in order to achieve energy efficiency of the building in accordance with the class in which it falls. According to the current classification [1], they are as follows:

- for new buildings, in the process of design or construction: at least class B;
- for buildings put into operation in the period 1991 - 2009: at least class C;
- for buildings put into operation before 1990: at least class D.

METHODOLOGY

The main criteria are the energy performance (EP) of the building and compliance with the reference values (Table 1).

For the electrical designers' part, the number of indicators M are from group 3 [1]:

- total annual cost of heating, cooling, ventilation, hot water, lighting and appliances [kWh];
- total annual specific cost of heating, cooling, ventilation, hot water, lighting and appliances [kWh].

Table 1. EP reference values of buildings

Confines	Energy consumption class
$EP \leq 0.5 \cdot EP_{\max,r}$	A
$0.5 \cdot EP_{\max,r} \leq EP \leq EP_{\max,r}$	B
$EP_{\max,r} \leq EP \leq 0.5 \cdot (EP_{\max,r} + EP_{\max,s})$	C

$0.5.(EP_{\max,r}+EP_{\max,s}) \leq EP \leq EP_{\max,s}$	D
$EP_{\max,s} \leq EP \leq 1.25 \cdot EP_{\max,s}$	E
$1.25 \cdot EP_{\max,s} \leq EP \leq 1.5 \cdot EP_{\max,s}$	F
$1.5 \cdot EP_{\max,s} \leq EP$	G

where: $EP = \{P_i, i = 1, 2 \dots M\}$; M is the number of indicators for EE; P is determined according to Ordinance No RD 16-1058/2009; $EP_{\max,r}$ and $EP_{\max,s}$ are reference values for total specific consumption of electricity for heating, cooling, ventilation, DHW, lighting and appliances [kWh].

A classification according to Table 1 can be made using the second indicator.

The reference values are obtained using limit values of the heat transfer coefficients U_{\max} [W/m².K] and concern the design part of HVAC. The obtained values for specific energy consumption [kWh/m²] have the character of thermal energy. In accordance with the methods used, they are monthly and/or annual averages. In them lighting is included taking into account the heat output per m². Also, the HVAC part does not consider the problem of what electricity consumption achieves the required energy in kWh (heat) for heating, cooling, ventilation and DHW.

The energy indicators used by HVAC designers are:

$$EP_{HVAC} = \sum_{i=1}^n Q_i \cdot e_i \quad (1)$$

$$EP_{HVAC} = (Q_H + Q_C + Q_{AC} + Q_{HW}) \cdot e_i \quad (2)$$

where: Q_H is the energy required for heating [kWh/m²]; Q_C is the required energy for cooling [kWh/m²]; Q_{AC} is the energy required for ventilation [kWh/m²]; Q_{HW} is the energy required for DHW [kWh/m²]; e_i reports the losses for production and transmission of the required energy (in case of primary energy carrier electricity $e_i = 3$).

For the "Electrical" design, when knowing the selected HVAC facilities, the following indicator can be used:

$$EP_{HVAC.EL} = W_{HVAC.EL} = \sum_{i=1}^n \frac{Q_i}{\eta_i} \cdot e_i \quad (3)$$

$$EP_{HVAC.EL} = \left(\frac{Q_H}{\eta_H} + \frac{Q_C}{\eta_C} + \frac{Q_{HW}}{\eta_{HW}} \right) \cdot e_i \quad (4)$$

where: $\eta_C = (2,2 \div 3,1)$ and $\eta_H = (1,6 \div 1,8)$ for air conditioners; $\eta_{HW} = 1$ for electric water heaters.

When put on the lighting in EP, indicator EP_{EL} is:

$$EP_{EL} = W_{HVAC.EL} + W_{L.EL} \quad (5)$$

The specific annual indicator LENI (Lighting Energy Numeric Indicator) is used.

$$LENI = \frac{W_{L.EL}}{W_L + W_P} = \frac{A}{A} \quad (6)$$

where: A is total illuminated area [m²]; W_L is electrical energy from the lighting load [kWh/y]; W_P is electrical energy from emergency lighting [kWh/y].

The following formulas are used:

$$W_L = \frac{\sum: [(P_N \cdot F_C) \cdot [t_D \cdot F_0 \cdot F_D + t_N \cdot F_0]]}{1000} \quad (7)$$

$$W_P = \frac{\sum: [P_{PC} \cdot (t_Y - t_D - t_N) + P_{EM} t_{EM}]}{1000} \quad (8)$$

where: P_N is installed power [W]; P_{PC} is parasitic power [W]; P_{EM} is power from emergency luminaires [W]; t_Y is 1 year period 8760h; t_D is period of operation of the luminaires during the day; t_N is period of operation of the lights at night; t_{EM} is period for charging the emergency lights; F_C is a factor determined by the use of installed power; F_0 is determined by the presence of people; F_D is determined by the presence of natural light.

To assess the energy efficiency of buildings in the design and construction of "smart home" systems indicators defined by the EK 15232 standard can be used [4]. In accordance with it, for each building, depending on the used automation system, the respective BAC (Building Automation and Control) efficiency class is determined. BAC classes are from A to D, divided into two groups for residential and non-residential buildings. Based on the classification of efficiency, depending on the type of building, BAC efficiency factors are selected: $f_{BAC.HC}$ and $f_{BAC.L}$. The first shows the impact of automation systems on improving energy efficiency for the heat used, and the second shows the same for the electricity used. In buildings where the main

energy carrier is electricity, automation systems have a twofold effect:

- reducing the total electricity consumption of the systems;
- improving the operation of HVAC systems, which leads to a reduction in electricity consumption.

Quantitative assessment is performed based on the following methodology:

- for heating systems $Q_{H,Tot,BAC}$ [kWh/m².y]

$$Q_{H,Tot,BAC} = (Q_{H,nd,B} + Q_{H,sys}) \cdot \frac{f_{BAC,HC}}{f_{BAC,HC,ref}} \quad (9)$$

$$Q_{H,Tot,BAC} = Q_H \cdot \frac{f_{BAC,HC}}{f_{BAC,HC,ref}} \quad (10)$$

where: $Q_{H,nd,B}$ is heat energy for heating and losses in the heating system; $f_{BAC,HC}$ is a reference BAC factor.

- for cooling systems $Q_{C,Tot,BAC}$ [kWh/m².y]

$$Q_{C,Tot,BAC} = (Q_{C,nd,B} + Q_{C,sys}) \cdot \frac{f_{BAC,HC}}{f_{BAC,HC,ref}} \quad (11)$$

$$Q_{C,Tot,BAC} = Q_H \cdot \frac{f_{BAC,HC}}{f_{BAC,HC,ref}} \quad (12)$$

- for lighting systems $Q_{OCB,BAC}$ [kWh/m².y]

$$Q_{OCB,BAC} = W_{OCB} \cdot \frac{f_{BAC,EL}}{f_{BAC,EL,ref}} \quad (13)$$

$$EP_{eл,BAC} = \left[\left(\frac{Q_H}{\eta_H} + \frac{Q_C}{\eta_C} \right) \cdot \frac{f_{BAC,HC}}{f_{BAC,HC,ref}} \right] \cdot e_i + \left[\left(\frac{Q_{HW}}{\eta_{HW}} + W_{OCB} \right) \cdot \frac{f_{BAC,EL}}{f_{BAC,EL,ref}} \right] \cdot e_i \quad (14)$$

Formula (14) is used to estimate the EE of buildings in the presence of a "smart house" system. [4]

ELECTRICAL ENERGY RESEARCH

An assessment of the electricity efficiency and the effect of the introduction of a "smart house" system for a single-family, two-storey, residential building in Aytos, Burgas Municipality has been made.

The building is a two-storey house with a total floor area of 342 m² and a floor area of 189 m². The building has a living room, a bathroom and a covered veranda on the first level and three bedrooms and two bathrooms on the second level.

The calculated electrical loads are based on the installed electrical loads:

$$P_{ins.} = 23kW; K_e = 0,65; P_{sym.} = 15kW$$

In the present project, smart technology will be used to increase the energy efficiency of the home by building an intelligent electrical installation and automating the management, namely:

- lighting and heating control;
- control of electric water heaters;
- management of household appliances;
- management of blinds and garage doors.

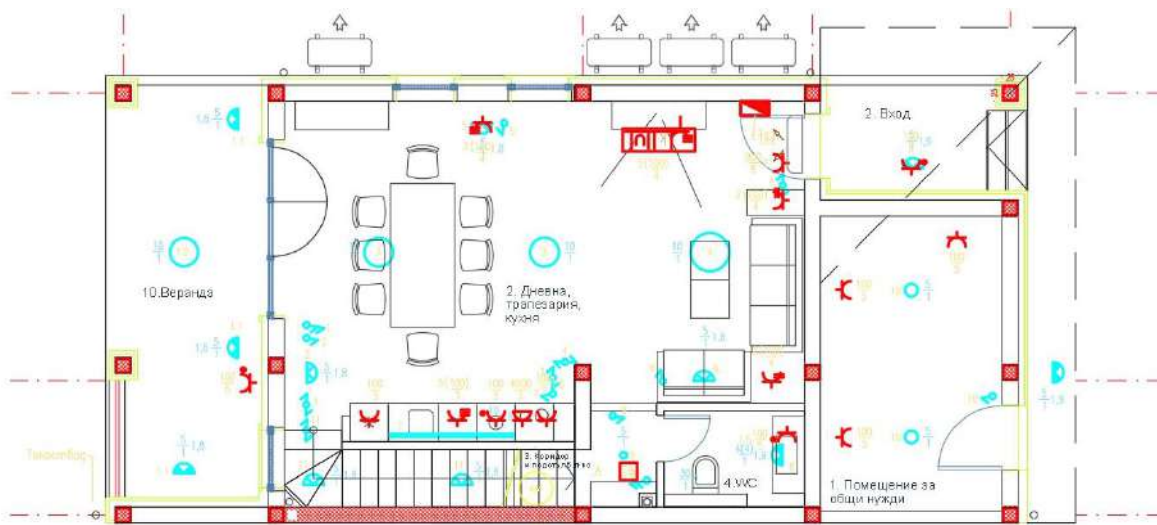


Fig. 2. Plan of the power installations on the first floor

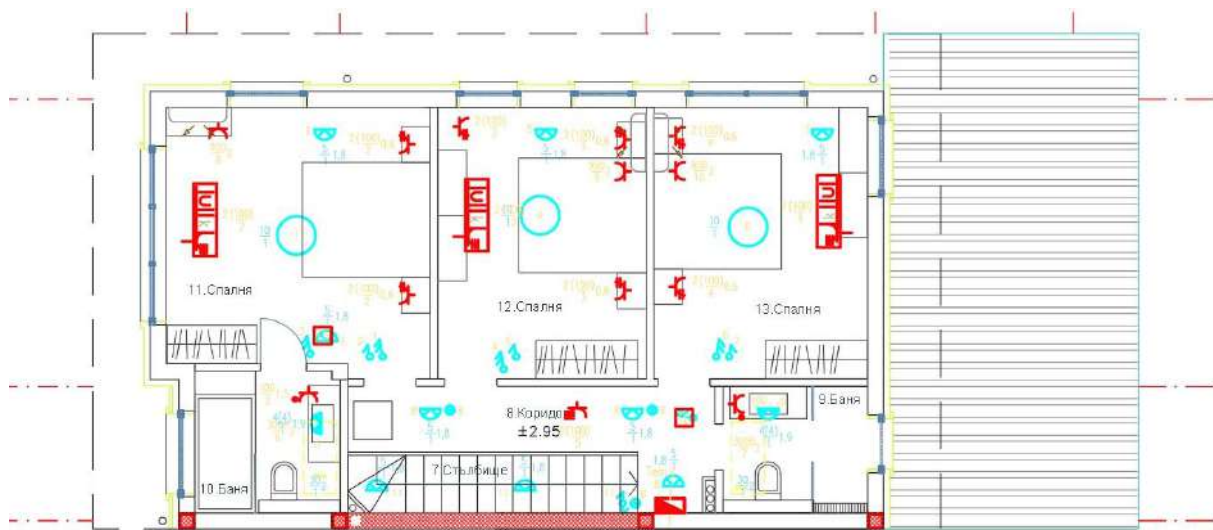


Fig. 3. Plan of the power installations on the second floor

The automation system consists of the following elements:

- main module CU3 - 02M with RF module (SKU: 3239 standard);
- power supply module PS3-100/iNELS (SKU: 4889 standard), for main module;
- separator BPS3-01M-02M;
- connecting server (SKU: 4920EN);
- switching, addressable, 12-channel mechanism SA3-O12M, for lighting control;
- universal dimmable device, two-channel DA3-22M (SKU: 3262 standard), for light intensity control of LED lamps;
- wall smart switches for lighting WSB3-40, WSB3-20 and WSB3-40;

- Wi-Fi based module VC-SH-HUB, to control the air conditioners;

- Wi-Fi smart switch BESTCON SCB1E, which serves to control electric water heaters through Wi-Fi based module VC-SH-HUB.

HVAC facilities used in the project:

- air conditioners: 900W / 220V (4 pcs.);
- duct fans: 30W / 220V (3 pcs.);
- electric water heaters: 3000W/ 220V (3 pcs.);
- LED lighting fixtures.

Based on the shown methodology and the projects under parts “HVAC” and “Electrical”, the respective indicators have been calculated:

Table 2. Electrical powers design of the building for HVAC and lighting

HVAC and DHW facilities			Lighting
Q_H	Q_C	Q_{HW}	$Q_{L,EL}$ (LENI)
[kWh/m ² .y]	[kWh/m ² .y]	[kWh/m ² .y]	[kWh/m ² .y]
23.19	21.48	10.99	
$W_{HVAC,EL}$ [kWh/m ² .y]			4
59.66			

Total floor area of the building $A = 342m^2$;
BAC class of the building is A.

$$\frac{f_{BAC,HC}}{f_{BAC,HC,ref}} = 0,81; \quad \frac{f_{BAC,EL}}{f_{BAC,EL,ref}} = 0,92;$$

$$EP_{EL} = EP_{BAC,EL} = 49,94 \left[\frac{kWh}{m^2} \cdot y \right];$$

$$EP_{max,r} = 59,66 \left[\frac{kWh}{m^2} \cdot y \right].$$

EE characteristic of the building EP meets the condition $0.5 \cdot EP_{\max.r} \leq EP \leq EP_{\max.r}$. The building is therefore class B in terms of EE.

The calculations show that with the introduction of the "smart house" system, EE savings will be made in the amount of 9.72 [kWh/m².y].

With respect to the specific building, which has an area of 342m², this means that the energy savings will be in the amount of 3324 [kWh/y].

RESULTS AND DISCUSSION

An assessment was made of the impact of building automation on electricity efficiency and the classification of buildings by BAC class.

The energy efficiency of the building is calculated, with the "Smart Home" system and without this system. Calculations show that with the introduction of the intelligent system, savings in

electricity consumption of 3324 [kWh/year] will be made.

REFERENCES

1. Ordinance No 7 / 15.2004, am. 11.2017, "*Energy efficiency, heat storage and energy saving in buildings*".
2. Ordinance No RD16-1058 / 09.2009, am. 02.2016, "*Energy consumption indicators and energy performance of buildings*".
3. Law on Territory Planning, 03.2001, am. 07.2020г.
4. Gyurov V., *Improving energy efficiency in buildings using "smart home" electrical design*, Proceedings of the TU - Sofia, v. 60, book 1, 2010.

MODELING OF SINGLE PHASE INVERTER SYSTEM IN SIMULINK SOFTWARE

Vasil Ivanov

E-mail: vasil_bi@mail.bg

ABSTRACT

SIMULINK software models graphs and charts as a modern method for creating mathematical models. A simulation structure of blocks in Simulink programming environment has been built.

Key words: filter, amplitude frequency response, duty cycle, Simulink.

INTRODUCTION

Voltage inverter control systems

The voltage at the output of the inverters has a strictly defined form, which depends on the control algorithm of the power devices in the circuit. Depending on the system of alternating voltages supplying the load in the output, single-phase and three-phase voltage inverters are most often used.

The shape of the current through the load, provided that a voltage with a strictly defined shape is applied to it, depends on the nature and parameters of the load circuit [3].

When using the method of symmetrical PWM control, signals are obtained for adjusting the power devices. The pulses in the half-cycle are symmetrical with respect to the beginning and the end. In the case of unregulated control of the output voltage, the PWM generator produces rectangular pulses for the output voltage with a control algorithm of 0.5, which are asymmetric in half-cycle.

The main elements of the power circuit of inverters are semiconductor devices controlled by a key method. These are most often bipolar transistors with isolated gate (IGBT), power field-effect transistors with induced channel (power MOSFET) or thyristors excluded from the gate (GTO thyristors).

Simulink single-phase inverter system project

Different schemes of single-phase voltage inverters are known, as well as different algorithms for controlling power devices and forming the output voltage curve in them. The most widely used are:

- single-phase inverters with rectangular shape of the output voltage - modified sine wave

Single-pulse PWM with fixed and adjustable width of control pulses is modelled.

- single-phase inverters with sinusoidal pulse - width modulation PWM control. They are modelled with one period and two period sinusoidal PWM function.

RESEARCH METHODS

The stages of modelling and measurement of a single-phase inverter with a modified sine wave were as follows:

1. The main output parameters of the inverter system are set;

2. The curves of currents and voltages in the two modes with different fill factors are measured;

3. The magnitudes of harmonics with serial numbers h_3 , h_5 , h_7 , as well as their initial phases are reported by a PowerGUI block;

4. The losses from active power in the line to the load are calculated by summing the active powers of the most influential harmonics.

5. The total power consumption from the consumption is analyzed and the efficiency of the inverter system is determined by comparing the two modes of operation;

- Output data for practical implementation of the inverter system:

$U_{dc}=300V$, $R_T=5 \Omega$, $L=0.025H$, $f_1=50Hz$;

The first step of the project is to create the schematic diagram of the model in the Simulink software environment, shown in Fig. 1 [1, 2, 3]. The inverter system is modelled by several basic elements represented graphically in the scheme: source (U_{dc}), bridge single phase voltage inverter (U_{ac} , f_1) and active inductive load ($R_T L$). Measuring instruments, oscilloscopes, are also included [4, 5].

Power IGBT transistors T1, T2, T3 and T4 with parallel diodes to the EC junction are controlled by pulse generators, shown in Fig. 2. For T1 and T2, two fill factors are programmed 50% (35%), and for T3 and T4 50% (50%), for two simulation modes.

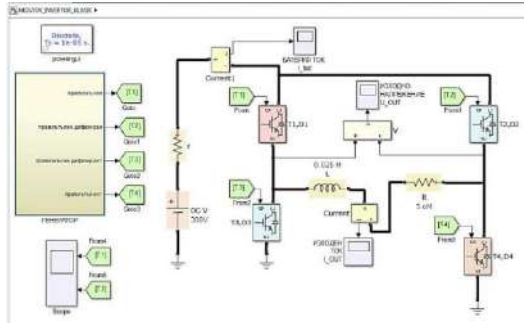


Fig. 1. Schematic diagram of a model inverter system

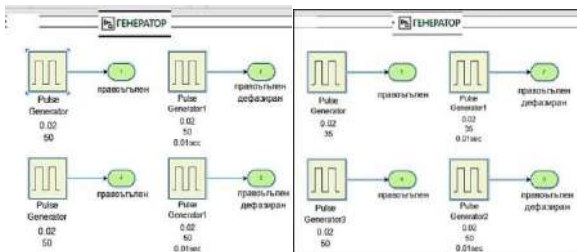


Fig. 2. Models created in the subsystem of Fig. 1 as rectangular pulse generators with fixed fill coefficients;

The complementary couples T1 and T2 are connected to the positive terminal, while T3 and T4 are connected to the negative terminal of a DC voltage source (rechargeable batteries or photovoltaic modules). The transistors have built-in diodes connected to the power supply in the opposite direction of their conductivity. The output parameters of the electrical circuit are measured using oscilloscope models for I_{OUT} , U_{OUT} . The voltage and current curves I are shown in the following figures and are in the form of a signal with two different control algorithms.

EXPERIMENT

Simulation results and evaluation of efficiency

• Starting the model with fill factor 50%/50%

Diagrams of the magnitudes of the harmonics from the output voltage with an unregulated control algorithm 50%/50% are shown in Fig. 3.

From the amplitude-frequency characteristic (AFC) the effective values and the initial phases for the voltage harmonics are taken into account:

First harmonic $U_{h1} = 267.8V$ and $THD_U = 48.49\%$

Initial phase of U_{h1} for first harmonic $\psi_{U1} = 0.4^{\circ}$.

$U_0 = 0.96V$, $I_0 = 10.93A$;

$U_{h3} = 89.6V$, $\psi_{U3} = 0.1^{\circ}$;

$U_{h5} = 53.8V$, $\psi_{U5} = -0.1^{\circ}$;

$U_{h7} = 38.4V$, $\psi_{U7} = -0.2^{\circ}$;

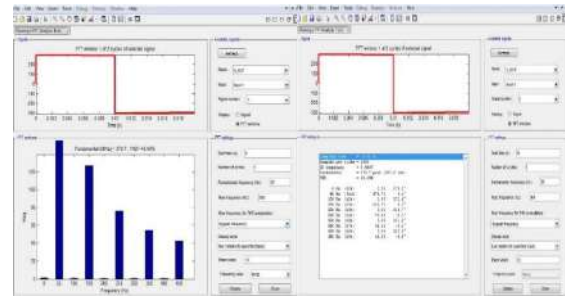


Fig. 3. Frequency spectrum and shape of the output voltage generated by the PowerGUI unit, at a duty cycle of 50% / 50%.

From the results for the frequency response in Fig. 4. the effective values and the initial phases for the output current harmonics are taken into account at the following programmed conductivity interval in the half-cycle:

First harmonic $I_{h1}=29.9 A$ и $THD_I= 29.42\%$.

Initial phase of I_{h1} for first $\psi_{I1} = -40.9^{\circ}$.

$I_{h3} = 4.94A$, $\psi_{I3} = -36.6^{\circ}$;

$I_{h5} = 2.4A$, $\psi_{I5} = -26.8^{\circ}$;

$I_{h7} = 1.58A$, $\psi_{I7} = -20.4^{\circ}$.

The power losses along the lines to the load are calculated by summing the active powers of the most influential harmonics, with serial numbers h_3, h_5, h_7 .

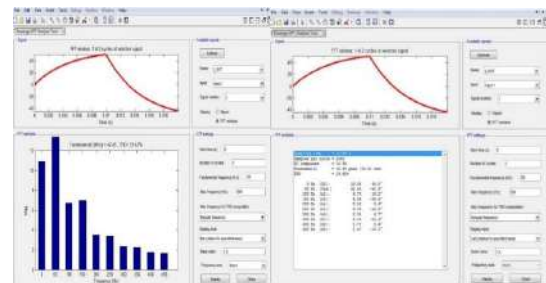


Fig. 4. Spectral synthesis and shape of the output current at 50% / 50%.

The integrated active power is calculated by the Fourier row by summing the given harmonics from the spectrum:

$$P_{out} = U_0 \times I_0 + \sum P_h \times \cos \varphi_h \quad (1)$$

The phase difference taking into account the displacement between the initial phases of voltage and current is determined for the first harmonic by:

$$\varphi_1 = \psi_{U1} - \psi_{I1} \quad (2)$$

The useful active power consumed by the load is calculated for the magnitudes of the first harmonics of current and voltage and shows the conversion efficiency through the voltage inverter:

$$P_1 = U_{h1} \times I_{h1} \cos \varphi_1 \quad (3)$$

After substitution with values for the reported data, it is obtained that:

$$\begin{aligned} P_0 &= 10.5 \text{ W}, \\ P_1 &= 8007 \times \cos(41.2^\circ) = 8007 \times 0.8 = 6406 \text{ W}; \\ P_3 &= 443 \times \cos(36.7^\circ) = 443 \times 0.84 = 372 \text{ W}; \\ P_5 &= 129 \times \cos(26.7^\circ) = 129 \times 0.9 = 116 \text{ W}; \\ P_7 &= 60.7 \times \cos(20.2^\circ) = 60.7 \times 0.95 = 57.6 \text{ W}. \end{aligned}$$

The calculated useful active power delivered to the load is:

$$P_{useful} = P_0 + P_1 = 6406 + 10.5 = 6416.5 \text{ W}.$$

The calculated loss of active power on the supply line is:

$$\begin{aligned} P_{loss} &= P_3 + P_5 + P_7 = 372 + 116 + 57.6 = 548.6 \text{ W}. \\ P_{loss} \% &= P_{loss} / P_{useful} \times 100 = 8.5\% \end{aligned}$$

• **Starting the model with fill factor 35%/50%.**

The magnitude of the harmonics from the frequency spectrum and the waveform of current and voltage are shown in Fig. 5 and 6. From Fig. 5 the effective values of the initial phases for the voltage harmonics are taken into account as a percentage:

First harmonic $U_{h1} = 238.9\text{V}$ and $THD_U = 29.7\%$

$$\begin{aligned} \text{Initial phase of } U_{h1} \text{ for first } \psi_{U1} &= 27.1^\circ, \\ U_0 &= 0.47\text{V}, I_0 = 5.2\text{A}; \\ U_{h3} &= 14.2\text{V}, \psi_{U3} = 77.8^\circ, I_{h3} = 2.1\text{A}, \psi_{I3} = 8.9^\circ; \\ U_{h5} &= 38\text{V}, \psi_{U5} = -44.8^\circ, I_{h5} = 0.7\text{A}, \psi_{I5} = -60.3^\circ; \\ U_{h7} &= 38\text{V}, \psi_{U7} = 8.4^\circ, I_{h7} = 1\text{A}, \psi_{I7} = -35.4^\circ. \end{aligned}$$

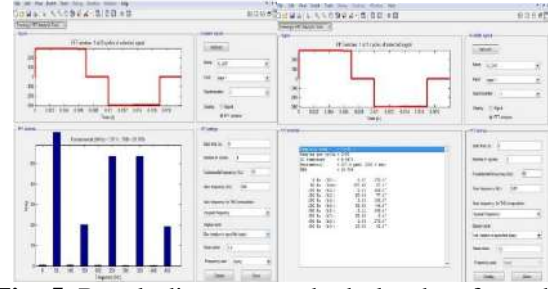


Fig. 5. Result diagrams and tabular data from the frequency synthesis of the output voltage with a control algorithm 35%/50%.

From Fig. 6 the rms values and the initial phases for the output current harmonics are taken into account at the thus programmed conductivity interval in the half-cycle:

First harmonic $I_{h1} = 27.8\text{A}$ and $THD_I = 14.74\%$.
Initial phase of I_{h1} for first $\psi_{I1} = -22.9^\circ$.

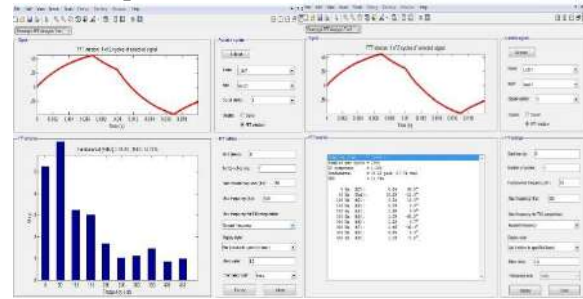


Fig. 6. Result diagrams and tabular data from the frequency synthesis of the output current with a control algorithm 35%/50%.

After substitution with values for the reported data, it is obtained that:

$$\begin{aligned} P_0 &= 2.44 \text{ W}; \\ P_1 &= 7095 \times \cos(50^\circ) = 7095 \times 0.71 = 5038 \text{ W}; \\ P_3 &= 29.8 \times \cos(69^\circ) = 29.8 \times 0.47 = 14 \text{ W}; \\ P_5 &= 27 \times \cos(15.5^\circ) = 27 \times 0.97 = 26.2 \text{ W}; \\ P_7 &= 38 \times \cos(43.8^\circ) = 38 \times 0.77 = 29.4 \text{ W}. \end{aligned}$$

The calculated useful active power delivered to the load is:

$$P_{useful} = P_0 + P_1 = 5038 + 2.44 = 5040.4 \text{ W}.$$

The calculated loss of active power on the supply line is:

$$P_{loss} = P_3 + P_5 + P_7 = 14 + 26.2 + 29.4 = 69.6 \text{ W}.$$

The percentage of losses in the inverter system with a symmetrical 35% / 50% control algorithm is:

$$P_{losses} \% = \frac{P_{loss}}{P_{useful}} \times 100 = 1.38\%$$

CONCLUSIONS

1. The comparative analysis shows a reduced harmonic composition when simulating the inverter system with a fill factor 35%/50% and $P_{\text{loss}} \% = 1.38\%$. At a fill factor of 50% / 50% the losses of active power are $P_{\text{loss}} \% = 8.5\%$.

2. The rectangular voltage pulses with control on algorithm 35%/50% have a reduced spectral composition, because the half-period is symmetrically located. Thus, it approaches the shape of the sinusoid, imitating a modified sine wave with better performance from the asymmetrically placed rectangular pulse.

3. The model gives an accurate forecast of the efficiency of the inverter system to make it a reality when choosing different electrical loads. Deteriorated harmonic composition in the output voltage spectrum affects the performance of sensitive consumers. It has been proven that the scheme of the model with a control algorithm 35%/50% is better.

The simulation analysis of a voltage inverter with a rectangular shape of the output signal proves its widespread use in the autonomous photovoltaic systems for low power, automotive power converters, UPS and etc.

Inverters can supply electrical loads such as lighting fixtures, pumps, television and radio receivers, computer stations, sites remote from the public power supply network and structures intended for uninterruptible power supply.

No filter was applied in the studied model, which takes into account the increased harmonic composition of the inverter system. When installing a cutting filter in the output circuit higher harmonics can be suppressed, which will improve the power factor, efficiency and quality of the energy applied to the load.

The economic efficiency of the application of single-phase inverters is low cost with the good technical characteristics.

REFERENCES

- [1] Materials from PhD dissertation "Study of the influence of photovoltaic systems on electrical networks", certificate № PY-HC-2017-13, issued on 23.06.2017 to Vasil Borisov Ivanov, Ruse.
- [2] Yordanov, J. Application of MATLAB in Engineering Research Part 1, Ruse, 2004. <http://ecet.ecs.uni-ruse.bg>.
- [3] Antchev, M., "Energy efficiency of power electronic devices", Avangard Prima Publishing House, ISBN 378-954-323-731-9, Sofia, 2010.
- [4] Diakonov P., Simulink 5/6/7: Self-taught. DMK Press, 2008. ISBN 978-5-94074-423-8.
- [5] Hudyakov, Vl., German – Galkin, S., Power electronics, №1, №2, №3, №4/2005, №1/2006, №4/2007, №1/2008, №2/2008, №4/2008, №4/2009, №2/2010, №4/2011. www.finestreet.ru

DETERMINING THE AREA OF THE AUTOMOBILE TIRE CONTACT FOOTPRINT USING GENERALIZED NETS

Yuliy Petrov
E-mail: yulipetrov@abv.bg

ABSTRACT

In this article the generalized nets method for calculating the tire contact footprint area is applied. The method is based on the digital processing of an image and on Bresenham's algorithm for determining the actual outlines of the footprint and the calculation of its total area. Generalized nets are one of the most popular techniques for describing the processes formally and abstractly.

Key words: generalized nets, total area, tire contact footprint, outline

INTRODUCTION

Determining the automobile tire contact footprint area is strictly connected to the tire's grip on the pavement. This grip depends on both various atmospheric factors and the supporting surface. There are many methods for determining the tire contact footprint. One of these is described in [1], applying various mathematical methods and digital processing of the image. The footprint is taken by applying a layer of paint to the tire that is being tested. The tire has a specific internal pressure. The footprint is made on a piece of paper after pressure has been applied to the tire. The area of the resulting footprint can be processed in two ways:

1. Manually, by using a planimeter to calculate the area of the contact footprint;
2. By using a computer program which determines the number of pixels in the image. These pixels compose the contact footprint in digitized form.

The core issue, which is also seen in traditional manual methods, is to determine the exact outline of the tire contact footprint.

After thorough research on already existing methods of image processing, the method "convex hull" has been chosen in [1].

The goal of the present article is to describe the algorithm for determining the area of the tire contact footprint by using generalized networks.

EXPOSITION

Presented in this article is a generalized network model of a general structure for calculating the tire contact footprint, using the "convex hull" method [1]. The methodology for creating the generalized networks includes:

- creating a static structure for the modelling process;
- coverage of the dynamic of the modelling process;
- description of the functionality of the modelling process for a period of time;
- determining the data which is of interest to the modelling function as a rolling circle method.

Generalized network model (Fig 1):

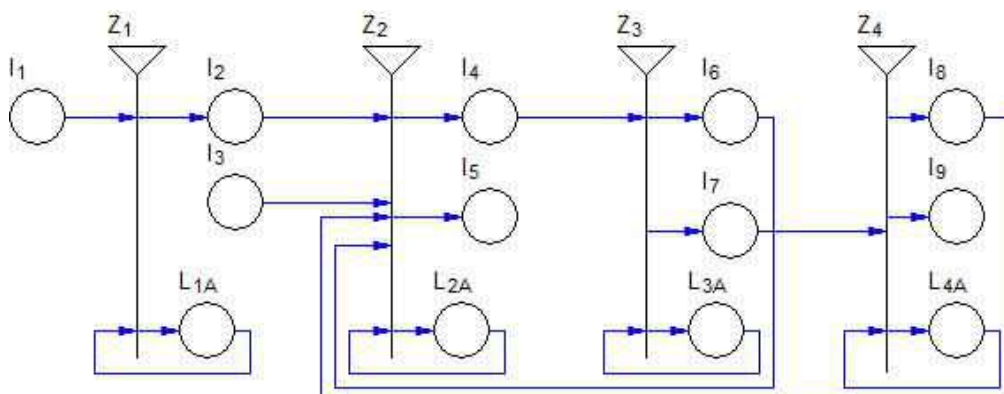


Fig. 1. Generalised network model for rolling circle method

A generalised net model is developed with an introduced set of transitions:

$$A = \{Z_1, Z_2, Z_3, Z_4\}$$

where the transitions describe the following processes:

Z_1 = “the contact footprint in the digitized image”;

Z_2 = “calculate a set of circle points”;

Z_3 = “the found black pixels are stored”;

Z_4 = “search new black pixel”.

The transitions have the following description:

$$Z_1 = \langle \{l_1, l_{1A}\}, \{l_2, l_{1A}\}, R_1 V\{l_1, l_{1A}\} \rangle$$

where:

$$R_1 = \begin{array}{c|cc} & l_2 & L_{1A} \\ \hline l_1 & false & true \\ L_{1A} & W_{1A,2} & true \end{array}$$

$W_{1A,2}$ = “the processed image is binary”.

The token from position l_1 enters position L_{1A} and does not change its characteristics. The token from position L_{1A} splits into one token, which enter positions l_2 , obtaining the same characteristics: “image is binary”.

$$Z_2 = \{l_2, l_3, l_6, l_8, l_{2A}\}, \{l_4, l_5, l_{2A}\}, \\ R_2, V\{l_2, l_3, l_6, l_8, l_{2A}\}$$

where:

$$R_2 = \begin{array}{c|ccc} & l_4 & l_5 & L_{2A} \\ \hline l_2 & false & false & true \\ l_3 & false & false & true \\ l_6 & false & false & true \\ l_8 & false & false & true \\ L_{2A} & W_{2A,4} & W_{2A,5} & true \end{array}$$

$W_{2A,4}$ = “existence of black pixel”

$W_{2A,5}$ = “error when selecting a black pixel”

The tokens from positions l_2, l_3, l_6, l_8 merge into L_{2A} . The token from position L_{2A} enters position l_4, l_5 where it obtains characteristics: “black pixel available” and “selected pixel outside the image”.

$$Z_3 = \langle \{l_4, l_{3A}\}, \{l_6, l_7, l_{3A}\}, R_3 V\{l_4, l_{3A}\} \rangle$$

where:

$$R_3 = \begin{array}{c|ccc} & l_6 & l_7 & L_{3A} \\ \hline l_4 & false & false & true \\ L_{3A} & W_{3A,6} & W_{3A,7} & true \end{array}$$

$W_{3A,6}$ = “a new centre of the circle is available”

$W_{3A,7}$ = “no black pixel”

The token from position l_4 enters position l_{3A} and does not change its characteristics. The token from position l_{3A} splits into two tokens, which enter positions l_6, l_7 obtaining characteristics: “next centre of the checking circle” and “no black pixel found”.

$Z_4 = \langle \{l_7, l_{4A}\}, \{l_8, l_9, l_{4A}\}, R_4, V\{l_7, l_{4A}\} \rangle$
where:

$$R_4 = \begin{array}{c|ccc} & l_8 & l_9 & L_{4A} \\ \hline l_7 & false & false & true \\ L_{4A} & W_{4A,8} & W_{4A,9} & true \end{array}$$

$W_{4A,8}$ = “there are change the trajectory”

$W_{4A,9}$ = “image has been processed”

The token from positions l_8 enters position L_{4A} and does not change its characteristics. The token from position L_{4A} splits into two tokens, which enter positions l_8, l_9 , obtaining characteristics: “new position” and “area calculation”.

After the transition of the output tokens with these characteristics, it is possible to record real tire contact footprint and area calculation.

RESULTS

Fig. 2 shows the tire contact footprint image, processed using the “convex hull” method in Matlab, and the same image processed via the rolling circle method, where the radius of the checking circle used for the image in Fig. 2b is 40 pixels, and the radius used for the image in Fig. 2c is 10 pixels.



Fig. 2. a) a simple image processed applying the “convex hull” method; b) and c) the same image processed applying the rolling circle method with radius of the checking circle 20 and 50 pixels respectively

CONCLUSIONS

What is suggested is a new approach to the digital method for determining the tire contact footprint area developed by using a new enclosing box technique. The method we propose allows the bounding contour to get closer to the shape of the footprint. The aim of our future work will be the estimation and optimization of the method performance.

REFERENCES

[1] Erbakanov L., Staneva L., Vardeva I, Petrov Y., Tire Contact Footprint Area Measurement Using an Alternative Bounding Box Method, *Int. Journal of Engineering Research and Applica*

tion, ISSN : 2248-9622, Vol. 7, Issue 8, (Part -3) August 2017, pp.01-04

[2] Vardeva I, Gochev V, Calculation of estimations of messages by generalized nets and intuitionistic fuzzy truth values, *IEEE 6th International Conference “Intelligent Systems”*, 2012

[3] Vardeva I, Generalized net model for building a virtual private dial-up network, *Issues in IFSs and GN*, Vol.9 (2011), pp.70 – 76

[4] Gocheva P., Hinov N., Gochev V., Generalized net based estimations on switching topologies in electronic circuits, *AIP Conference Proceedings 2048*, 060025 – pp.1-6 (2018)

[5] Gocheva P., Hinov N., Gochev V., Modeling of Electronic Circuits with Generalized Nets, *2018 IX National Conference with International Participation (ELECTRONICA)*, DOI:10.1109

FINDING THE VELOCITY OF AN OBJECT SITUATED ON A MOVING OBJECT WHEN COLLIDING WITH A STATIONARY OBJECT AND THE MOBILE PART IS EJECTED

Yuliyana Petrova, Stancho Pavlov
E-mail: yulipetrov@abv.bg

ABSTRACT

In theoretical mechanics, impact is seen as a physical phenomenon. The main and determining property of impact as a process is the instantaneous change of speed at this point in the system. The change in the internal state of the object accompanying the impact of other objects is not considered in the theory of mechanics. The article, using the methods of mathematical apparatus and physical properties in theoretical mechanics, determines the location of impact after a collision with a stationary vehicle. The precise location of the object before the impact and the mechanism of its movement after the impact is extremely important in the investigation process applicable in assessing the velocity of the vehicle in motion during a traffic accident: collision with another vehicle or fixed barrier.

Key words: mechanism, accident, vehicle, investigation, moving body

INTRODUCTION

Application problems: on top of a moving object is a mobile part /object/ subjected to motion [1]. The system of these two parts collides into a stationary object and the mobile part ejects at a certain angle and initial velocity. In another case, if the velocity at the collision is less than the given initial velocity, then the mobile part remains with the moving object after the collision [2, 3].

Let the velocity at the collision of the moving object be $V = v_o + v_1$, then the mobile part has velocity v_o at an angle of α when colliding with the stationary object. The landing position of the mobile part, the angle α , the initial velocity v_o are known. Let us find the velocity V of the mobile part at the moment of collision, choosing the coordinate system, as shown in Fig. 1:

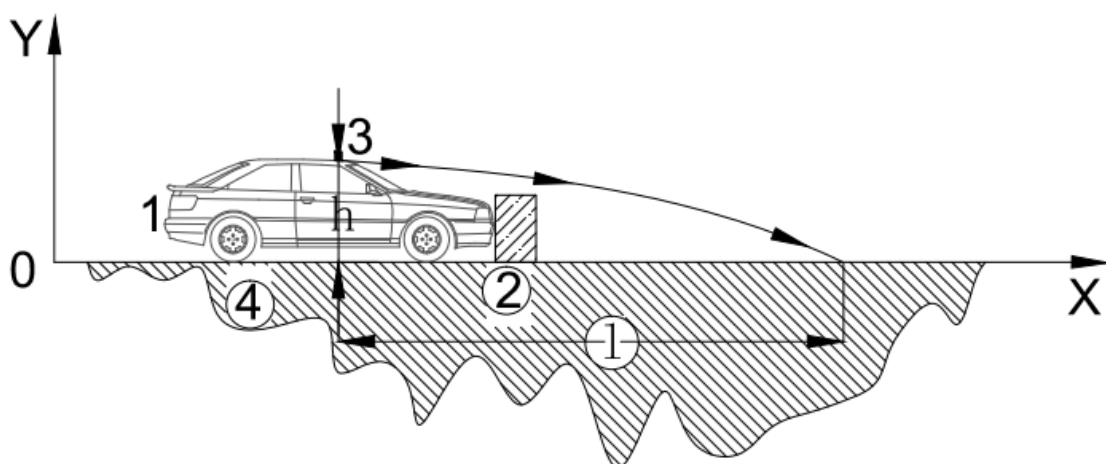


Fig. 1. Staging the task of moving, movable and immovable body

At the moment of collision, the height is h . The mobile part at the same moment is at the height $y = -H$ and the displacement (X) on horizontal plane [4, 5, 6].

$$\begin{cases} x = v_1 \cos \alpha t \\ y = h + v_1 \sin \alpha t - \frac{gt^2}{2} \end{cases} \quad (1)$$

The kinematic equation of movement of the mobile part is eq. (1). We can find the time from the first equation and substitute it in the second equation. In this way we find y as a function of x.

$$y = -\frac{g}{2v_1^2 \cos^2 \alpha} x^2 + tg\alpha x + h \quad (2)$$

We observe in the final state of the mobile part two coordinate points (X, H), we get:

$$\begin{aligned} H &= -\frac{g}{2v_1^2 \cos^2 \alpha} X^2 + tg\alpha X + h \\ \Leftrightarrow \frac{g}{2v_1^2 \cos^2 \alpha} X^2 &= +tg\alpha X + h + H \end{aligned} \quad (3)$$

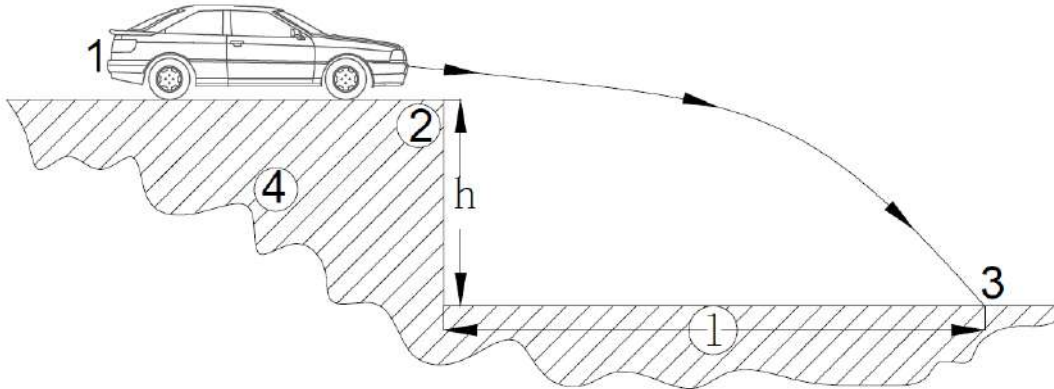


Fig. 2. Formulation of the task

The time of the second object to impact the horizontal axis at point A is t.

From the formula of conservation of impulse, it follows that:

$$m_1 v_1 = m_2 v_2 \Rightarrow v_2 = \frac{m_1 v_1}{m_2}, \quad (5)$$

where (x, y) are the coordinates of point A at the chosen coordinate in Fig. 2.

Because of the laws of kinematics [10]:

$$x = v_2 t; y = \frac{gt^2}{2} \quad (6)$$

From the last equation for v_1 we can write:

$$v_1 = x \sqrt{\frac{g}{2 \cos \alpha [(h + H_1) \cos \alpha + x \sin \alpha]}} \quad (4)$$

The angle of ejection due to collision in an experimental trial is measured.

APPLICATION PROBLEMS: A MOVING OBJECT COLLIDES INTO A STATIONARY OBJECT, FIND THE VELOCITY OF THE STATIONARY OBJECT AFTER THE COLLISION

The first object with mass m_1 moves with velocity v_1 and collides with the second stationary object with mass m_2 . The second object (after moving object collides with it) slides down an angled surface and collides with the horizontal axis at point A. We need to find the velocity v_1 . The masses m_1 , m_2 and the coordinates of point A are known (Fig. 2) [7, 8, 9].

where (x, y) are the coordinates of point A at the chosen coordinates in Fig. 2. We isolate t from the first equation and substitute it in the second equation. We get v_2 from x and y.

From the law of conservation of impulse [11] v_1 is defined:

$$v_1 = \frac{m_2}{m_1} v_2 = x \cdot \frac{m_2}{m_1} \sqrt{\frac{g}{2y}} \quad (7)$$

CONCLUSIONS

The presented mechanisms accurately determine the velocity of the moving body in impact in two types of tasks:

1. Determining the velocity of a moving body with a moving body on it in a collision with a stationary body;

2. Determining the velocity of the body in collision with a second, stationary body according to the final position of the second.

REFERENCES

[1] Panovko Y., "Osnova prikladnoj teoti I kolebanii i udara", Leningrad, 1976.

[2] Ivanov A., "Zadacha ob udare tvvrdeh tel", Sorosobskii obrazovatelnoj jurnal, Tom 7, №5, 2001.

[3] RU Pat. E01H 5/12 (2016)

[4] Aleksandrov E., Sokolinskij V., Prikladnaya teoriya I razcheta udarnah system, UDK 621:621.8.02.031.3, 1969, Moscow

[5] Shmaeva E., Zotov A. Dinamika, Teoriya udara, YFA 2015.

[6] A. Güven Öztas, Application of impulse theory to vehicle collisions, Tr. J. of Engineering and Environment Science 23 (1999), 455-465.

[7] Nikolaev V., On two types of impacts in mechanics, Lomonosov Moscow State University, Faculty of Physics, 2005

[8] Lejbovich M., Teoriya udara v zadachah i primerah, Habarovk, Izdatelstvo TOGU, 2016.

[9] Anindiya Chatterjee, Rigid body collisions & Some general considerations, new collision laws and some experimental data, January 6.1997.

[10] Ivanov I., Destruction of a cast iron cylinder head in operation and after welding recovery, Acta Technica Corviniensis – Bulletin of Engineering, 2017, Tome X, Fascicule 1, 107-110

[11] Ivanov I., Kirov S., Destruction of harness nooses during mining construction, Scientific Proceedings of STUME (2017), NDT days 2017, Number 1, 352-354

DEVELOPING COMPETENCES BY TRAINING STUDENTS IN AUTOMOTIVE DIAGNOSTICS

Magdalena Dyulgerova, Toncho Boyukov
E-mail: mdyulgerova@abv.bg, toncho_b@abv.bg

ABSTRACT

An important factor for the successful realization on the labour market of students of technical specialties is the study of subjects that provide professional knowledge by forming both key and professional competences. The training in automotive diagnostics leads to the development and expansion of the range of competences. The hands-on use of digital technologies for diagnostics forms professional competences for establishing car problems and transferable competences in personal efficiency and self-improvement.

Key words: technical education, building competences, diagnostic

INTRODUCTION

The successful professional adaptation and prospective career of graduate students is the compliance of the level and character of their professional training and their personal qualities with the requirements of the business and jobs of the future.

However, a number of employers think that novice engineers do not have enough practical skills. Furthermore, they lack key skills, such as communication, responsibility, and teamworking [1, 3, 4].

The development of educational competences involves acquiring individual knowledge and skills by students as well as the mastery of a complex process in which a set of educational components is determined for each selected area of study. What is specific for the goals for the development of competences is that they are not only the result of the teacher's activities but also of the students' pursuits and development in the process of acquiring social experience.

Today's social and technical reality needs workers who are competent both in their professional field and "in a field that, it would seem, is not clearly connected with their professional existence".

At present, it is necessary to develop competence models for engineering specialists adapted to the specific conditions of their professional activities.

An important factor for the successful realization on the labour market of students of technical

specialties is to develop their profile by introducing subjects that provide professional knowledge by forming both key and professional competences. The competence profile of a person in a key position contains two main components: a job description and a competence framework, which is the set of required competences for the position.

One of the key subjects in the profile of technical specialties is the diagnostics of machines and systems. The application of the new achievements of science and technology in transport requires the use of both classical methods and new diagnostic tools in the training. The new information technologies which make use of computation and computer networks allow for a new, modern educational environment to be established as the basis for the development and improvement of the educational system.

EXPOSITION

The educational policy in technical specialties is aimed at building competences in the field of engineering and technology.

Competence is defined as the joint use of personal abilities and attributes, skills and knowledge to effectively perform a job, role, function, task, or duty [5].

In the conceptual model of MyCompetence, competence is an employee's set of knowledge, skills, attitudes and behaviours of to achieve results (levels of performance) in a given professional role or organization [6, 7]. Competence is an expression of the individual's ability to do his

job successfully. Competence is a concept that is considered in the context of demonstrated behaviour in a specific situation and in the performance of a specific task, role, etc. Competence is closer to "I know how" than to "I know what".

The training of students of technical specialties is based on "qualification characteristics" outlining the skills which a bachelor of technical subjects in the area of transport has to acquire.

A specialist who has acquired a Bachelor's degree in "Engineering and technology in transport" needs a high professional level in technology for the design, manufacture, repair, and technical operation of equipment intended for transportation of passengers and various types of cargo, including liquid and gaseous cargo. They need to obtain knowledge related to the analysis and synthesis of equipment designed for the transportation of passengers and goods; manufacture, testing, installation, maintenance, and repair of such equipment.

The classification used in MyCompetence formulates cluster competences applying several criteria, according to the field: digital, communicative, organizational, and professional.

MyCompetence defines 17 clusters of the same type of competences. The clusters include key and specific competences.

Considering the qualification characteristics of the specialty and the block model of the syllabus [2], it can be concluded that there is a need to build specific and develop key competences.

Specific competences are defined as strictly professional, mainly technical and technological knowledge and skills related to the specific nature of the functions performed in a particular position, i.e. what employees need to know so that they can do their job successfully and efficiently in accordance with the requirements of their position. These competences are related to the specific nature of the profession and the tasks of the position (workplace), the equipment, tools and technology used, the business processes and operations, and the specific regulations and standards regarding their position.

There are three types of competences: universal, transferable and unique.

Transferable competencies include skills and abilities needed to perform several roles in varying degrees of importance and mastery. Examples of these are leadership and management skills.

Unique competencies refer to specialized know-how or abilities required for a specific role or job. Technical competences include the underlying knowledge and skills of "the portion of the

iceberg that remains above the surface of water", described in observable and measurable terms that are necessary in order to perform a particular task assigned to a person achieving quantitative targets and conforming to qualitative requirements.

The development of an engineer's competence profile at university is limited within the provided academic hours and therefore, competences from the 17 clusters have to be selected.

One of the subjects forming the profile of the engineer is "Diagnostics of transport equipment". It is studied in the fourth year, when students are already familiar with the general principles of reliability of transport units and systems and with concepts such as failure, operability, maintainability, etc. Students have improved their logical thinking, they have understood that quality is a necessary element for the reliability of both a single element and a complex system, both at the design and operational stages.

The study of car diagnostics should lead to the expansion and deepening of the range of competences. The choice of competences was made after analyzing the clusters from MyCompetence, taking into account the Bulgarian qualifications framework. According to MyCompetence, the competences are specific, and according to Europass, they are professional.

Our choice of focus was on specific/professional competences from three clusters: Working with regulations, standards and requirements; Repair and maintenance; and Design, development and implementation.

In parallel, transferable (organisational, according to Europass) competences from the Personal efficiency and self-improvement cluster are enhanced during the training. The training begins with the formation of the Working with regulations, standards and requirements cluster competences, as follows:

- Application of health and safety standards: acquaintance with the instructions, rules and regulations for health and safety at work, environmental protection, and fire and emergency safety in the performance of daily duties. Strict observance of all rules is exercised, emphasizing the fact that transport is a high-risk sector.

- Application of normative regulations and standards: acquaintance with the application of the requirements for the specific automotive sector standards.

- Compliance with standards and norms: examples are given of situations that show the need for their timely and complete implementation,

strictly adhering to the norms and standards adopted by the company. In the course, there is an opportunity for practical training in a real work environment in a partner company.

After understanding the importance of knowledge and compliance with standards and rules, classes are held to form competences from the Repair and maintenance cluster:

- Diagnostics of motor vehicles: the aim is to form competences for organizing and carrying out diagnostics in the correct technological order, determining the technical condition of the mechanisms, systems and units of conventional and electric vehicles.

- Care for the technical condition of the vehicle: competences for understanding the vehicle as a system, for systematic and precise control of the technical condition of the vehicle, detection of technical errors that pose a risk to safety, and taking the respective reliable measures for their removal.

- Maintenance of systems and equipment: inspection, diagnostics and maintenance of systems and equipment, strictly observing the standards for their proper and appropriate maintenance.

- Damage prevention: timely identification and prevention of the risks of damage and accidents.

- Operation of a motor vehicle: maintenance activities on the motor vehicle, observing the legal framework regarding the requirements for technical condition of vehicles.

Together with the development of the listed competences, the following are improved: analysis of test data: interpretation and analyses of the data collected during the tests, formulation of conclusions, new ideas or solutions.

The selected competences are the basis for the development of the following professional competences: Carrying out repair work, Repair of motor vehicles, and Servicing, which are formed in other courses provided later in the syllabus.

The development of professional competences also determines the parallel development of transferable (organizational, according to Europass) competences, which are summarized in the Personal efficiency and self-improvement cluster. In car diagnostics training, opportunities are created to develop key competences needed for many other areas.

Special attention is given to the development of observation, concentration and attention span. These competences develop as a result of practising the two methods of diagnostics: subjective, by which probable failures can be observed visu-

ally, by olfactory means, or noise detection; and objective, by onboard or external diagnostic equipment. The systematic approach is used by setting tasks for purposeful focusing on a certain cars system, its elements, their individual characteristics and details. It is necessary to concentrate on a specific goal, object, process, activity, operation, signal, etc. At the same time logical thinking is developed and conclusions are drawn from the collected information.

Decisions to determine the failure are made on the basis of monitoring and analysis of the situation. Practical, active thinking is developed with regards to predetermined goals, and based on visual, auditory and other perceptions in work operations. Students can reach a new level of knowledge in the form of concepts and ratiocinations about their properties and spatial-object relations.

The use of modern computerized methods is very effective in building key and professional competences for detecting vehicle failures.

Each vehicle is equipped with an onboard computer. Onboard diagnostic (OBD) information systems are designed to automatically monitor and record technical condition data, the correct technical operation of vehicles and driver performance.

Modern vehicles use onboard computers which control fuel metering, auxiliary emissions controls, valves, etc., regulate anti-lock braking, control transmission, and vehicle speed controls. OBD II is an extension of such a computer. A tester, which is an example of outboard diagnostics, is required to access the stored problem code. The task of outboard diagnostics is to analyze the fault code of the control units.

The choice of a fault-finding algorithm is the basic step in establishing the causes of the ability loss. The most effective method is the logical approach to determinate probable failures of vehicle systems and elements.



Fig. 1 Launch diagnostic tester

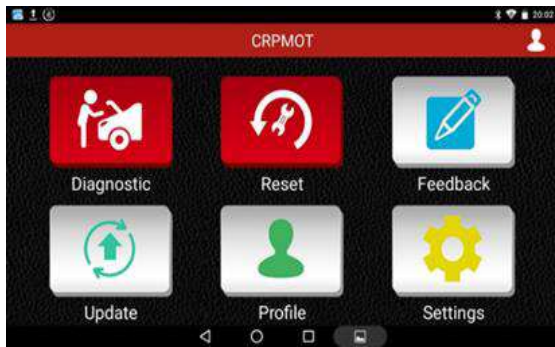


Fig. 2 Diagnostic tester menu



Fig. 3 Function choice

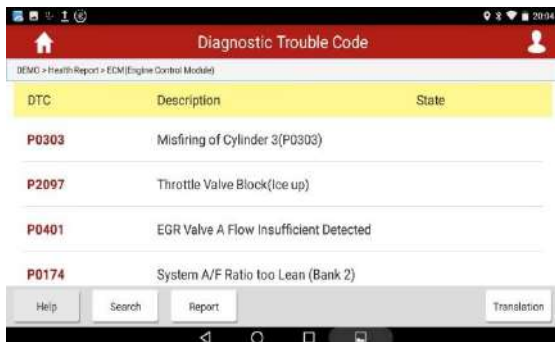


Fig. 4 Selection of a test element

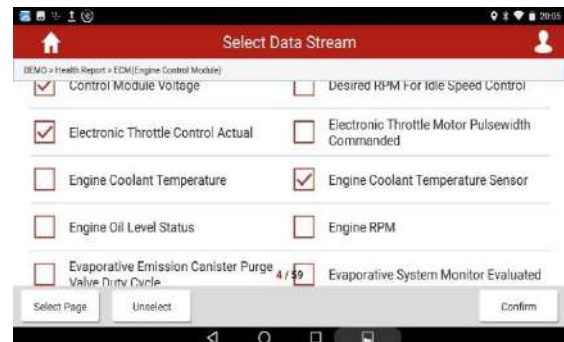


Fig. 5 Read parameters/measured value block

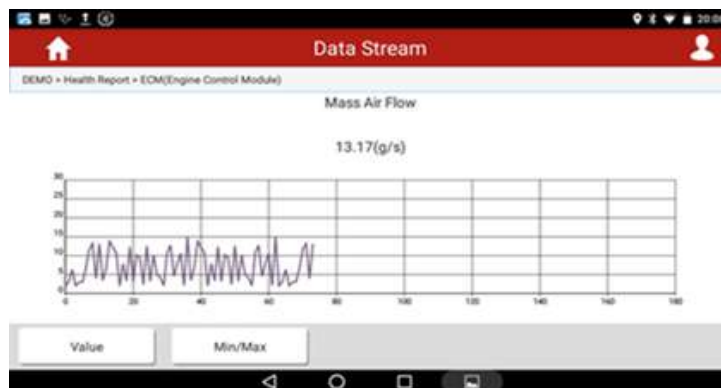


Fig. 6 Monitoring of parameters

This approach gives a lot of possibilities for developing competences for understanding the vehicle as a system, for systematic and correct control of the technical condition.

The training is based on the acquired knowledge of automotive technology and the reliability of transport systems.

The practical exercises use computer technology to diagnose a car. Launch CRP MOT diagnostic equipment is used for developing specific competences in diagnostics. The tester is a multi-brand diagnostic scanner, including more than 48 car brands with diagnostic capabilities for all

parts of the car electronic systems and the 10 most commonly used special functions and basic adaptations. The equipment is based on a complete Android operating system (Fig. 1). All diagnostics information is displayed on the LCD graphic display of the tester. The set also includes the commonly used BMW-20 pin and MB-38 pin adapters for old sockets.

The laboratory exercises start with an introduction to the principle of operation and the use of a diagnostic system tester. Students need to develop skills for understanding the standards and norms which are used in car diagnostic. At

the beginning of the practical classes students have to get skills such as connecting the tester connector to the diagnostic car connector; selection of the vehicle manufacturer type; choice of the appropriate section which provides the list of fault codes (Fig.3) from the tester menu (Fig. 2); after resetting errors in the memory, selection of the appropriate section in the tester menu and determination of the new parameters.

In addition to the numeric code, diagnostic units also provide a definition of the fault code (Fig. 4). All accumulated fault codes can be reset.

The initial information on the possible cause of the damage is stored in "Read parameters/Measured value block" (Fig. 5).

The specified fault code does not necessarily refer to an actual component failure. Before replacing individual components, the information should be read carefully to determine the next diagnostic steps.

It is possible to monitor the parameters in real time in graphical form (Fig.6).

In the process of training important competences are developed, namely concentration and professional knowledge. They are required for an analysis of the information and establishing the character of the element failure or reduction of system availability.

During the practical task, all values that are measured, monitored and evaluated, as well as the reference values of the system are recorded and then provided in written form as a protocol.

CONCLUSION

The use of digital technologies for system diagnostics in the training of students of technical specialties develops the professional competences for establishing car failures. They acquire skills to recognize the fault codes given by the onboard computer and know the symptoms of

probable failure. Students obtain knowledge about the main parameters controlled by the computer and the parameters which can be determined without using a tester. As a result, they acquire competences for logical determination of the possible failure causes and the possible solutions for repair and prevention of failure. In addition, students get transferable competences in personal efficiency and self-improvement.

ACKNOWLEDGEMENTS

This study was supported by the Scientific Research Sector of University Prof. Dr Assen Zlatarov, Burgas, Project No 424/2019.

REFERENCES

1. Chantov, V. Kompetencii i kompetentnost (me-zhdu znanieto i mozhneto). *Novi informacionni tehnologii v obrazovatelniya process*, 2012, in Bulgarian
2. Dyulgerova, M. Izpolzovane na strukturno-blokov model za razkriwane na mezhdupredmetnite wryzki pri obuchenieto v tehniceskite specialnosti., *Assen Zlatarov University Annual*, Vol. XLV, Book 1, 2016, Burgas, in Bulgarian
3. Myagkov, A. Studenti tehnichekogo wuza: profesionalnyie kompetencii i ovidaniya na rinke truda. *Sociologicheskie issledovaniq*, 2016, № 6, in Russian
4. Piralova, O. Teoreticheskie osnovi optimizacii obucheniq profesionalnym disciplinam v usloviyah sovremennogo technicheskogo wuza. *Akademia estestvoznaniya*, 2011, in Russian
5. <https://ec.europa.eu/esco/portal/skill>
6. <https://mycompetence.bg/bg/static/9>
7. <http://machines.competencemap.bg/language/bg/uploads/files/analysis1/analysis>

Assen Zlatarov University
ANNUAL, Vol. XLIX, BOOK 1, 2020
TECHNICAL AND NATURAL SCIENCES

Editor-in-Chief
Prof. Margarita Terzieva, DSc

Co-editors
Assoc. Prof. Penka Peeva, PhD
Assoc. Prof. Liliya Staneva, PhD
Asst. Prof. Ivan Sokolov

Technical Assistant
Iliana Ishmerieva

Design and layout
Libra Scorp Publisher
www.meridian27.com

Printed in M&BM Ltd.
www.mbm-bg.com

Edition of
Assen Zlatarov University
www.btu.bg

ISSN 2603-3968

BURGAS, 2020

ISSN 2603-3968



9 772603 396002